

**Status des  
Regressionstestens für  
ASTEC V2.0r2**



## **Technischer Bericht/ Technical Report**

Reaktorsicherheitsforschung -  
Vorhabens Nr.:/  
Reactor Safety Research-Project No.:  
RS1190

Vorhabensitel / Project Title:  
Gezielte Validierung von  
COCOSYS und ASTEC sowie  
Unsicherheits- und Sensitivi-  
tätsanalyse zum Iodverhalten

Specific Validation of COCOSYS  
and ASTEC and Uncertainty and  
Sensitivity study on Iodine

Berichtstitel / Report Title:  
Status des Regressionstestens  
für ASTEC V2.0r2

Autor / Authors:  
H. Nowack  
M. Pelzer

Berichtszeitraum / Publication Date:  
August 2012

Anmerkung:  
Das diesem Bericht zugrunde lie-  
gende F&E-Vorhaben wurde im  
Auftrag des Bundesministeriums  
für Wirtschaft und Technologie  
(BMWi) unter dem Kennzeichen  
RS1190 erstellt durchgeführt.

Die Verantwortung für den Inhalt  
dieser Veröffentlichung liegt beim  
Auftragnehmer.



## **Kurzfassung**

Der Integralcode ASTEC wird gemeinsam von IRSN und GRS entwickelt, um Stör- und Unfälle in Leichtwasserreaktoren vom einleitenden Ereignis bis hin zur Freisetzung von radioaktiven Stoffen in die Umgebung zu simulieren. Die Entwicklungsarbeit der GRS konzentriert sich dabei auf das Containment Modul CPA (Containment Part of ASTEC), dessen Modellierung auf den GRS-Code COCOSYS zurückgeht. Um sicherzustellen, dass bei der Weiterentwicklung von COCOSYS keine ungewünschten Nebeneffekte auftreten, ist für diesen Code bereits ein Regressionstesten eingeführt worden. In diesem Verfahren werden Rechnungen zu ausgewählten Experimenten und Kraftwerksanlagen durchgeführt. Dabei wird jeweils derselbe Datensatz mit zwei unterschiedlichen Code-Versionen ausgeführt. Anhand von ausgewählten physikalischen Parametern wird die aktuelle Code-Version für jeden Rechenfall mit der vorhergehenden Version verglichen. Im Falle von Experimentnachrechnungen werden auch Vergleiche mit experimentellen Daten durchgeführt. Aufbauend auf den Erfahrungen des Regressionstestens für COCOSYS ist ein vergleichbares Verfahren für ASTEC mit dem Fokus auf das Modul CPA erstellt worden. Dieses Verfahren dient der Bewertung von Unterschieden zwischen Rechnungen mit verschiedenen ASTEC-Versionen und ist damit nicht als Programmvalidierung zu verstehen. Auf diese Weise lassen sich eventuelle Fehler oder ungewollte Auswirkungen auf andere Modellen schnell auffinden. Damit liefert das Regressionstesten einen wichtigen Beitrag zur Qualitätssicherung von ASTEC.

Der Bericht über das Regressionstesten wird weitgehend automatisch erstellt, dabei werden die Abweichungen zwischen zwei verschiedenen Codeversionen dargelegt. Als Anhang wird ein solcher erster Bericht bereitgestellt. Dieser legt den derzeitigen Stand des Regressionstestens für die ASTEC-Versionen V2.0r1 und V2.0r2 dar.

## **Abstract**

The integral code ASTEC is jointly developed by IRSN and GRS for the simulation of incidents and accidents in light water reactors from the initiating event up to the release of radioactive material into the environment. The development at GRS is focused on the containment module CPA (Containment Part of ASTEC), whose modelling is based on the GRS code COCOSYS. To assure that the development process of COCOSYS causes no unintended side effect, a regression testing procedure has already been introduced for this code. Within this procedure calculations of experiments and plant scenarios are performed with the same input deck but two different code versions. For every test case the recent code version is compared to the preceding code version on the basis of chosen physical parameters. In the case of post-calculations of experiments also comparison to experimental data is given. Based on the experiences gained with the regression testing for COCOSYS a comparable procedure has been developed for ASTEC with focus on the CPA module. This procedure is used for the evaluation of differences between different ASTEC versions. Therefore, it has a different purpose than the validation of the code. In this way bugs or unintended side-effects in other modules can be detected early during the development process. Hence, the regression testing is an important contribution to the quality assurance of ASTEC.

The report about the regression testing is automated to a wide extent. Within this report the differences between two code versions are explained. The first version of this report is given as appendix. This report shows the recent state of the regression testing for the ASTEC versions V2.0r1 and V2.0r2.

## Inhaltsverzeichnis

|   |                          |   |
|---|--------------------------|---|
| 1 | Einleitung .....         | 1 |
| 2 | Schlussfolgerungen ..... | 4 |
| 3 | Verteiler .....          | 5 |
| 4 | Anhang .....             | 7 |



# 1 Einleitung

Zur Simulation der verschiedenen physikalisch-chemischen Vorgänge bei Stör- und Unfällen in Kernkraftwerken werden von der GRS der Systemcode COCOSYS und der deutsch-französische Integralcode ASTEC entwickelt. Bei COCOSYS handelt es sich um ein Codesystem auf Basis mechanistischer Modelle, mit denen die relevanten Wechselwirkungen zwischen den verschiedenen Phänomenen im Containment simuliert werden können. ASTEC beschreibt als Integralcode den gesamten Störfallablauf vom einleitenden Ereignis mit der Freisetzung von Spaltprodukten aus dem Reaktorkern über das Reaktorkühlsystem und das Containment bis in die Umwelt. Im Rahmen des Vorhabens RS1190 erfolgt die Validierung dieser beiden Codesysteme.

Für COCOSYS ist bereits ein Verfahren zum Regressionstesten aufgesetzt worden, um Fehler bei der fortschreitenden Entwicklung des Codes zu entdecken und den Modellierungsfortschritt zwischen verschiedenen Versionen darzustellen. Dazu werden jeweils mehrere Rechenfälle, d. h. Experimentnachrechnungen und Anlagenszenarien mit unterschiedlichen Codeversionen nachgerechnet. Aus dem Vergleich der Ergebnisse beider Codeversionen und zusätzlich mit experimentellen Ergebnissen lassen sich Rückschlüsse auf den Modellierungsfortschritt ziehen. Außerdem erlaubt dieses Vorgehen das Finden von Programmierfehlern oder unbeabsichtigter Nebeneffekte bei der Weiterentwicklung einzelner Teilmodelle. Aufbauend auf den Erfahrungen, die aus dem Regressionstesten für COCOSYS gewonnen worden sind, ist ein solches Regressionstestverfahren auch für den Code ASTEC entwickelt worden. Da der Schwerpunkt der GRS bei ASTEC auf der Entwicklung des Containment-Moduls CPA (Containment Part of ASTEC) liegt, ist das Regressionstesten auf dieses Modul fokussiert. Aber auch das Iodmodul IODE und das Modul MEDICIS zur Berechnung der Schmelze-Beton-Wechselwirkung werden im Regressionstesten für ASTEC behandelt. Für einige Testfälle ist auch ein Vergleich mit COCOSYS-Ergebnissen gegeben.

Der im Anhang dargelegte Bericht vergleicht die ASTEC Versionen V2.0r1 und V2.0r2. Bei einigen Rechenfällen erfolgt außerdem ein Vergleich mit der COCOSYS Version V2.3v9. In Tabelle 1 sind die für das Regressionstesten vorgesehenen Rechenfälle aufgelistet. Die bereits in diesem Bericht enthaltenen Rechenfälle sind mit einem Häkchen gekennzeichnet. Bereits bei dem aktuellen Stand werden alle Themen im Regressionstesten berücksichtigt. Die übrigen Testfälle werden parallel zur weiteren Entwicklung von ASTEC ergänzt. Die Auswahl soll zukünftig an die Entwicklungsziele von ASTEC angepasst bzw. ergänzt werden.

**Tabelle 1      Überblick über die behandelten Rechenfälle**

| <b>Thema</b>                | <b>Experiment</b>      | <b>Status</b> | <b>COCOSYS</b> |
|-----------------------------|------------------------|---------------|----------------|
| Sprühsysteme                | HDR E11.1              | ✓             |                |
|                             | MISTRA MASP1           | ✓             | ✓              |
| Aerosolverhalten            | BMC VANAM-M3           | ✓             | ✓              |
|                             | KAEVER test K148, K187 | ✓             |                |
| Iodchemie                   | ThAI Iod11             | ✓             | ✓              |
|                             | PHEBUS RTF-1           | ✓             | ✓              |
| Wasserstoffverbrennung      | ENACCEF RUN 153        | ✓             |                |
|                             | BMC Hx23               | ✓             |                |
| Schmelzebetonwechselwirkung | OECD CCI2              | ✓             |                |
|                             | COMET L3               | ✓             |                |
| Druckabbausysteme           | GKSS M1                | ✓             | ✓              |
|                             | EREC BC-V213 SLB-G02   | ✓             | ✓              |
| Typische Anlagenrechenfälle | KONVOI                 |               |                |
|                             | SWR-72                 | ✓             | ✓              |
|                             | WWER 1000              |               |                |

✓ Bereits in diesem Bericht behandelt

Genau wie beim Regressionstesten für COCOSYS, ist die Prozedur in der Scriptsprache Python entwickelt worden. Dabei ist die Berechnung der Testfälle sowie die grafische Auswertung automatisiert worden. Die in dem Bericht zum Regressionstesten verwendeten Grafiken werden verlinkt eingefügt. Dadurch wird das Erstellen späterer Versionen des Regressionstestberichts weitgehend automatisiert. Dieser Bericht wird als lebendiges Dokument weiterentwickelt, wobei bei neu herausgegebenen Anwenderversionen auch ein Bericht über das Regressionstesten erscheinen soll. Zur Beurteilung des Entwicklungsfortschritts von ASTEC ist es notwendig, zu jedem Testfall verschiedene charakteristische Parameter zu bestimmen. Im Falle von Experimenten werden zusätzlich Vergleiche mit Messergebnissen herangezogen. Auf diese Weise können die mit verschiedenen Programmversionen erzielten Ergebnisse bewertet und unerwünschte Nebeneffekte bei der Codeentwicklung frühzeitig entdeckt werden. Neben der Qualitätssicherung durch das Finden von Modellfehlern dient das Regressionstesten damit auch der Dokumentation des Entwicklungsfortschritts von ASTEC.

Im Bericht zum Regressionstesten werden die maßgeblichen Code-Änderungen, die zwischen den verglichenen Versionen erfolgt sind, angegeben. Dies erlaubt Rückschlüsse auf die Ursachen bei unterschiedlichen Rechenergebnissen zwischen den verglichenen Versionen.

Dieser Bericht gibt den aktuellen Stand des Regressionstestens für einen Vergleich der Versionen V2.0r1 und V2.0r2 wieder. Zusätzlich erfolgen bei einigen Rechenfällen Vergleiche mit COCOSYS V2.3v9. Der aktuelle Bericht „Status of regression testing - Comparison of ASTEC V2.0r2 with V2.0r1 and with COCOSYS V2.3v9“ zum Regressionstesten in englischer Sprache ist als Anhang beigefügt.

## 2 Schlussfolgerungen

Die hier im Regressionstesten behandelten Experimente decken die Punkte Sprühsysteme, Aerosolverhalten, Iodchemie, Wasserstoffverbrennung, Schmelzebetonwechselwirkung, Druckabbausysteme, sowie typische Anlagenrechenfälle und damit alle angestrebten Phänomene ab. Es ist nötig die Matrix der behandelten Rechenfälle in Zukunft an die Modellierungsfortschritte in ASTEC anzupassen.

Die durchgeführten Arbeiten zeigen bereits den Nutzen des Regressionstestens. So sind z. B. die stark verbesserten Ergebnisse im Iod-11 Rechenfall auf das Finden und Beheben eines Bugs bei der Wärmeeinspeisung in Strukturen zurückzuführen, der erst beim Regressionstesten im Vergleich zu COCOSYS-Ergebnissen aufgefallen ist. Dieser Bug-fix erklärt auch die Unterschiede in den SWR-72 Rechnungen. Die Ergebnisse der Wasserstoffverbrennungsrechnungen sind ein Beispiel dafür, wie der Entwicklungsfortschritt an stark bearbeiteten Modellen durch das Regressionstesten wiedergegeben werden kann. Kleinere Unterschiede sind zum Beispiel an dem Versuch COMET L3 sichtbar, die auf Arbeiten am MEDICIS Modul zurückzuführen sind. Die Iodrechnungen zeigen starke Unterschiede zwischen COCOSYS und ASTEC. Das liegt an den unterschiedlichen Iodmodellen, AIM in COCOSYS und IODE in ASTEC. Das Regressionstesten erlaubt einen Vergleich beider Modelle.

Diese Beispiele zeigen die Eignung des Regressionstestens als ein Mittel zur Qualitätssicherung während der weiteren Entwicklung von ASTEC und im speziellen des Moduls CPA. Der aktuelle Regressionstestbericht ist im Anhang enthalten.

### 3 Verteiler

|                          |                                        | Exemplare<br>gedruckte Form | Exemplare<br>pdf |
|--------------------------|----------------------------------------|-----------------------------|------------------|
| <b>BMWi</b>              |                                        |                             |                  |
| Referat III B 4          |                                        | 1 x                         |                  |
| <b>GRS-PT/B</b>          |                                        |                             |                  |
| Projektbegleiter         | (dre)                                  | 3 x                         | 1 x              |
| <b>GRS</b>               |                                        |                             |                  |
| Geschäftsführung         | (stj, wfp)                             |                             | je 1 x           |
| Bereichsleiter           | (erv, stc, ver, prg, luw, rot,<br>zir) |                             | je 1 x           |
| Abteilungsleiter         | (som)                                  |                             | je 1 x           |
| Projektleiter            | (klh, ren)                             |                             | je 1 x           |
| Projektbetreuung         | (bar, wal)                             |                             | je 1 x           |
| Informationsverarbeitung | (nit)                                  |                             | 1 x              |
| Autoren                  | (noh, pel)                             | je 1 x                      | je 1 x           |
| Bibliothek               | (Köln)                                 | 1 x                         |                  |
| <b>Gesamtauflage</b>     |                                        | <b>Exemplare</b>            | <b>7</b>         |



## **4 Anhang**





## **Status of ASTEC-CPA Regression Testing**

Comparison of ASTEC V2.0r2 with V2.0r1 and  
with COCOSYS V2.3v9

Holger Nowack  
Martin Pelzer

Revision 0  
December 3, 2012

---

---

## Contents

|       |                                                                             |     |
|-------|-----------------------------------------------------------------------------|-----|
| 1     | <b>Introduction</b> .....                                                   | 1   |
| 2     | <b>Procedure for the ASTEC-CPA regression tests</b> .....                   | 3   |
| 2.1   | <b>General</b> .....                                                        | 3   |
| 2.2   | <b>Execution of ASTEC runs for the regression testing using a GUI</b> ..... | 3   |
| 3     | <b>Development of ASTEC V2.0r2 versus V2.0r1</b> .....                      | 6   |
| 4     | <b>Regression tests</b> .....                                               | 7   |
| 4.1   | <b>Spray systems</b> .....                                                  | 7   |
| 4.1.1 | HDR E11.1 .....                                                             | 7   |
| 4.1.2 | MISTRA MASP1.....                                                           | 15  |
| 4.2   | <b>Aerosol behaviour</b> .....                                              | 25  |
| 4.2.1 | BMC VANAM-M3 .....                                                          | 26  |
| 4.2.2 | KAEVER Tests.....                                                           | 32  |
| 4.3   | <b>Iodine behaviour</b> .....                                               | 47  |
| 4.3.1 | THAI Iod-11 .....                                                           | 47  |
| 4.3.2 | PHEBUS/RTF-1 .....                                                          | 54  |
| 4.4   | <b>Hydrogen combustion</b> .....                                            | 60  |
| 4.4.1 | ENACCEF RUN 153 .....                                                       | 60  |
| 4.4.2 | BMC Hx23.....                                                               | 67  |
| 4.5   | <b>Molten corium concrete interaction (MCCI)</b> .....                      | 72  |
| 4.5.1 | OECD-CCI-2 .....                                                            | 73  |
| 4.5.2 | COMET L3 .....                                                              | 78  |
| 4.5.3 | Summary.....                                                                | 85  |
| 4.6   | <b>Pressure suppression systems</b> .....                                   | 85  |
| 4.6.1 | GKSS M1 .....                                                               | 85  |
| 4.6.2 | EREC BC-V213 SLB-G02 .....                                                  | 91  |
| 4.7   | <b>Typical NPP test cases</b> .....                                         | 98  |
| 4.7.1 | BWR-72 (KRB II – C).....                                                    | 98  |
| 4.7.2 | KONVOI PWR.....                                                             | 108 |
| 4.7.3 | WWER-1000 .....                                                             | 108 |
| 5     | <b>Summary</b> .....                                                        | 109 |
| 6     | <b>References</b> .....                                                     | 110 |

## 1 Introduction

Regression testing is understood as the calculation of defined test cases with each version of the ASTEC code prior to its release. This is done to check how newly introduced models or model extensions influence the calculation results, i.e. whether side effects lead to unexpected results. For that purpose experiments are selected, which quality is generally accepted and which cover one or more significant phenomena. To assure the quality of ASTEC, each new release version (also termed as user version) will be tested by this procedure prior to its release against the results of calculations with a previous code version.

This regression testing is done by GRS in parallel to the periodic testing of ASTEC at IRSN for deeper analysis of the CPA module. While IRSN tests all modules of ASTEC, GRS is concentrating on the CPA module, for which GRS is mainly responsible. IODE and MEDICIS modules are included into some cases of the GRS regression testing as well.

For each test some selected experimental parameters are compared with the results of the last ASTEC user version and the version foreseen to be released. Deviations between the calculation results and experimental results as well as deviations between the compared ASTEC versions will be assessed.

Additionally to the experiments, some typical NPP test cases are included to check the capability of ASTEC for real plant conditions. Logically, these plant calculations can be compared among different ASTEC versions only.

The regression testing procedure for ASTEC is based on the experiences gained by the regression testing procedure with COCOSYS /ARN 08/. For test cases that are also available in the COCOSYS regression testing procedure also a comparison to the COCOSYS results is given.

The regression testing procedure is a powerful tool for the detection of bugs inside the ASTEC code that occur during the development process. Thus, it allows an early fixing of programming errors prior to the release of a new code version. Beside this, the comparison with experimental data offers a good insight in the model improvements made between different ASTEC releases.

The regression testing cannot be understood as the validation of the code, i.e. there is no principal discussion on the models, physical phenomena or the experimental results. Tests are explained to the extent necessary for the principal understanding of the results. Specialists for the particular ASTEC models give suggestions, which parameters are of main interest and typical for the model to be assessed. Deviations between experimental data and the ASTEC calculations will be proven with respect to their assessment, i.e. whether the new version gives the same result or even a better agreement with the tests. In case of poorer results these will be explained. Detailed results (e.g. reports or experimental data) of the basic validation of the ASTEC models will be collected and added to the regression testing package in electronic form.

The report on regression tests is a "living" document, i.e. the applied experiments and the covered area of phenomena will be enlarged permanently with the on-going development of ASTEC. This document describes the status of the regression testing as a

---

first release of this report. Therefore, a comparison between the already released versions ASTEC V2.0r1 and V2.0r2 is given here.

## 2 Procedure for the ASTEC-CPA regression tests

### 2.1 General

The regression testing procedure for ASTEC is based on the regression testing procedure for COCOSYS. The following Table 2.1-1 shows the test cases included/planned for the ASTEC regression tests. At the moment 12 experimental test cases and 3 plant calculations are included in the test-matrix with focus on CPA. In the current state still two plant test cases for NPP application are missing, but the total number of 12 experimental test cases and 1 additional plant test case is already sufficient to test the modelling progress of ASTEC CPA.

**Table 2.1-1 Calculations chosen for regression testing**

| Topic                              | Experiment             | ASTEC | COCOSYS |
|------------------------------------|------------------------|-------|---------|
| Spraying systems                   | HDR E11.1              | ✓     |         |
|                                    | MISTRA MASP1           | ✓     | ✓       |
| Aerosol behaviour                  | BMC VANAM-M3           | ✓     | ✓       |
|                                    | KAEVER test K148, K187 | ✓     |         |
| Iodine chemistry                   | THAI Iod11             | ✓     | ✓       |
|                                    | PHEBUS RTF-1           | ✓     | ✓       |
| Hydrogen combustion                | ENACCEF RUN 153        | ✓     |         |
|                                    | BMC Hx23               | ✓     |         |
| Molten corium concrete interaction | OECD CCI2              | ✓     |         |
|                                    | COMET L3               | ✓     |         |
| Pressure suppression systems       | GKSS M1                | ✓     | ✓       |
|                                    | EREC BC-V213 SLB-G02   | ✓     | ✓       |
| Typical NPP test cases             | BWR-72                 | ✓     | ✓       |
|                                    | KONVOI                 |       |         |
|                                    | WWER 1000              |       |         |

✓ already included in this report

### 2.2 Execution of ASTEC runs for the regression testing using a GUI

The ASTEC-CPA regression testing is centrally performed on the PC "PC1970" under Windows 7 operating system. The PC is embedded into the GRS network and it can be accessed via the "Remote Desktop Connection" tool of Windows (authorisation, i.e. User-ID and password are needed). The data for the regression testing are located on the C drive of this PC.

This PC and in particular the regression testing data are linked with the GRS backup system "IBM TSM Backup". Thus, all information is saved frequently and data can be restored in case of problems.

In order to establish a defined procedure for the regression testing the calculation of the different datasets is automated as far as possible. For this a script **main\_thread.py** has been developed using the freeware programming language Python ([www.python.org](http://www.python.org)).

This script uses a defined directory tree (see Figure 2.2-1):

- the input datasets and design members for plotting are located in the directory ‘inputs\_designmember’,
- the different ASTEC versions are stored in directories with the name ‘astecv + version number’,

For example the ASTEC version V2.0r2 is stored under ‘astecv20r2’. All calculations with a certain ASTEC version are calculated within the corresponding ASTEC version directory.

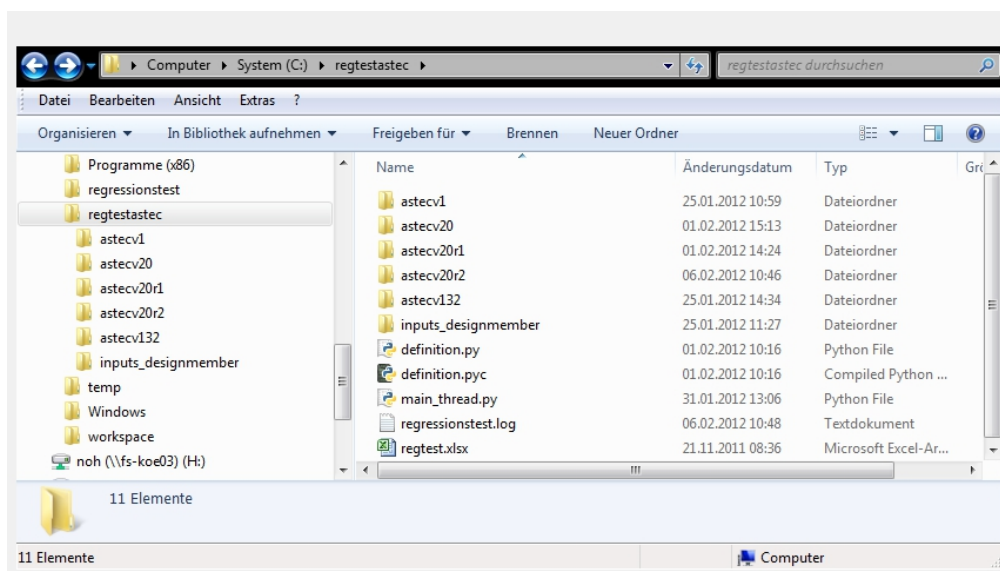


**Figure 2.2-1 Directory structure for the regression testing**

The calculations as well as the plotting of the results is automated and stored in graphic files of Windows "EMF" format. These graphic files are automatically included in an MS Word document of the (i.e. the present) regression testing report. This procedure allows the generation of a new version of the report with as less effort as possible. Thus, this report is a kind of a 'living document' that is generated anew with every new user version of ASTEC.

After starting the main procedure "main\_thread.py" a graphical user interface occurs as shown in Figure 2.2-2. It allows choosing the datasets and ASTEC versions that will be used for the calculations. It is also possible to mark the "No calculation" option. This is useful, if a calculation has already been performed, but a new plotting of the relevant parameters is necessary. The listing of the datasets and employed ASTEC versions is defined in the procedure "definition.py" as is seen in Figure 2.2-3. The lists "astecversions" and "inputs" can be extended by further regression test cases. The drawing of the GUI is performed automatically after extending these lists.

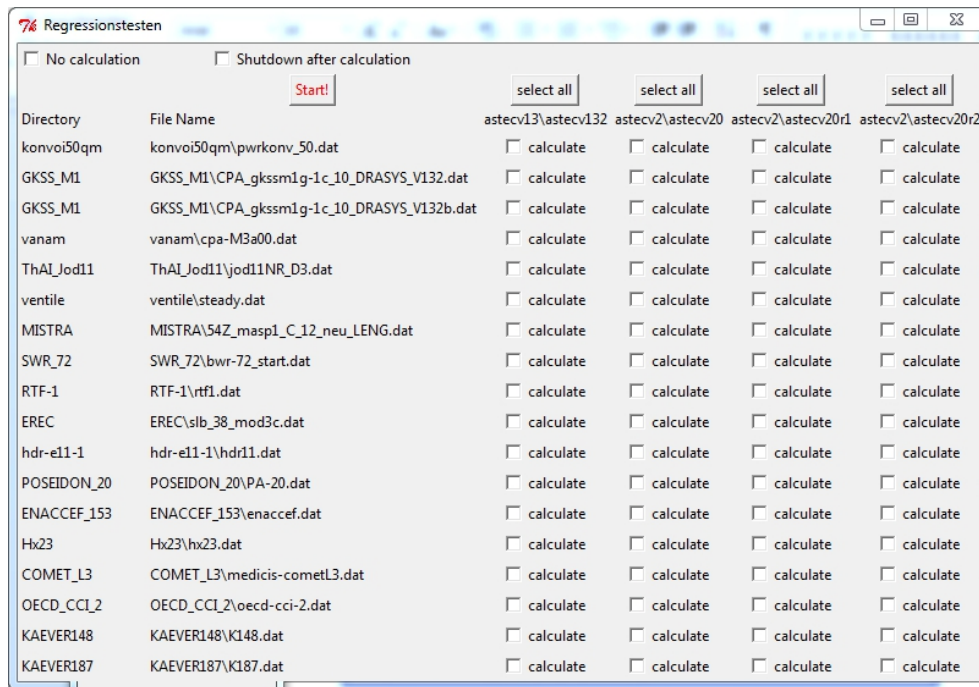


Figure 2.2-2 Graphical user interface of the regression testing

```

1  astecversions = []
2  inputs = []
3
4  astecversions.append("astecv13\astecv132")
5  astecversions.append("astecv2\astecv20")
6  astecversions.append("astecv2\astecv20r1")
7  astecversions.append("astecv2\astecv20r2")
8  # astecversions.append("astecv20dev\astecv1")
9
10 inputs.append(("konvoi50qm\pwrkonv_50.dat", "konvoi50qm\RESTART_0.dat"))
11 inputs.append("GKSS_M1\CPA_gkssm1g-1c_10_DRASYS_V132.dat")
12 inputs.append("GKSS_M1\CPA_gkssm1g-1c_10_DRASYS_V132b.dat")
13 inputs.append("vanam\cpa-M3a00.dat")
14 # inputs.append("sliptest\slip.dat")
15 # inputs.append("sliptest\noslip.dat")
16 inputs.append("ThAI_Jod11\jod11NR_D3.dat")
17 inputs.append("ventile\steady.dat")
18 inputs.append("MISTRA\54Z_masp1_C_12_neu LENG.dat")
19 inputs.append("SWR_72\bwr-72_start.dat")
20 inputs.append("RTF-1\rtf1.dat")
21 inputs.append("EREC\slb_38_mod3c.dat")
22 inputs.append("hdr-e11-1\hdr11.dat")
23 inputs.append("POSEIDON_20\PA-20.dat")
24 inputs.append("ENACCEF_153\enaccef.dat")
25 inputs.append("Hx23\hx23.dat")
26 inputs.append("COMET_L3\medicis-cometL3.dat")
27 inputs.append("OECD_CCI_2\oecd-cci-2.dat")
28 inputs.append("KAEVER148\K148.dat")
29 inputs.append("KAEVER187\K187.dat")
30
length: 1161 lines: 30 Ln: 1 Col: 1 Sel: 0 Dos\Windows ANSI INS

```

Figure 2.2-3 Definition of ASTEC versions and input files - definition.py

### 3 Development of ASTEC V2.0r2 versus V2.0r1

The changes on the code basis between the different ASTEC versions of the V2.0 branch are explained in /CHA 11/. In the following the changes between V2.0r1 and V2.0r2 that are relevant for the CPA, IODE, and MEDICIS modules investigated in this report are summarized.

Within CPA-THY, the flame FRONT model has been substantially improved. The flame front velocity is now calculated by the FEBE solver. So the time step is no longer directly used in the flame front model input. Some changes have been introduced that are useful for plant calculations. Now, it is possible that ignitions start at any time in different zones provided that an ignitable composition exists. Re-ignition of already burnt zones is also possible, if the ignition limit is fulfilled after a first deflagration phase again. Rupture discs, doors, and pipes serve as possible flame front propagation paths. Further, the flame front propagation depends on the hydrogen concentration in adjacent zones depending on horizontal, upward, or downward direction.

In addition to the FRONT model, some changes have been made in order to calculate pressure head losses in junctions caused by filter devices and some modifications have been performed for FAN systems.

In the AFP part a model for dry aerosol resuspension has been included in CPA.

The IODE module is strongly linked to CPA as it calculates iodine behaviour in the containment. Considerable development has been performed on IODE between the two versions compared. The storage of adsorption/desorption coefficients were missing in the database. This has been corrected in the current version. Important for the user is that the reaction names in IODE have changed, in order to give an understandable system of reaction names that is more users friendly. From a modelling point of view also relevant improvements were conducted. These changes have been done on the simulation of the I-/Ag reaction in the liquid phase, the formation of volatile I<sub>2</sub> under irradiation, and the reaction kinetics of disproportionation of HIO. For plant calculations, the Ruthenium chemistry is by default included in the code.

Also molten corium concrete interaction is covered by this regression testing procedure. Between the two versions compared, MEDICIS model improvements have been performed that allow the successive modelling of MCCI in two different cavity chambers. In particular, improvements have been made on the distribution of corium during the pouring phase from a higher cavity region into a lower cavity.

This overview shows that the largest differences between the compared versions are expected on experiments that deal with the FRONT module and the IODE module. For details on the modelling progression the original document /CHA 11/ is available.

## 4 Regression tests

Following main phenomena are covered by the regression tests (corresponding to the structure of the next sections in this chapter):

- thermal hydraulics,
- aerosol behaviour,
- iodine behaviour,
- molten core concrete interactions (MCCI)

as well as technical systems used in different types of NPP as:

- pressure suppression systems (PSS) including bubble condenser,
- spray systems and
- passive systems.

Additionally, one of some typical NPP test cases is included to check the ability of ASTEC to allow for typical plant conditions.

Basis for the following test cases are validation calculations and applications to real plants performed by different ASTEC users. In close cooperation with the specialists for the different main phenomena representative tests and parameters of main interest were selected. Detailed results for each test facility, test conditions, experimental and calculation results can be found in the original validation reports referenced.

### 4.1 Spray systems

The modelling capabilities for spray systems are checked on the basis of HDR E11.1 and MISTRA MASP1 experiments.

#### 4.1.1 HDR E11.1

##### 4.1.1.1 Test facility

The HDR (Heißdampfreaktor – German for hot steam reactor) facility is the containment of a decommissioned hot steam reactor. With a height of 60 m it has the same dimension in height as operating PWR containments. Its diameter is 20 m and its total volume amounts to 11 300 m<sup>3</sup>.

The HDR-E11 experiments had the primary goal to provide an experimental database for the verification of severe accidents computer codes. The main objectives were:

1. Steam-air-hydrogen distribution
2. Global convection behaviour

3. Local heat transfer
4. Energy distribution
5. Internal and external spray system behaviour
6. Thermodynamic annulus behaviour
7. Filtered venting

A sketch of the HDR containment is given in Figure 4.1-1. It shows two different break locations that can be used for steam injection from an installed pressure vessel that simulates a blow down (BD) and by external steam injection from a nearby coal power plant (EX). During the E11.1 experiment the complete injection is directed to the upper release point.

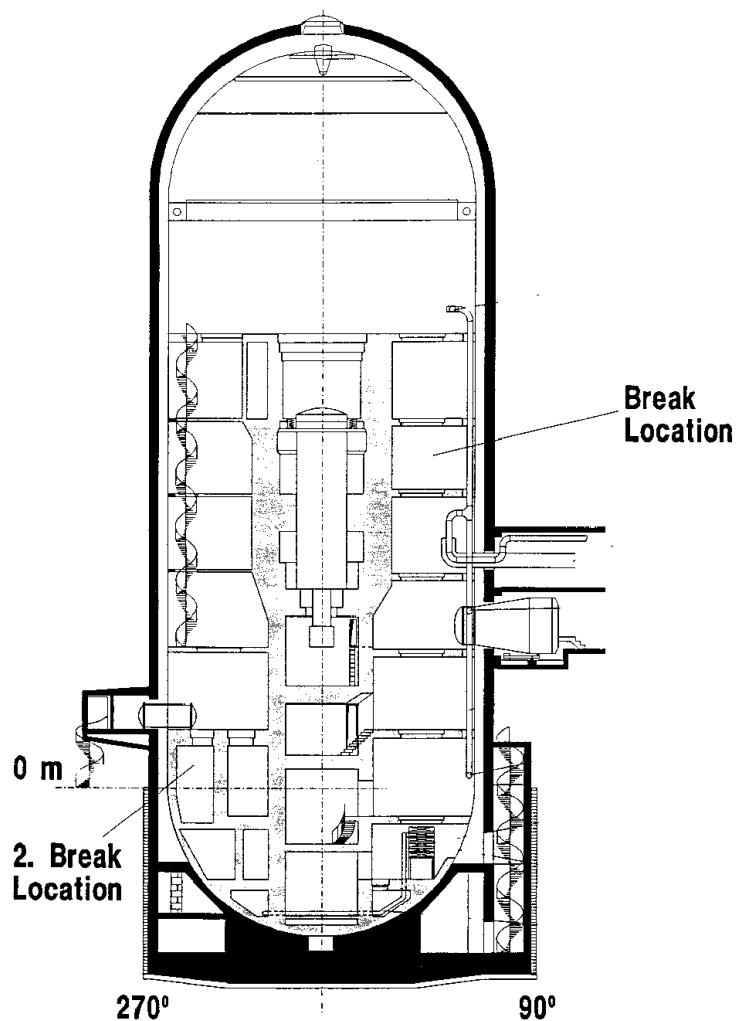
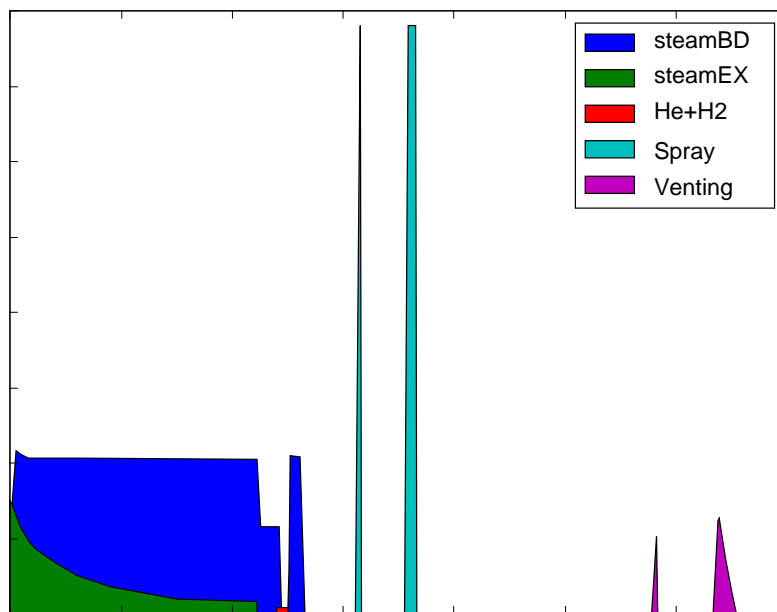


Figure 4.1-1 HDR containment

#### 4.1.1.2 Experiment E11.1

The experiment HDR E11.1 was performed in order to simulate a break location in a middle or high position inside the containment that would lead to significant light gas

stratification. In the experiment a helium-hydrogen mixture is used in order to prevent burnable gas configurations. The mixture consists of 40 vol% H<sub>2</sub> and 60 vol% He that leads to a molar weight of 3.2 g/mole. A spray system inside the containment is operated during the experiment that makes it valuable for the validation of spray system models. The course of the experiment is shown in Figure 4.1-2. It shows the injection rates of steam coming from the blow down vessel (BD) and the external steam supply (EX) in the beginning of the experiment. The injection of light gas (He+H<sub>2</sub>) at about 12 h lasts 0.5 h. Due to the low molecular mass the mass flow rate is very low compared to the steam injection. The spray system is operated during two different periods. The rates in the figure are calculated values from water mass inside the spray water tanks from the CPA results. The venting mass flow rates at the end of the calculation are also results of CPA.



**Figure 4.1-2 Injection, spray, and venting mass flow rates**

#### 4.1.1.3 Nodalisation

The used CPA nodalisation is illustrated in Figure 4.1-3. It is based on a COCOSYS dataset used for validation purposes and described in /HÜT 02, ALL 07/. It consists of 171 zones that model all inner containment zones as well as the annulus of the HDR. The reactor zones are modelled by 90 zones and the dome part by 40 zones. The annulus consists of 25 zones. The details of the ASTEC CPA dataset are described in /BAC 08/.

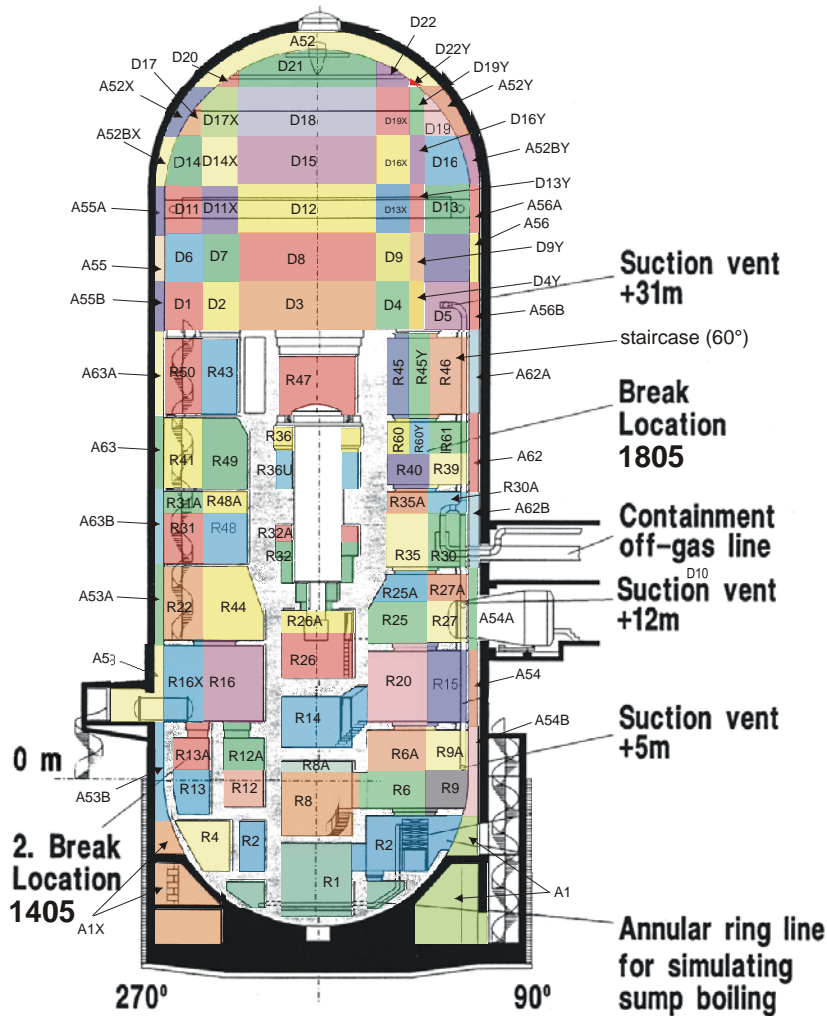
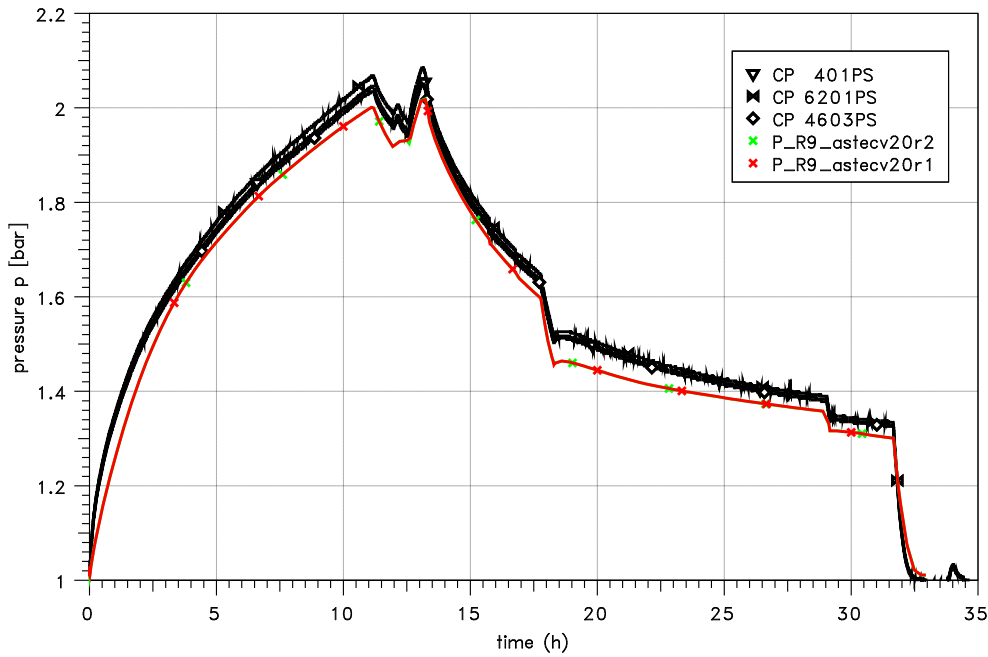


Figure 4.1-3 HDR Nodalisation

#### 4.1.1.4 Results

In the following a comparison between the ASTEC version V2.0r2 and the older version V2.0r1 is presented. In the new version it is no longer possible to calculate with a compound HEH2 that describes the used mixture of the light gases helium and hydrogen. Therefore, the new calculation was changed in so far that hydrogen and helium are calculated as separate compounds, while the old calculation still uses the artificial compound HEH2. Figure 4.1-4 shows a comparison of the pressure inside the HDR during the E11.1 experiment measured and calculated by CPA. Until ~ 14 h the pressure increases due to the injection of steam and the short period of light gas injection. The pause of steam injection can be observed by a short decrease of the total pressure at about 12 h. After finishing the injection the pressure decreases because of condensation. The second phase of the experiment starts with the initiation of the spray system at 17.5 h and is visible by a short and strong pressure decrease. The CPA result shows a slightly lower pressure compared to the experiment. The difference is always smaller than 0.1 bar.

HDR E1 1.1 Experiment



**Figure 4.1-4 HDR E11.1, Total pressure**

The following graphics show the temperatures during the experiment on a lower level of the containment, on the height of the injection, and in the dome area of the HDR facility. The temperatures in the lower part of the containment are displayed in Figure 4.1-5. No great influence is visible in this region of the containment due to the injection of steam in the upper release point. The results of the simulation are in good accordance with the experiment. The temperatures in the height of the injection position are displayed in Figure 4.1-6. The temperatures rise up to 130 °C in these compartments. Also for these zones the accordance between the CPA results and the experiment are very good. Figure 4.1-7 shows the temperatures inside the dome region. The temperatures increase up to 120 °C and are also post-calculated very well by CPA.

HDR E1 1.1 Experiment

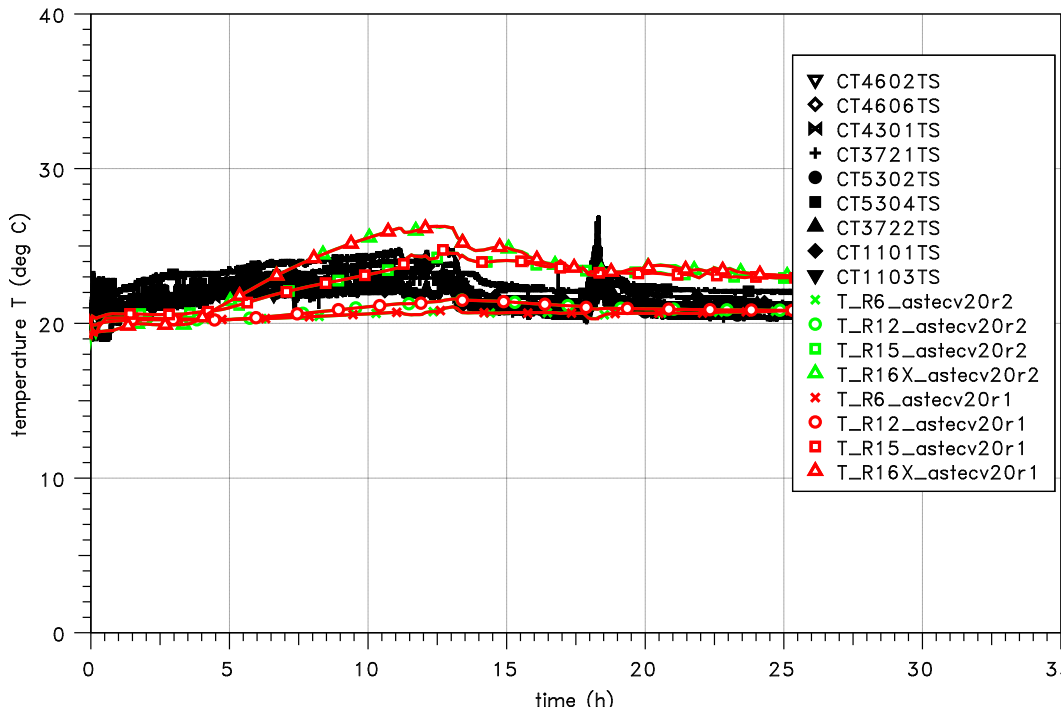


Figure 4.1-5 HDR E11.1, Temperatures in lower part of containment

HDR E1 1.1 Experiment

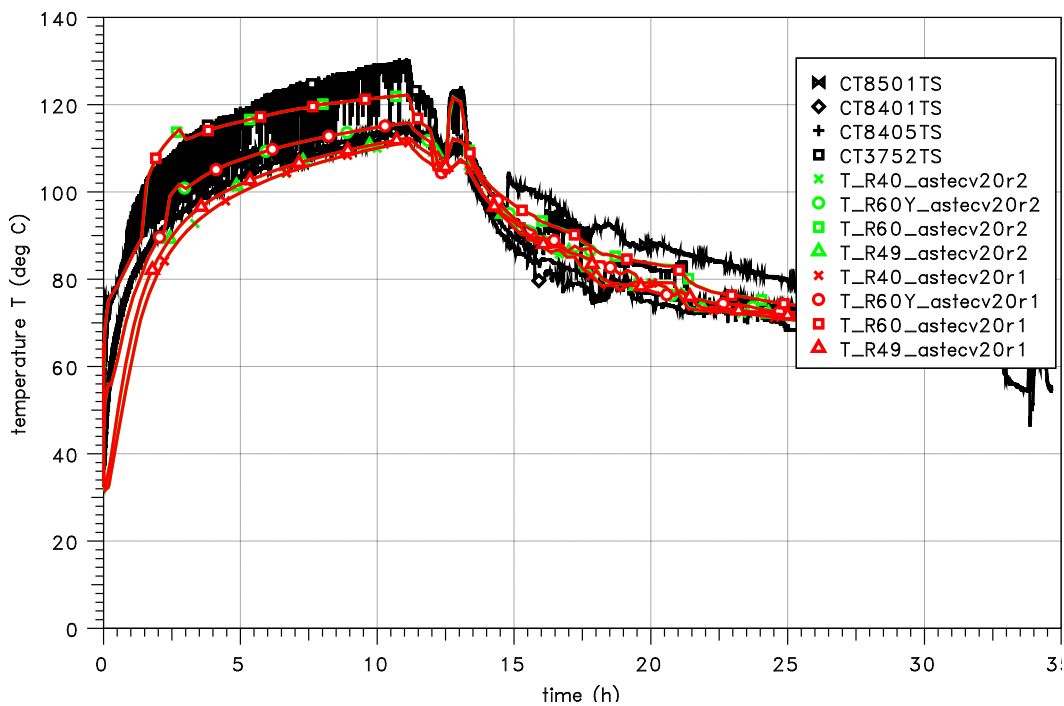
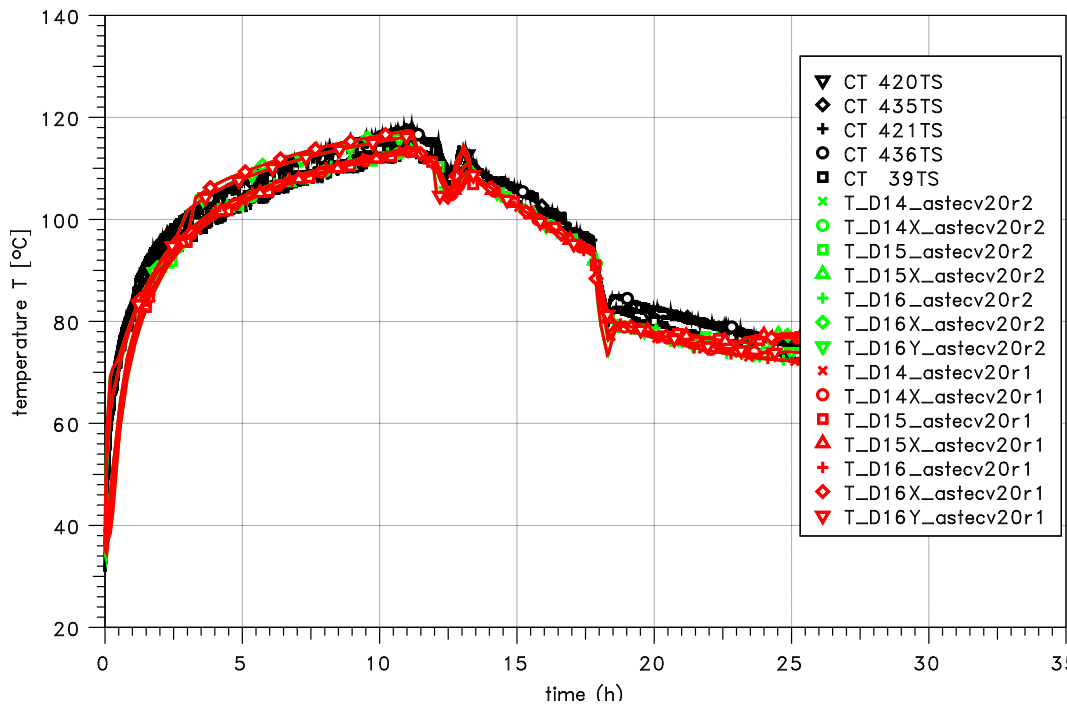


Figure 4.1-6 HDR E11.1, Temperatures on injection height

HDR E11.1 Experiment



**Figure 4.1-7 HDR E11.1, Temperatures in dome**

The light gas concentrations during the experiment are also given for a lower position, the injection height, and the dome area of the HDR containment. Due to the different modelling with a compound HEH2 in the old version and separate components for HE and H<sub>2</sub> in the new version the graphics show HEH2 or the sum of the helium and hydrogen concentrations. Figure 4.1-8 shows the concentration of the light gas mixture H<sub>2</sub>+He in the lower part of the containment. Only a small increase of the concentration occurs in this region up to 30 h. The measurement shows concentrations of only 1 vol%, while the CPA results are up to 3 vol% after 30 h.

The concentrations of the light gas mixture at the height of the injection zone are presented in Figure 4.1-9. Directly after injection the values increase up to more than 15 vol%. The exact behaviour during this time depends on the exact position of the measurement, while the CPA results only show a mean value for a complete zone. Up to the operation of the spray system at about 17.5 h the concentration in this region decreases due to the mixing in the containment. The measured values decrease to 2.5 vol% and the CPA results to 6 vol%. Directly after the onset of spraying the calculated concentration increases up to 15 vol% because of the condensation process started by the spray system. This effect cannot be seen in the measured curve. It is in accordance with the stronger pressure decrease of the CPA results in comparison to the measurement during the spray phase in Figure 4.1-4. The measurement shows only a slight increase of the concentration up to 7 vol% at the time of venting at 32 h. This can also be explained by the normal condensation process inside HDR and up streaming flow from the lower compartments with lower light gas concentration.

The light gas concentration in the dome region is shown in Figure 4.1-10. Directly after the start of the injection at 12 h the concentration increases to 15 vol%. Due to mixing processes the concentration decreases below 10 vol% depending on the exact position. Up to the onset of the spray system at 17.5 h the concentration increases up to 15 vol% due to the steam condensation processes in the dome area. After spraying the

calculated concentration falls below the measured curve, while the measurement shows constant values.

The different modelling of the light gas mixture between both ASTEC versions has no significant influence on the calculated concentrations of the light gas.

HDR E1 1.1 Experiment

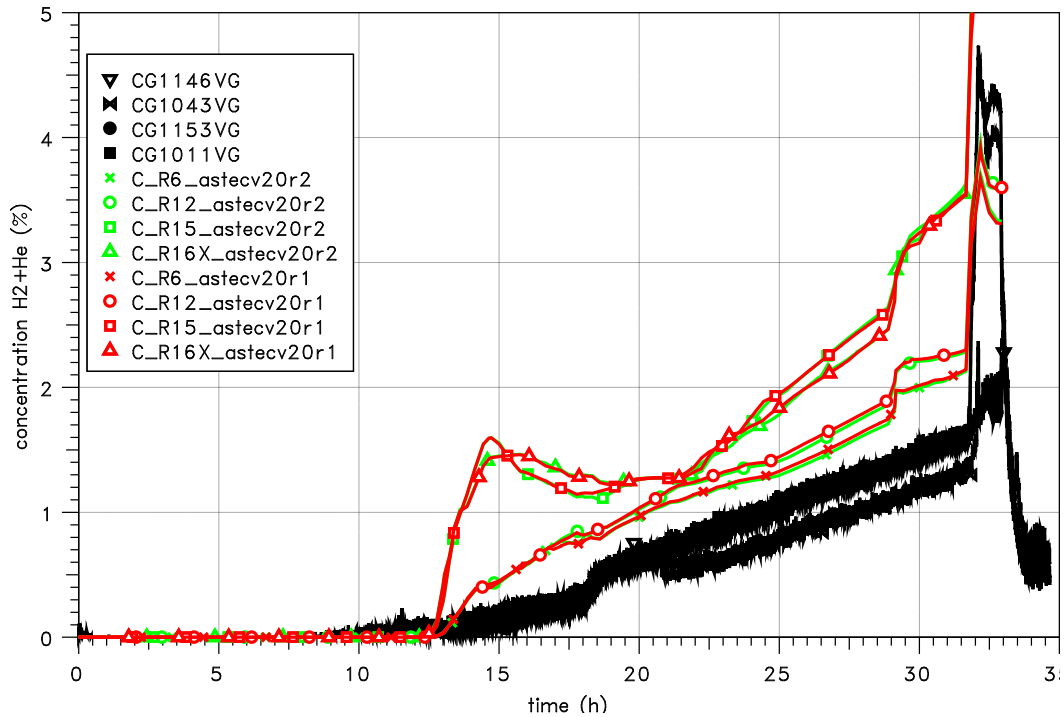


**Figure 4.1-8 HDR E11.1, Light gas concentration in lower part of containment**

HDR E1 1.1 Experiment

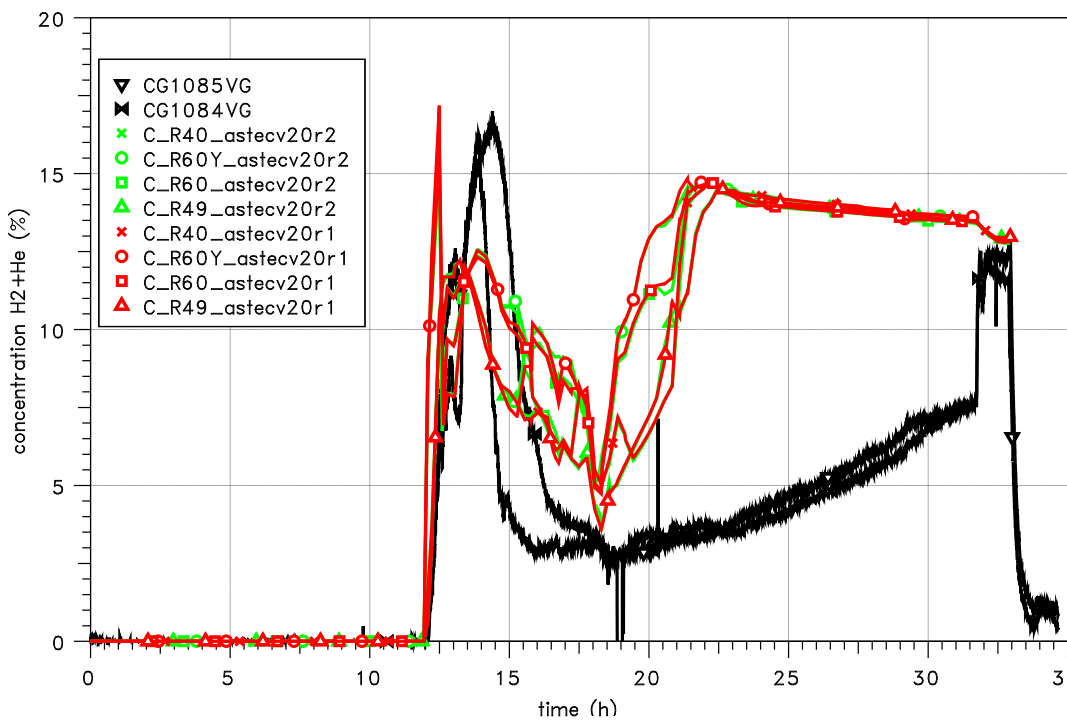


**Figure 4.1-9 HDR E11.1, Light gas concentration on injection height**

HDR E11.1 Experiment

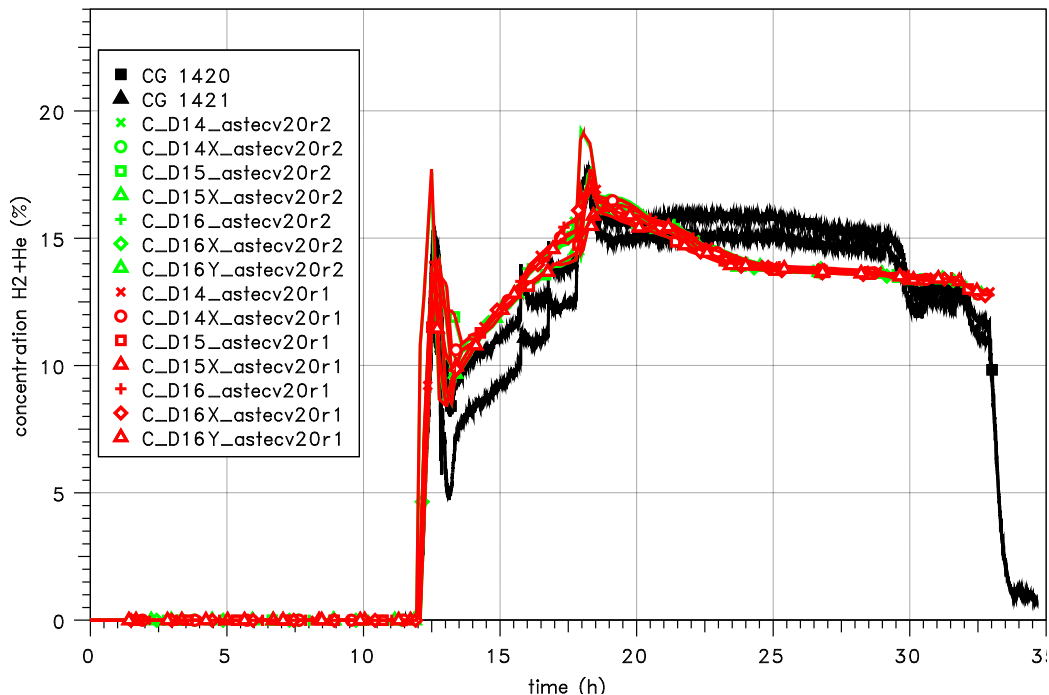


Figure 4.1-10 HDR E11.1, Light gas concentration in dome

#### 4.1.1.5 Summary

The post-calculation of the E11.1 experiment shows very good results concerning the thermo-hydraulic results for pressure and temperature. Concerning the concentrations of the light gas mixture depending on the position of the measurement strong differences between the measurement and CPA occur. But the general distribution of the light gas is well post-calculated by CPA. Condensation effects during the operation of the spray system are overestimated by CPA. This leads to a stronger decrease of the pressure inside the HDR facility and to a local overestimation of light gas concentration in the regions where the spray system is active.

The new ASTEC version V2.0r2 gives nearly the same results as the previous version V2.0r1. No unexpected deviations were found between the results of both code versions.

#### 4.1.2 MISTRA MASP1

The MISTRA test facility is located in Saclay (France) and operated by CEA. It is a coupled effect test facility, objective of which is to support modelling and validation of computer codes.

#### 4.1.2.1 Test facility

The MISTRA facility and its operating conditions are designed with reference to the conditions of a PWR containment in accidental situation. It comprises a vessel, inside which three condensers are set up, and external circuits (Figure 4.1-11). The linear length scale ratio of the test facility to a PWR containment is 1:10.

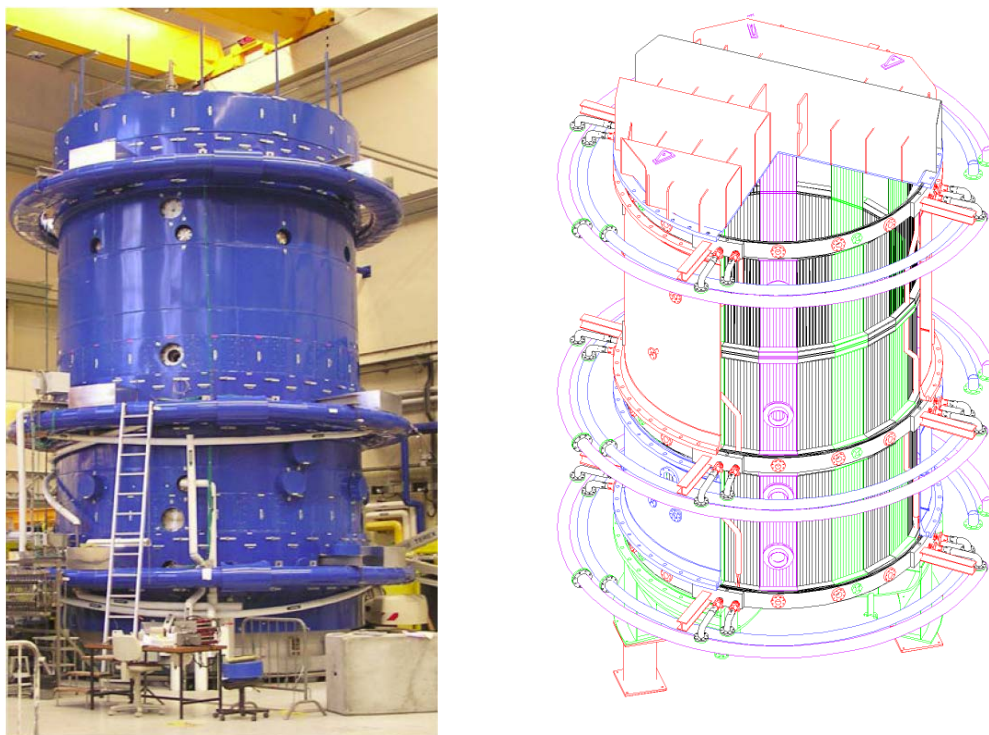


**Figure 4.1-11 MISTRA test facility, general and schematic views showing external circuits of three annular condensers**

The MISTRA facility is a cylindrical vessel of 99.5 m<sup>3</sup>, 4.25 m internal diameter and 7.38 m height /ABD 06, MAL 06/. It is constituted of two shells, a flat cap and a curved bottom, fixed together with twin flanges.

The facility is made of stainless steel with a wall thickness of 15 mm for the cylindrical wall, 25 mm for the bottom, 110 mm for the flanges and 119 mm for the ceiling. This ceiling thickness value is an equivalent thickness due to the presence of many stiffeners. The internal stainless steel surfaces amounts to about 118 m<sup>2</sup>. The total mass of stainless steel is about 40 t. The vessel has an external thermal insulation of 20 cm rock wool. The vessel is not temperature regulated, but can be preheated by steam, so that after a preheating phase the wall temperatures are similar to the inner atmosphere temperatures.

Three cylinders (called condensers) are inserted inside the vessel close to the vessel wall, providing a free gas volume with 3.8 m diameter. The condensers are not perfect cylinders but polygons with 24 faces (yellow drawn in Figure 4.1-12). The vertical space between two condensers is 0.12 m. However the space is partially hid with gutters. The total condensing area is 69 m<sup>2</sup> divided into 26.2 m<sup>2</sup> (lower condenser) and 21.4 m<sup>2</sup> for the middle and upper condenser each. A so-called 'dead volume' behind these condensers exists and some steam condensation can occur on the vessel walls. Each condenser has its own regulation circuit designed to provide circulating heated or

cooled water and, thus, ensuring a most stable and uniform condenser temperature. The outer sides of the condensers are insulated with synthetic foam of 20 mm thickness. Special gutters are installed to collect and quantify the condensate from the condensers. Steam condensation is also quantified by water collecting at different locations: along the cylindrical wall of the vessel, along the external part of the condensers and on the bottom.

A single spray nozzle is installed near the centre of the vessel roof. To avoid interaction of droplets with the condensers the spray is generated by a full jet nozzle with an angle of 30° (see Figure 4.1-12). The average spray droplet size generated is about 1 mm with an initial velocity of 25 m/s.

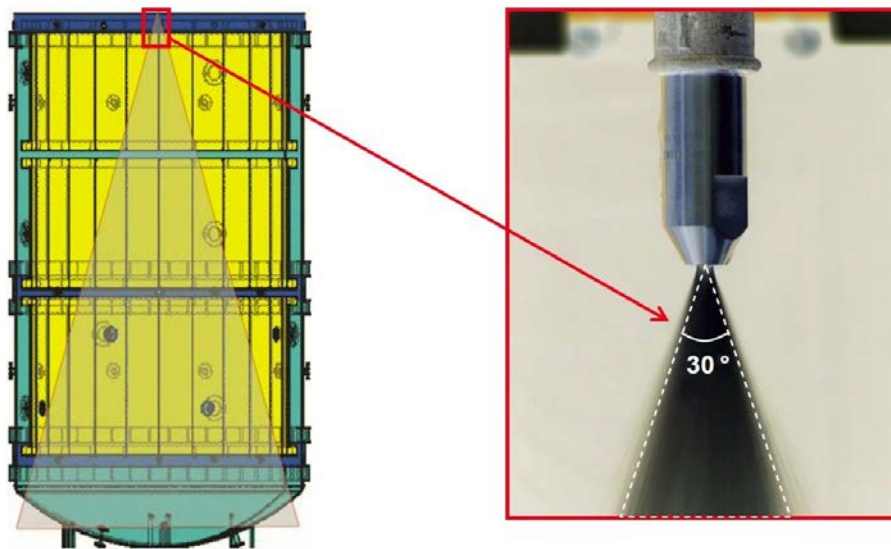


**Figure 4.1-12 MISTRA test facility, vertical cut including 3 condensers (yellow) and spray jet (grey) indications and spray nozzle detail**

A diffusion cone (injection nozzle) fitted with a removable cap is set up on the bottom of the vessel, on the central axis. It is designed for gas injection and steam/helium mixing (inside diffusion cone prior to injection into the vessel).

The measurements performed during the tests are related to total pressure, temperature (gas, liquid and wall), gas composition, velocity, and condensed mass flow rate. Sensors are located on the walls and in the gaseous volume.

The instrumentation mesh is located on four vertical half-planes: 105° (P1), 165° (P3), 225° (P2) and 345° (P0) in the main gas volume, but also in the 'dead volume' (Figure 4.1-13). The instrumental mesh grid on the half plane at 345° combines 10 vertical levels (N0 to N10) and 5 radial positions (R0 to R5). The instrumentation of the reference half-plane P0 is given in Figure 4.1-14. More information on the measurement can be found in /KLE 09a/.

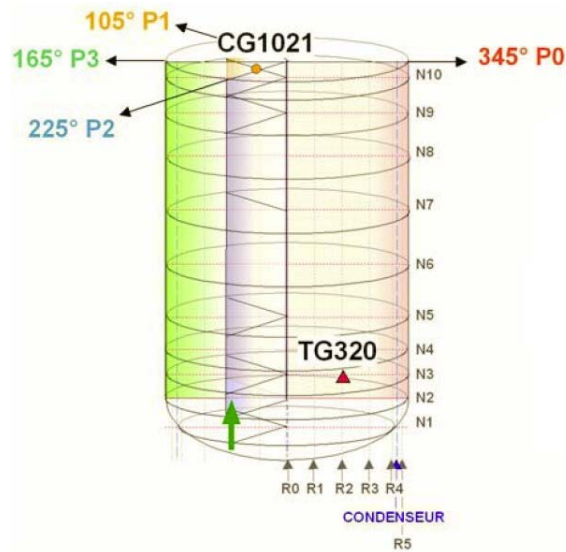


Figure 4.1-13 MISTRA test facility, instrumentation mesh

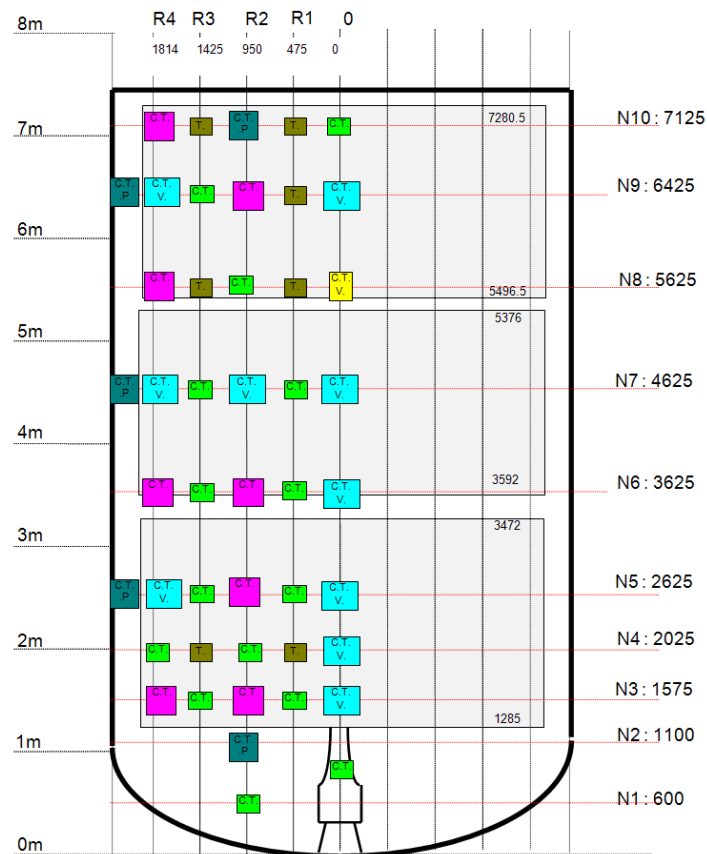


Figure 4.1-14 MISTRA test facility, instrumentation of reference half-plane P0 (used in MASPn experiments)

#### 4.1.2.2 MASPn spray experiments

The main intention of the spray tests series MASP0 to MASP2 was the modelling of the depressurization of the vessel atmosphere by a spray system. The tests provide data

for the validation of computer codes related to the droplet heat and mass transfer modelling and the gas thermodynamic modelling.

The tests were performed by CEA in summer 2004. Each of the 3 MASP tests started during the steady-state of an air-steam test called M5. The M5 tests consist of injection of superheated steam at 200 °C into the MISTRA vessel initially at room temperature and full of air (total pressure of 1 bar). The two top condensers are kept at a temperature of 140 °C and the bottom condenser at 80 °C. The pressure behaviour during an M5 test followed by the MASP1 is shown in Figure 4.1-15.

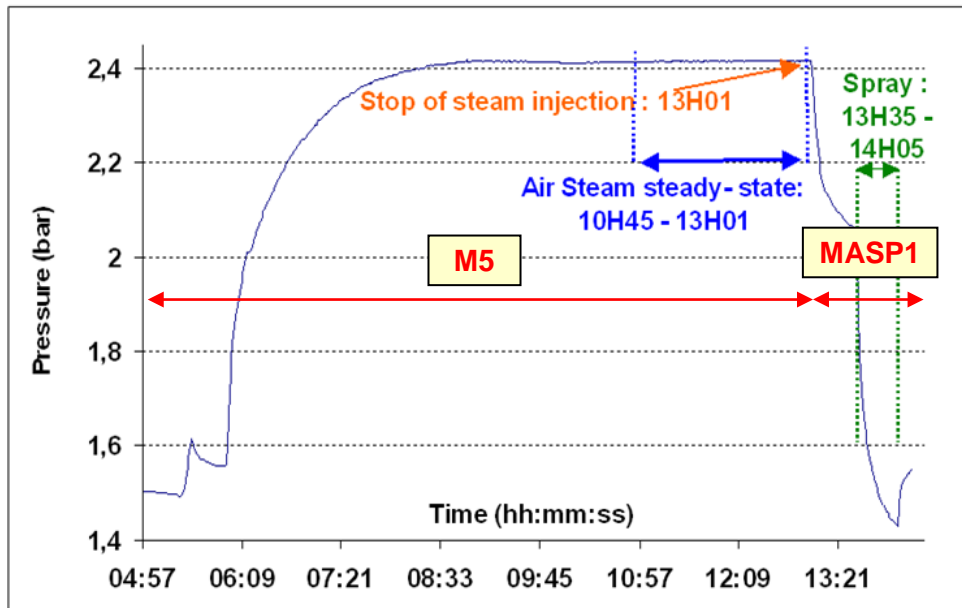


**Figure 4.1-15 MISTRA, M5 - MASP1 test sequence**

The MASP1 test started at the end of a M5 test with the average conditions given in Tab. 4.1-1. During the test the condensers are kept at the same temperature as in the foregoing M5 test (80 °C and 140 °C).

**Tab. 4.1-1 MISTRA, MASP1, initial test conditions**

| Condition                                             | MASP1 |
|-------------------------------------------------------|-------|
| Pressure (bar)                                        | 2.4   |
| Mean gas temperature (°C)                             | 124   |
| Steam volume fraction (deduced from mass balance) (-) | 0.45  |

The MASP1 test is composed of two phases:

1. depressurization by heat losses (0 – 1993 s),
2. spray activation during ~1800 s (1993 – 3780 s).

The spray characteristics are:

- droplets mass flow rate of 0.87 kg/s with a velocity of the mixture at the nozzle outlet of 25 m/s and a droplet diameter of 1 mm and
- 40 °C of the injected water.

More information on the test performance and the experimental data is given in /MAL 06, ABD 06/.

COCOSYS blind and open post-test calculations were performed by GRS in frame of the European SARNET project /KLE 09a/.

#### 4.1.2.3 CPA input deck

This test case is calculated with ASTEC CPA as well as with COCOSYS. The geometrical modelling used with both codes is the same, but the spray models available in CPA and COCOSYS are different. The nodalisation of the MISTRA vessel consists of 54 zones as presented in Figure 4.1-16. Four additional zones simulate the spray water tank, the two hot and the cold condenser (140 °C und 80 °C) and the environment. The nodalisation was selected such a way to represent the measurement gauges also (gauges on green marked radii R0 to R5 and on red marked levels N1 to N10).

The vessel is simulated by 4 radial rings at 14 axial layers. The zone names indicate the ring (names starting with R0 to R5) plus the layer (letter Z plus elevation of zone center). The inner two radii model the central vessel volume affected by the spray jet. The third radius simulates the space adjacent to the condensers and the outer radius simulates the space between vessel wall and condensers (so-called 'dead volume'). Below the lower cold condenser only 3 radial zones are modelled.

The nodes are connected by atmospheric junctions to simulate the atmospheric flows between the nodes by forced or free convection. Flow areas correspond to the geometry, i.e. virtual boundaries between nodes. The MISTRA vessel is assumed to be leak tight. Drain junctions are implemented to simulate flow processes of water, e.g. the drainage of water condensed on the lower cold condenser or from volume condensation in the nodes. Condensate is drained downward into the next zone. At the lower ends of the three condensers the water is drained out of the MISTRA vessel into the ENVIRON zone.

Heat transfer and heat conduction processes are considered by heat slabs. Structures are simulated in the CPA input deck for the three condensers, the ceiling, the vertical outer wall inclusive the flanges, the bottom and the insulated back sides of the condensers. The allocation of the structures to the nodes is illustrated in Figure 4.1-17. The surface areas and wall thicknesses are used as given in /MAL 06/. The heat losses to the environment are simulated with the CPA standard options, i.e. a combination of free and forced convection, condensation and wall-gas-radiation.

The spraying is modelled by a pump system injecting the water into the top central node R0Z713. Two parallel spray paths were defined, first one through the central part (R0\* nodes, see Figure 4.1-16) and second one simulating roughly the spray jet spreading through R2Z314 to R2Z060. According to the spray jet angel of 30° no direct droplets impingement to the condenser surface or the vessel side wall occurs. Other spray data as operation period, water droplet inlet temperature and droplet size were defined for the CSS model in ASTEC according to the specification /MAL 06/. In contrast to CPA, the COCOSYS calculation uses the IVO /IVO 93/ model. Since the spray model does not directly influence atmospheric flows (atmosphere entrainment due to spray jet) 13 FAN systems were implemented. They transport atmosphere from zone to zone according to the defined spray paths and simultaneous with the spray system operation.

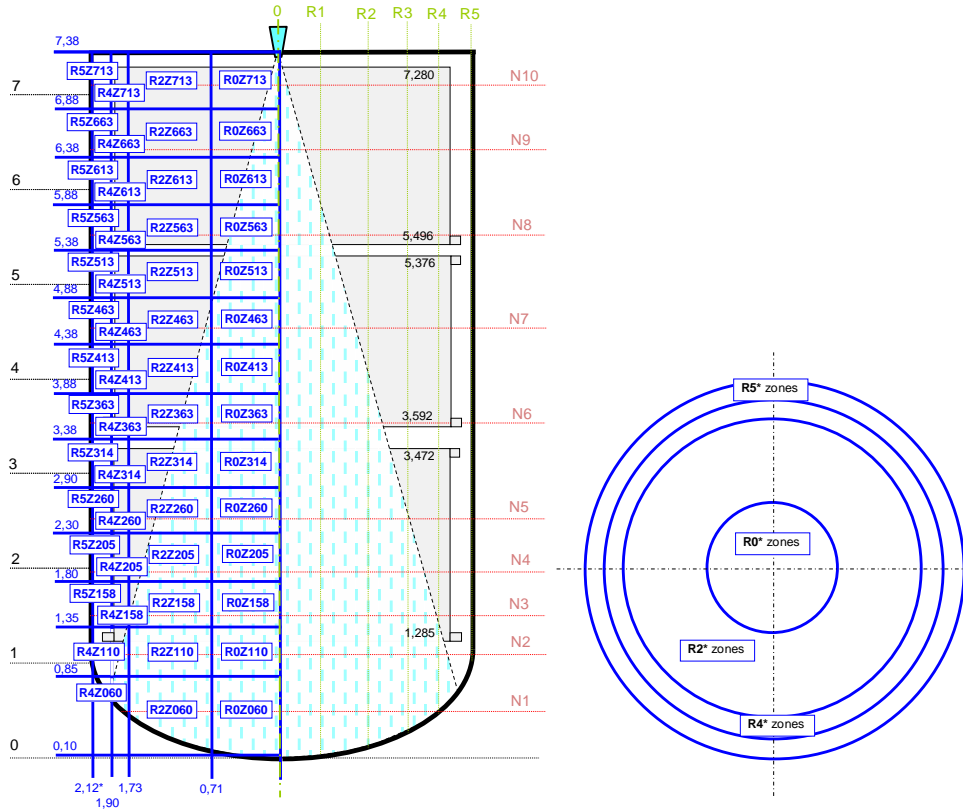


Figure 4.1-16 MISTRA, MASP1, 58 zone model including with zone names

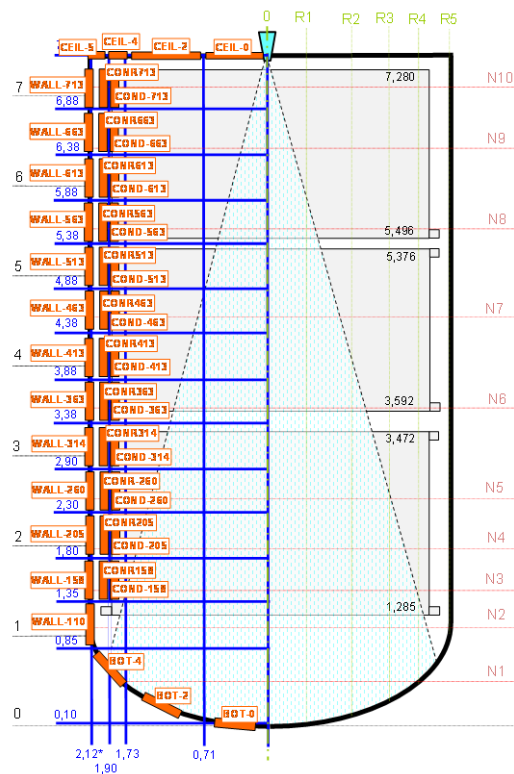


Figure 4.1-17 MISTRA, MASP1, 58 zone model, heat conducting structures

The initial conditions were not specified, but calculated (and adjusted according to experimental results) by CPA simulating the M5 phase. To reach a stratified atmosphere

the steam injection, the plume and the atmosphere entrainment were simulated according to suggestions given in /SCZ 04/: 11 FAN systems with upward directed, increasing volume flow rates according the Liepe formula.

More detailed information on the CPA input deck can be found in /KLE 09a/.

#### 4.1.2.4 Results

The outcome of the spray benchmark in the frame of the SARNET project inclusive the assessment of the delivered ASTEC and COCOSYS results can be found in /BLU 08/. Experimental data are available for the MASP1 and MASP2 tests with spray operation, whereas for the base test MASP0 only the measured pressure curve was delivered. Thus, detailed verification was done for the MASP1 test with spray mainly /KLE 09a/.

In the following figures for some key parameters a comparison between the experimental results (black dashed lines, marked with "exp"), the current COCOSYS version V2.3v9 (coloured solid lines, marked with "COC"), the previous ASTEC-CPA version V2.0r1 (red line), and the actual ASTEC version V2.0r2 is given.

The foregoing M5 steady-state phase is simulated in a simplified way by the injection of steam from -20 000 s to 0 s. That way, consistent initial conditions exist at the beginning of the MASP1 test. The MASP1 phase starts at 0 s. Thus, the shown time -2 000 s to 0 s is related to the M5 phase. More details on that are given in /KLE 09a/.

Figure 4.1-18 shows the comparison of measured and calculated pressure histories. The experimental pressure curve is well reproduced - in the M5 as well as during MASP1 phases. The difference between calculation and measurement is less than ~0.05 bar. Due to the empty MISTRA vessel the pressure is uniform in all zones. The COCOSYS calculation gives nearly the same pressure during the M5 steady-state phase as the two CPA calculations. The deviation during the spray phase is insignificant. Both ASTEC calculations deliver a slightly lower pressure during this phase and show no difference between both versions of CPA. The COCOSYS result is somewhat closer to the experiment than the CPA results for the spray phase, what is vice versa for MASP2 experiment /KLE 09a/.

Atmosphere temperatures for the radius R2 and different elevations (see also nodalisation on Figure 4.1-16) are given in Figure 4.1-19. One can see that during the foregoing M5 phase with the steam injection the temperature stratification is principally reproduced by COCOSYS and both CPA versions. Switching off the steam injection the temperatures drop fast and reach a new steady state after ~500 s. The stratification remains due to the operation of the hot and cold condensers. Starting at 2 000 s the spray cools down the atmosphere. Even during the spraying certain temperature stratification remains. This is principally reproduced, but the stratification is overestimated. Whereas the temperature in the lower zones is matched, the upper zones remain too warm in the COCOSYS calculation. The same behaviour is observed by both ASTEC versions but even more pronounced in comparison to COCOSYS. As mentioned above the spray model does not consider atmosphere entrainment and the applied FAN system volume flow rates were obviously estimated to low. Both CPA results are nearly identical.

SARNET WP12.2, MISTRA M5 + MASP1 spray experiment, 54Z\_masp1\_C\_12

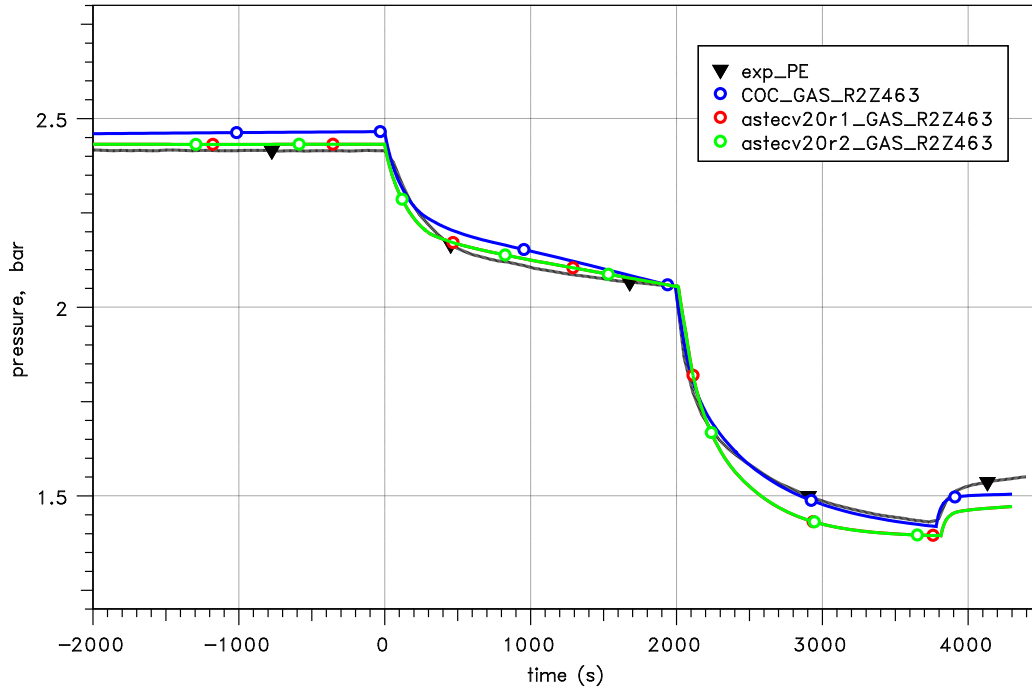


**Figure 4.1-18 MISTRA, MASP1, comparison of measured and calculated pressure**

SARNET WP12.2, MISTRA M5 + MASP1 spray experiment, 54Z\_masp1\_C\_12

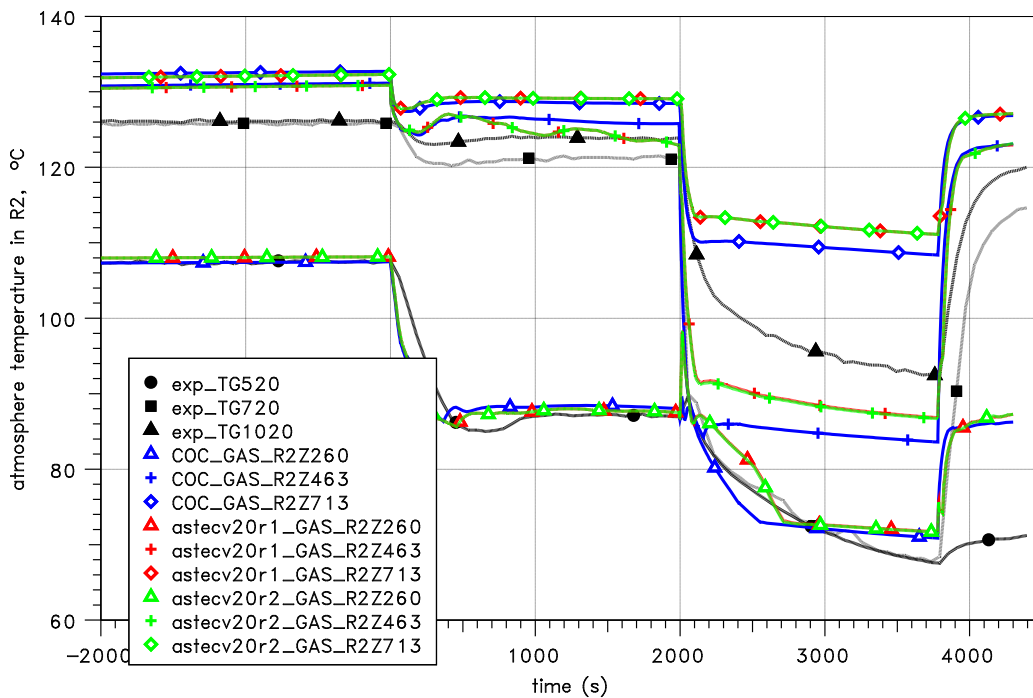


**Figure 4.1-19 MISTRA, MASP1, measured and calculated atmosphere temperatures in radius R2**

The sump water level rise during the experiment was derived from some temperature gauges, i.e. by a strong temperature drop due to coverage of the thermo elements measuring atmosphere to water temperature. The comparison of the COCOSYS result as well as both CPA results with these discrete points is shown in Figure 4.1-20. The

level behaviour is well reproduced by all codes. Only during the first 2 000 s of the MASP test COCOSYS calculates a slightly higher condensation rate compared to ASTEC.

Figure 4.1-21 shows the comparison of the calculated steam condensation at all condensers with the measurement. In fact, there is no condensation at hot upper and middle condensers (temperature of 140 °C is higher than the atmosphere) and condensate arises at the lower condenser only (marked in the figure by "exp\_Qcb"). Already for the M5 phase the initial condensation is calculated too high (78 g/s versus 68 g/s measured) within all three theoretical curves. Consequentially, in the experiment a larger part of the injected steam (in total 80 g/s) condensed at other surfaces. Nevertheless, with begin of the MASP1 phase there is a good coincidence with the measurement. The peak value of the condensation rate during spraying at ~2300 s is calculated well. It is remarked, that without the FANs simulating the atmosphere entrainment by the spray jet this peak is calculated significant smaller. This shows that this effect is of importance.

SARNET WP12.2, MISTRA M5 + MASP1 spray experiment, 54Z\_masp1\_C\_12

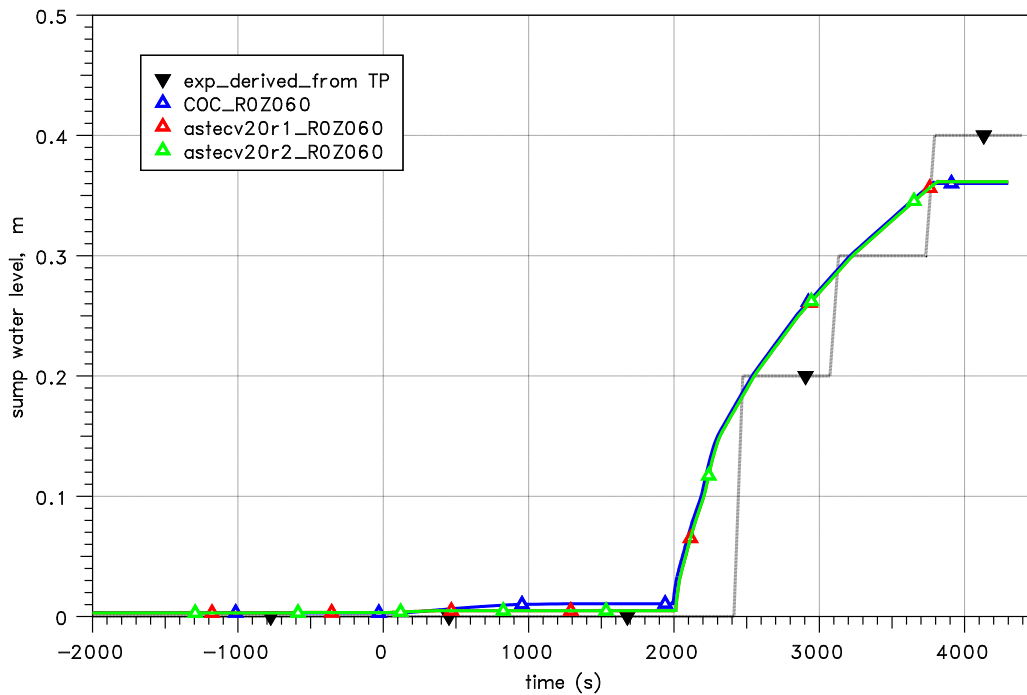
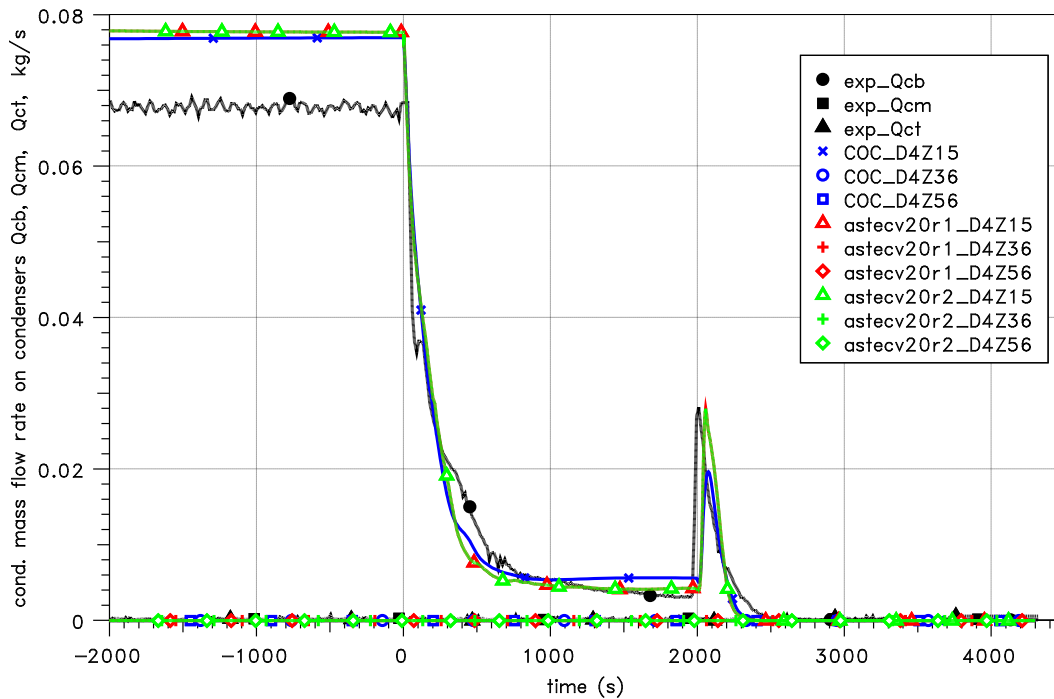


Figure 4.1-20 MISTRA, MASP1, measured and calculated sump water level

SARNET WP12.2, MISTRA M5 + MASP1 spray experiment, 54Z\_masp1\_C\_12



**Figure 4.1-21 MISTRA, MASP1, calculated and measured condensation rate at all condensers**

#### 4.1.2.5 Summary

Summarising, it can be stated, that the initial data of the M5 phase have a large influence on the whole process. The main thermal hydraulic effects of the spray, the strong pressure and atmosphere reductions, are well matched by COCOSYS as well as by ASTEC CPA.

The new ASTEC version V2.0r2 gives nearly the same results as the previous version V2.0r1. No unexpected deviations were found between the results of both code versions.

## 4.2 Aerosol behaviour

In the following the aerosol related models of ASTEC-CPA (i.e. in containment related models) are checked. Since the aerosol behaviour is strongly linked with the thermal hydraulics (e.g. atmospheric flows or condensation) some main thermal hydraulic results are given as well.

## 4.2.1 BMC VANAM-M3

### 4.2.1.1 Test facility

The Battelle Model Containment (BMC) has a free volume of 626 m<sup>3</sup>. It was built rotationally symmetric of reinforced concrete and is subdivided into several compartments. The VANAM test geometry (Figure 4.2-1) represents roughly the containment of a PWR.

The following locations are provided for injections:

- compartment R5 for the injection of steam or aerosol, respectively, suspended in a steam-air mixture,
- compartment R3 for the injection of steam or the re-injection of air, respectively (the latter only during the heat-up phase),
- R9 bottom part of the compartment R9 (annulus) for the removal and re-injection of air during the heat-up phase.

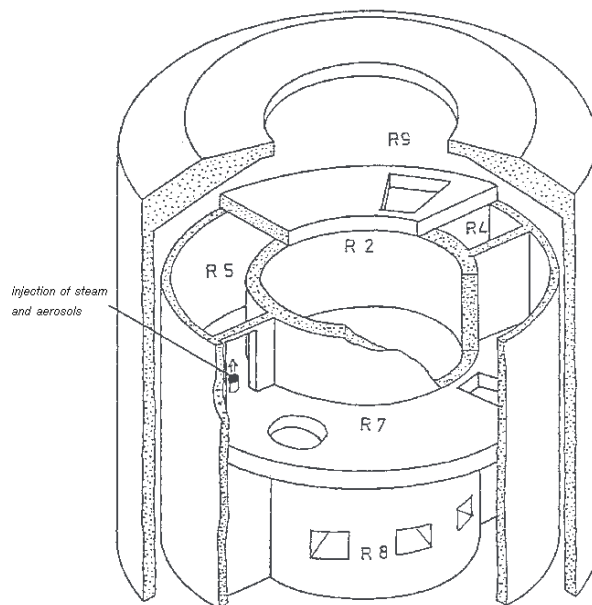


**Figure 4.2-1 BMC VANAM-M3, test geometry**

Most of the injected steam condenses at the containment structures. The condensate flows down into the sumps. Individual sumps can form in R3, R4, R5, R6, R7, R8 and R9.4 (lower part of annulus). During the phase 1 of the experiment sump water was drawn out of R9.4.

The experimental procedure is oriented on the core melt scenario ND\* according to the German Risk Study phase B /GRS 90/. The ND\* is a transient scenario caused by the loss of steam generator feed water supply with late depressurisation of the reactor pressure vessel. The different experimental phases are explained in Table 4.2-1:

**Table 4.2-1 Phases of the VANAM-M3 experiment /KAN 93/**

| Time (h)      | Phase | Explanation                                                                                                                                                                                                                                                                                                                                                                                                                                                                          |
|---------------|-------|--------------------------------------------------------------------------------------------------------------------------------------------------------------------------------------------------------------------------------------------------------------------------------------------------------------------------------------------------------------------------------------------------------------------------------------------------------------------------------------|
| 0.0 - 1.13    | -     | (no action)                                                                                                                                                                                                                                                                                                                                                                                                                                                                          |
| 1.13 - 17.2   | 1     | The test facility is heated up and the initial boundary conditions are adjusted: Steam is injected into R5. The injection rate is controlled to get a constant containment pressure of 1.25 bar. At the beginning of phase 1 there is a controlled air removal out of R9.4. Therefore steam can enter the lower regions of the model containment and heat up the structures. Towards the end of phase 1 air is re-injected into R9.4 and R3 in order to get the desired air content. |
| 17.2 - 18.23  | 2     | NaOH aerosol suspended in a steam-air mixture is injected into R5. The containment pressure is not controlled anymore and rises to 2.05 bar.                                                                                                                                                                                                                                                                                                                                         |
| 18.23 - 22.7  | 3     | All injections are stopped. Since the steam condensation on the outer containment wall is not compensated anymore by injection the pressure decreases to 1.25 bar.                                                                                                                                                                                                                                                                                                                   |
| 22.7 - 23.14  | 4     | NaOH aerosol suspended in a steam-air mixture is injected a second time into R5. The pressure increases.                                                                                                                                                                                                                                                                                                                                                                             |
| 23.14 - 25.26 | 5     | For the first 10 min all injections are stopped. Then steam is injected into the lower central room R3. The pressure increases to about 1.7 bar.                                                                                                                                                                                                                                                                                                                                     |
| 25.26 - 30    | 6     | The steam injection is switched back to R5. The pressure stabilizes around 1.7 bar.                                                                                                                                                                                                                                                                                                                                                                                                  |

#### 4.2.1.2 ASTEC-CPA input deck

For this calculation the simple nodalisation used for the ISP-37 calculation /SCZ 99/ has been taken:

- number of zones: 13
- number of junctions: 23
- number of structures: 49

The applied nodalisation is presented in Figure 4.2-2. The CPA input deck was automatically created from the same COCOSYS input deck using the COC2AST tool /DEI 03/.

The input deck used is not the original dataset provided by the ASTEC release version. In order to gain better comparability to COCOSYS results the characteristic length of most structures was changed from 0.01 m to 1 m.

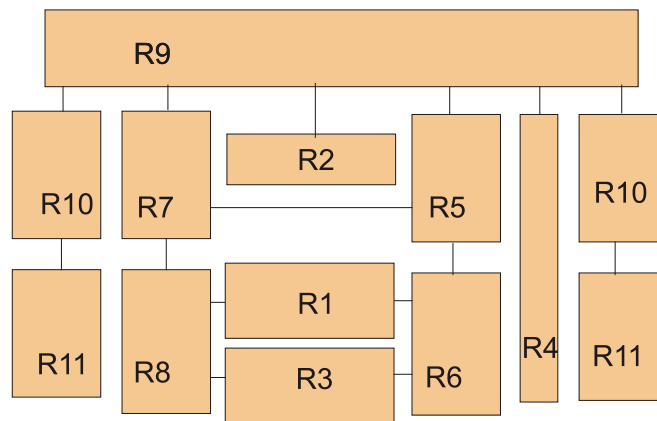


**Figure 4.2-2 BMC VANAM-M3, simple nodalisation**

#### 4.2.1.3 Results

In the following figures the results of ASTEC V2.0r2 (drawn by green lines in the figures) and V2.0r1 (red lines) are compared with the experiment (black lines). The COCOSYS result is given by a blue curve.

Figure 4.2-3 presents the comparison of the total pressure calculated with ASTEC-CPA, COCOSYS and the measurement. The main reason for the too high pressure in the initial phase of the experiment results from the limited knowledge about the leakage in the Battelle Model Containment. Only the air leakage has been estimated and therefore considered in the calculations; whereas the steam leakage is not taken into account. The maximal differences between COCOSYS and CPA are in the range of 0.05 bar.

VANAM M3 EXPERIMENT

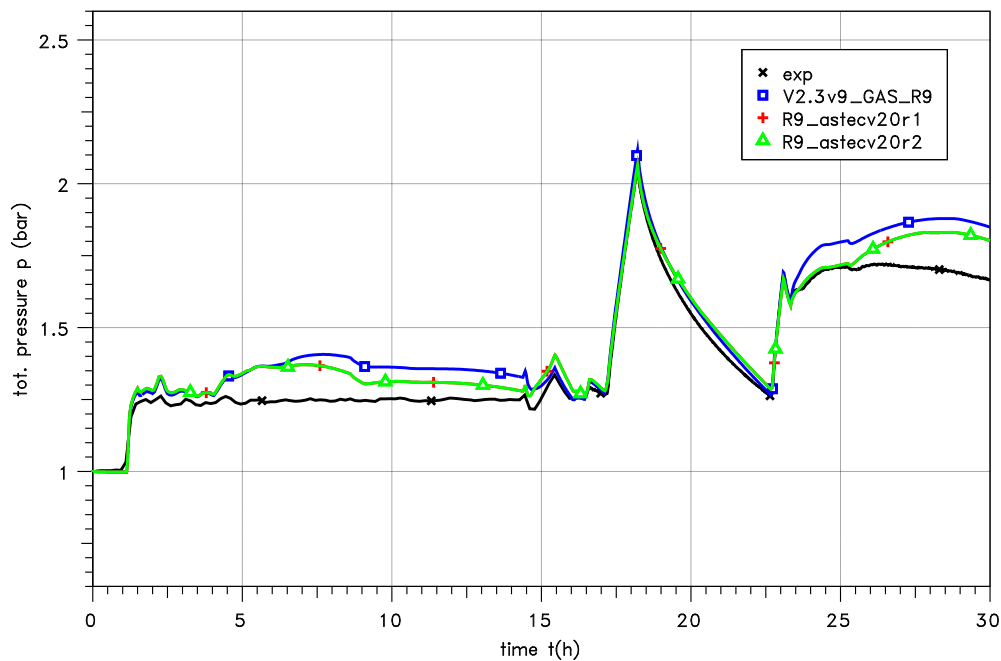


**Figure 4.2-3 BMC VANAM-M3, total pressure**

The nodalisation of this calculation is rather simple (as mentioned above, the same nodalisation as in the ISP-37 was applied), therefore the atmospheric stratification observed in the experiment cannot be simulated in detail. For the room R6 for example only one calculated temperature is available. The subdivision of the related rooms into more control volumes leads to a more detailed calculation of the temperature behaviour as it is shown in /SCZ 99/. It is pointed out, that in the COCOSYS and CPA calculations the non-equilibrium model NONEQUILIB has been used for all zones. Between COCOSYS and CPA only smaller differences are visible.

VANAM M3 EXPERIMENT

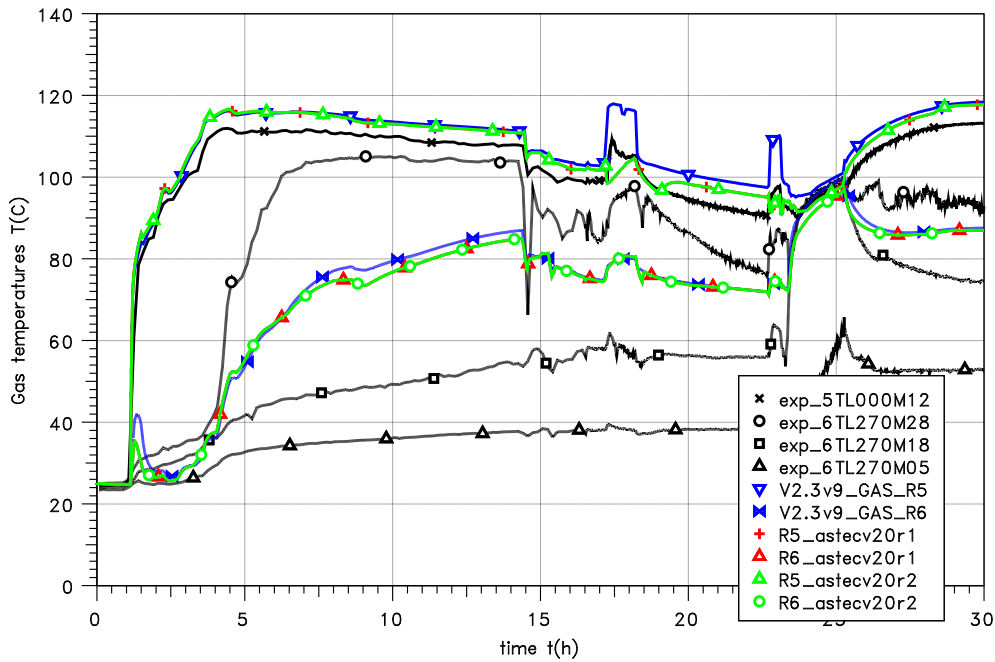


**Figure 4.2-4 BMC VANAM-M3, temperature stratification in R6**

One of the main influences on the aerosol behaviour is the humidity of the atmosphere. The example in Figure 4.2-5 shows the humidity in the room R8 in comparison with the experiment. The COCOSYS calculation shows (especially at around 15 h) a similar behaviour of the humidity compared to the experimental data. The CPA results are even closer to the experiment than the COCOSYS results.

VANAM M3 EXPERIMENT

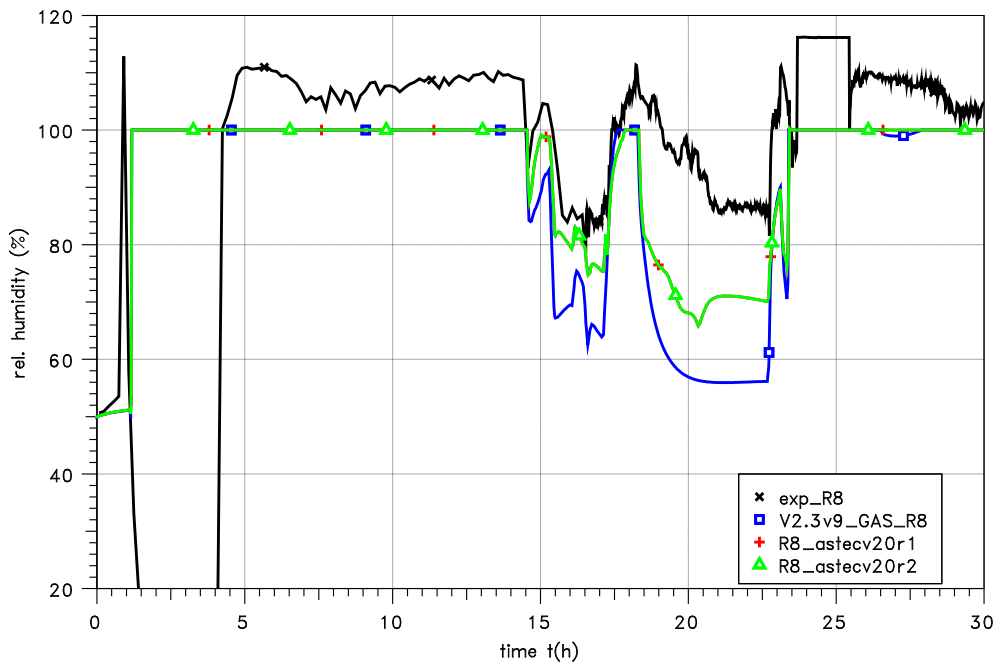


**Figure 4.2-5 BMC VANAM-M3, relative humidity in R8**

Figure 4.2-6 to Figure 4.2-8 present some calculated aerosol concentrations against the experimental data.

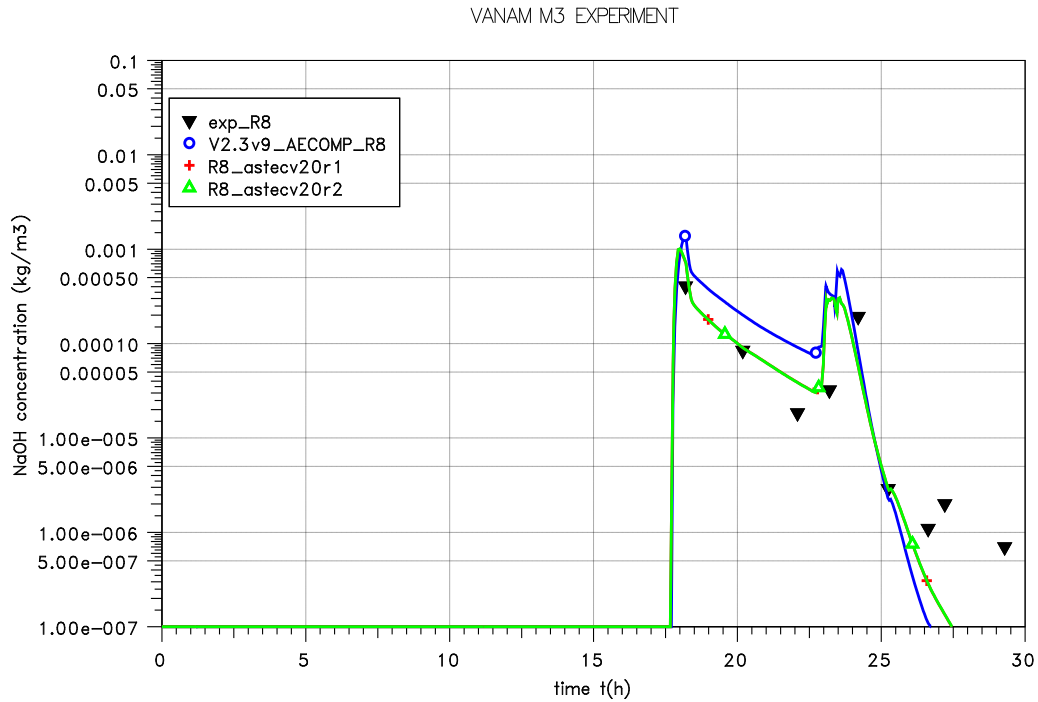


Figure 4.2-6 BMC VANAM-M3, aerosol concentration in R8

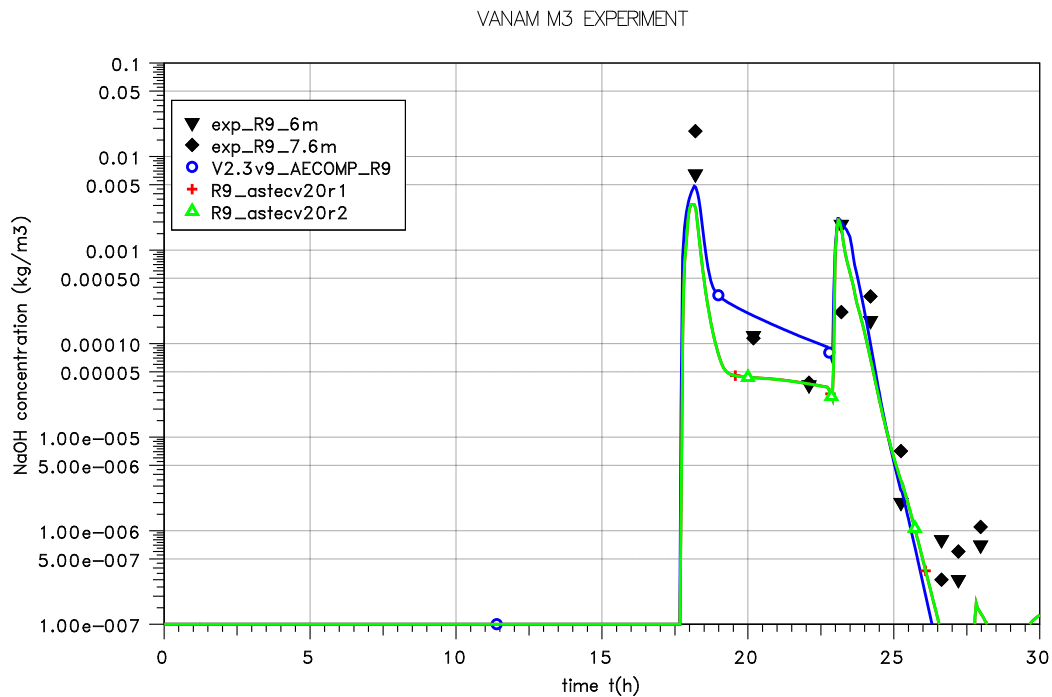
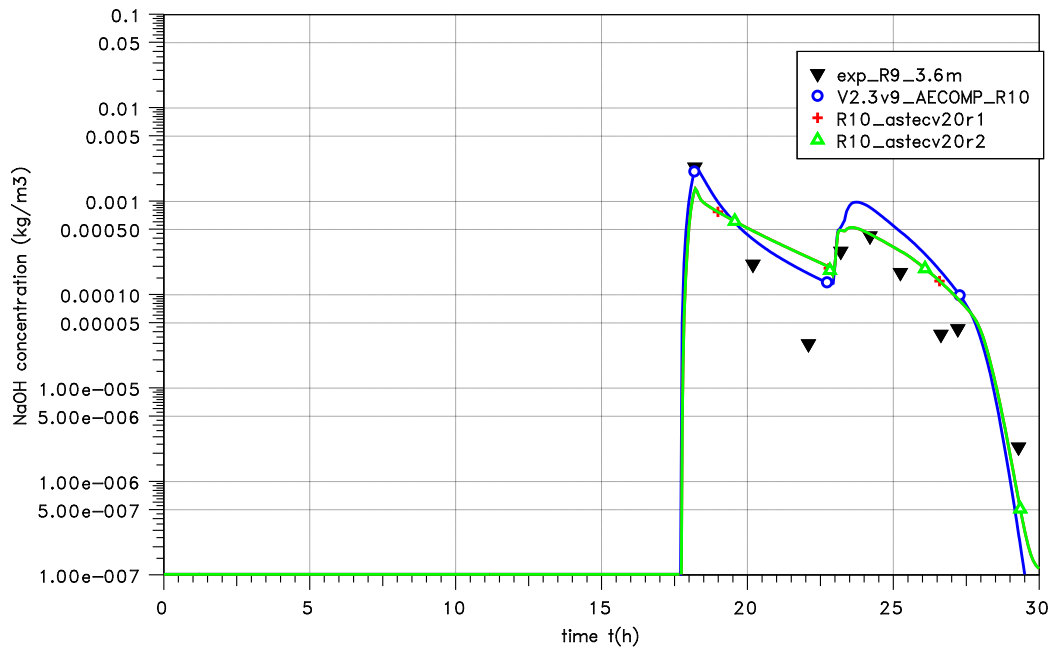


Figure 4.2-7 BMC VANAM-M3, aerosol concentration in R9

VANAM M3 EXPERIMENT



**Figure 4.2-8 BMC VANAM-M3, aerosol concentration in R10**

Concerning the aerosol results both the COCOSYS as well as the CPA results are in good accordance with the experiment.

**4.2.1.4 Summary**

The results gained with COCOSYS and CPA are reasonable for both the thermal hydraulic part as well as the aerosol behaviour. The calculated results match the measured concentrations, however they are somewhat different.

The new ASTEC version V2.0r2 gives the same results as the previous version V2.0r1. No unexpected deviations were found between the results of both code versions.

**4.2.2 KAEVER Tests**

The objective of five KAEVER tests, which were studied in OECD NEA International Standard Problem ISP 44, was the depletion of different hygroscopic (CsI, CsOH) and non-hygroscopic (Ag) aerosol particles in saturated conditions (condensing atmosphere) /FIR 02/. In particular, the influence of solubility and Kelvin-effect were the focus for investigation.

The KAEVER tests are rather simple – one room, steady state thermal hydraulic conditions. From the ISP44 KAEVER tests, a test using non-hygroscopic Ag-aerosols (K148) and a test using three, well-mixed aerosol species (Ag, CsI, CsOH: K187) were included in ASTEC regression testing.

#### 4.2.2.1 Test facility

The KAEVER test vessel operated by Battelle (Germany) was originally designed as 1:1 mockup for a nuclear reactor containment personal airlock /FIR 02/. Hence it is a horizontal cylindrical steel vessel with plane faces and a total volume of total 10.5 m<sup>3</sup> (Figure 4.2-9), which was finally used as test facility for aerosol experiments.

Due to its previous purpose, the test vessel is equipped with two doors having a complex opening mechanism (7\* in Figure 4.2-9). Most of the outer steel walls are thermally insulated and can be heated by electric resistance heater mats. Just parts of the doorway opening mechanism could not be insulated and are hence the main heat transfer paths to the environment. Furthermore, the opening mechanism forms a small leakage path for gases during an experiment as well.

The facility is equipped with several injection lines (steam at the bottom, aerosol at the top, nitrogen at the side), several gas sampling lines and thermocouples, pressure and humidity sensors.

The conditions inside the vessel during an experiment are generally well mixed.

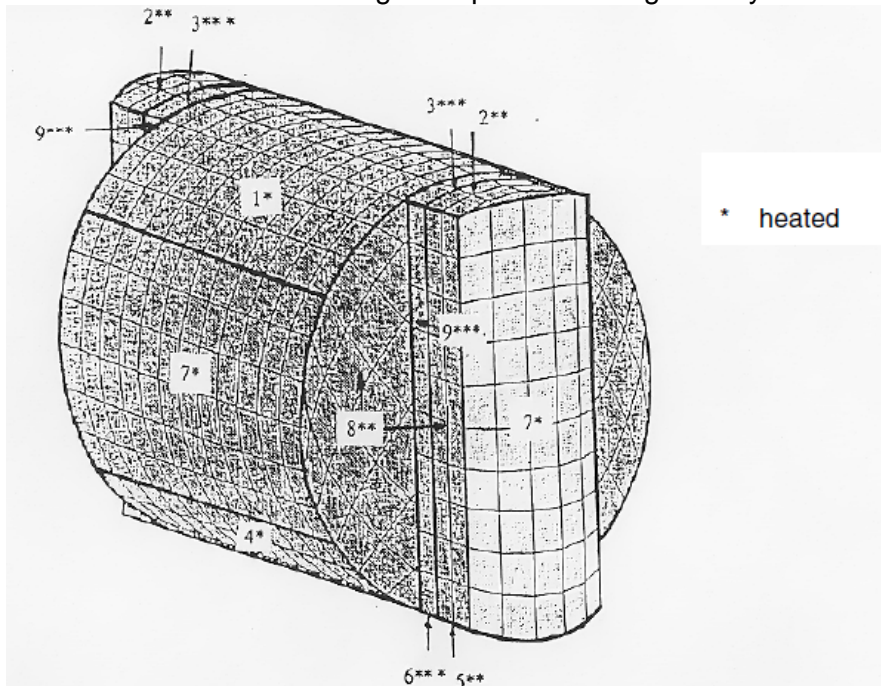
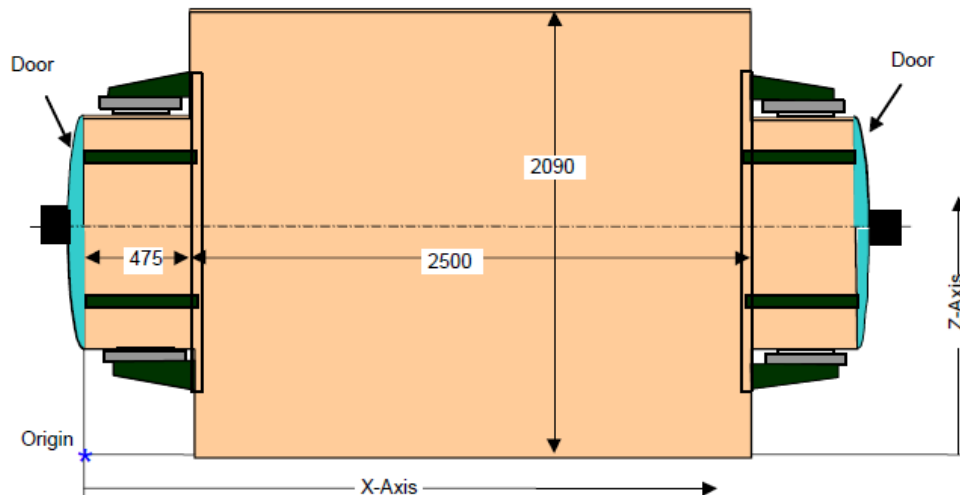


Figure 4.2-9 KAEVER test vessel /FIR 02/.



**Figure 4.2-10 Top view of the KAEVER test vessel /FIR 02/**

#### 4.2.2.2 Experiments

For both investigated tests, the KAEVER test vessel was heated up to 95 – 100 °C and saturated conditions (relative humidity >100 Vol%) were achieved by continued steam injection (preparation phase). Afterwards, the aerosols (Silver in K148, well-mixed Silver, CsI, CsOH in K187) were injected into the vessel while the steam injection carried on (phase II: lasted ~ 5 hours)

K148 experiment focused on the behaviour of non-hygroscopic aerosol material in saturated atmosphere (permanent condensation). Under these conditions, an important process is the condensation of steam on the aerosol particles (leading to particle growth). This condensation is affected by the Kelvin effect, i.e. the vapour pressure of a liquid increases with higher curved liquid/vapour interface (e.g. at smaller droplets) due to the surface tension. Hence the Kelvin effect hinders the condensation on small particles.

K187 experiment was used for the final “blind calculation” phase of ISP44. Well mixed non-hygroscopic, non-soluble silver, and hygroscopic and soluble CsOH and CsI were injected. Since the components are well-mixed and high soluble particles are present, the Kelvin-effect is assumed being negligible in this test.

#### 4.2.2.3 ASTEC input

The test vessel is simulated by a single zone. The surrounding hall of the vessel is simulated by one environmental zone.

The walls (heat structures) of the vessel are in accordance with the geometry of the facility (Table 4.2-2). Just one additional structure was added in order to take into account the heat losses due to the non-isolated parts of the door opening mechanism. The size of this heat structure was adjusted to get best agreement with the measured vessel temperatures.

The wall of the surrounding hall was simulated as well. It was connected to the vessel walls by radiative heat transfer and to the environment zone by convective heat transfer.

As suggested in ISP44 specification, a small junction between vessel and environment was introduced to take into account the small leakage flow through the doorway opening mechanism (pressure loss coefficient  $\zeta = 27,000$ , 26 mm<sup>2</sup> cross section for K148 and 47 mm<sup>2</sup> for K187).

However, the leakage size and size of the additional heat structure had to be adjusted for the simulation of each KAEVER experiment in ISP44 in a different way.

**Table 4.2-2 Aerosol deposition surfaces in ASTEC input**

| Surface                  | Area [m <sup>2</sup> ] |
|--------------------------|------------------------|
| Ceiling                  | 5.677                  |
| Bottom                   | 5.677                  |
| Vertical wall            | 18.265                 |
| Additional vertical wall | 2.35                   |

The aerosol injection rate was not measured directly in the test, but calculated afterwards /FIR 02/. As suggested in the ISP44 specification, this calculated aerosol injection rate was adjusted for the ASTEC input in order to meet the first measured aerosol concentration (directly after end of injection). The adjustment factor was 2.0 for K148 and 0.2 for K187.

Agglomeration and diffusiophoresis are taken into account while thermophoresis is switched off. The Kelvin effect is only calculated for K148 (surface tension of water  $\text{SURT} = 0.0512 \text{ N/m}$ ), since it is negligible for K187 due to the high solubility of the (well-mixed) particles. The solubility for Ag is set to 0 (Van't Hoff factor) and to 1.7 resp. 2.0 for CsI and CsOH. Further aerosol input parameters are given in Table 4.2-3.

The aerosols were accounted in 20 aerosol size classes. Water droplets are treated as own aerosol type.

**Table 4.2-3 Aerosol parameters in K148 and K187**

| Parameter                                 | K148  | K187                      |
|-------------------------------------------|-------|---------------------------|
| Injected Species                          | Ag    | Ag, CsI, CsOH             |
| Injected mass [g]                         | 4.3   | 11.4<br>(1.1 / 6.1 / 4.2) |
| Density [kg/m <sup>3</sup> ] <sup>1</sup> | 5000. | 1100.                     |
| Number median diameter [µm]               | 0.516 | 0.315                     |
| Standard deviation                        | 1.4   | 1.3                       |

<sup>1</sup> The silver particles in K148 do not contain much water due to the Kelvin effect. Hence the density is chosen to half of the density of elementary silver (like recommended in ASTEC user manual). The mixed aerosol particles in K187 are very likely to contain water – and hence their density is governed by the water density.

#### 4.2.2.4 Results

##### 4.2.2.4.1 K148: Plain Silver aerosol

The thermodynamic behaviour is well reproduced by the ASTEC calculation (Figure 4.2-11 and Figure 4.2-12). There are no differences between V2.0r1 and V2.0r2 calculation. The measured temperatures (Figure 4.2-12) indicate some thermal stratification inside the vessel. With the aerosol injected, the volume condensation rate increases (Figure 4.2-13), but is still only a tenth of the total wall condensation rate (Figure 4.2-14).

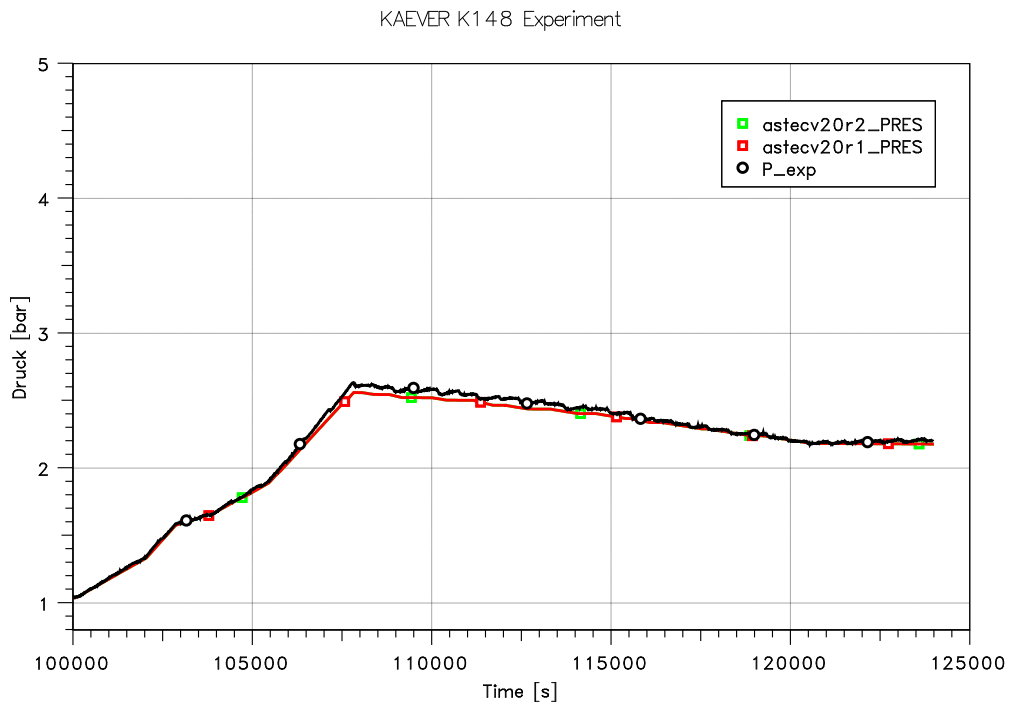


Figure 4.2-11 Pressure in K148 test phase II

KAEVER K148 Experiment

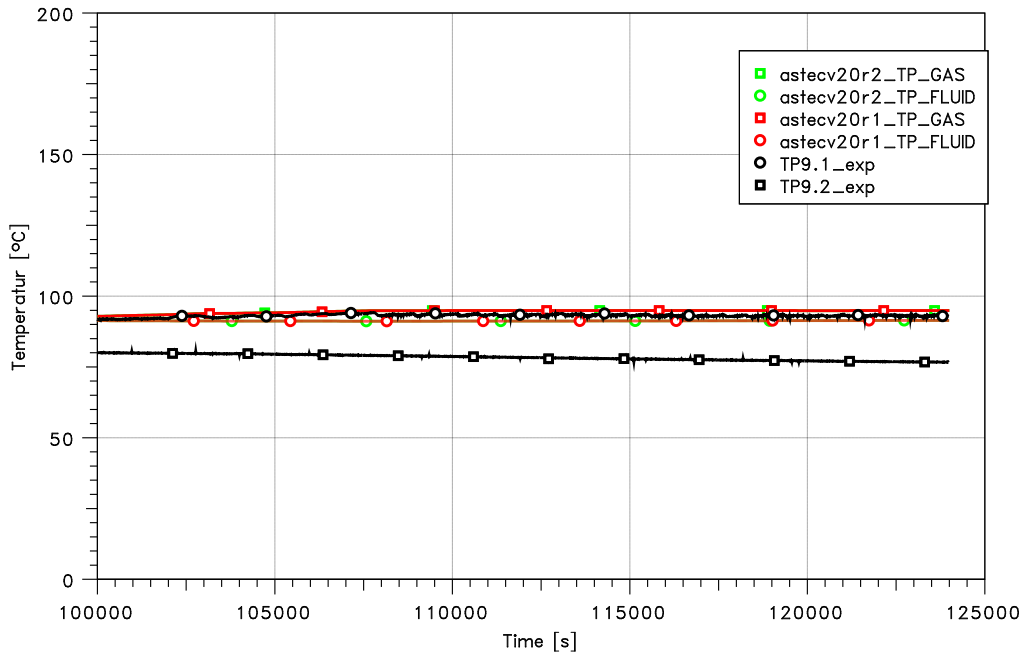


Figure 4.2-12 Gas temperature in the KAEVER test vessel for K148

KAEVER K148 Experiment

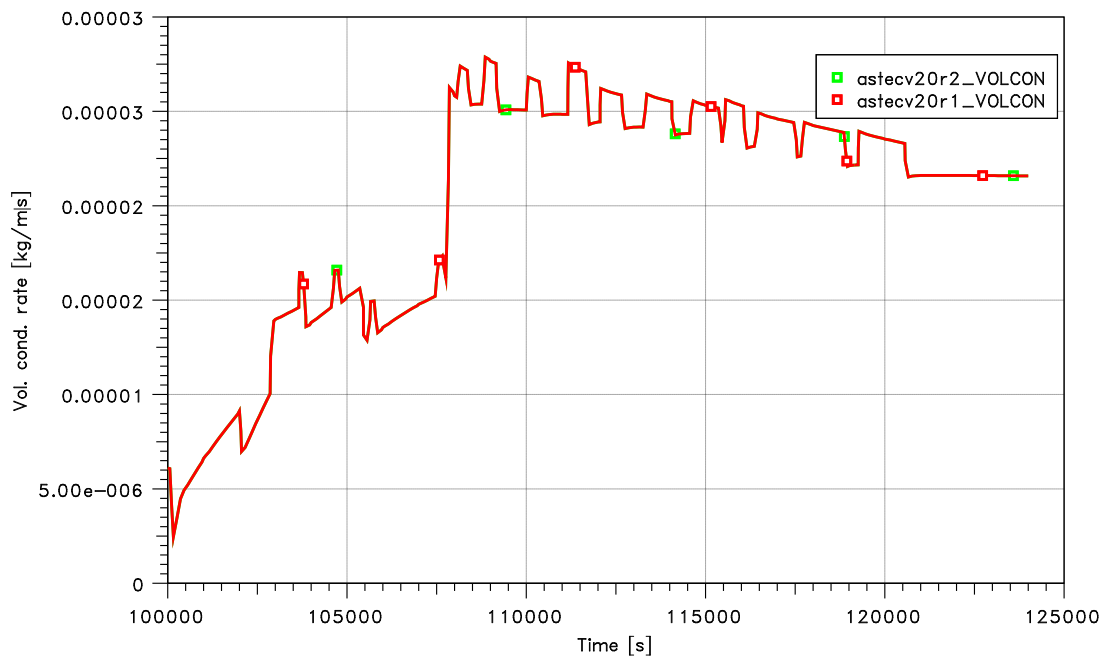
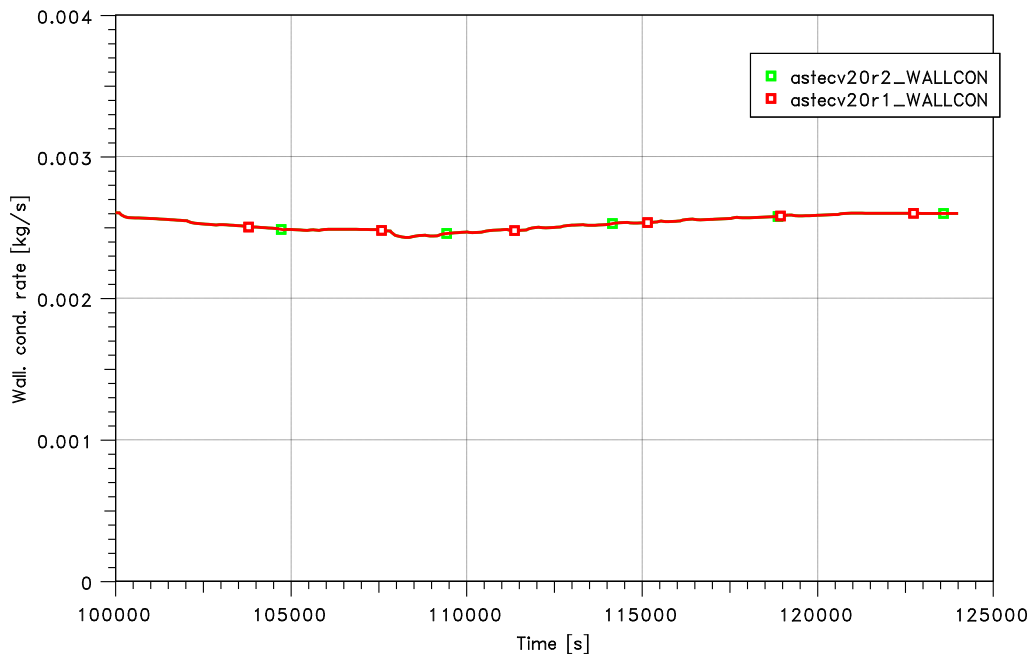


Figure 4.2-13 Volume condensation rates in K148 test calculations

KAEVER K148 Experiment



**Figure 4.2-14 Sum of all wall condensation rates in the KAEVER test vessel in K148 calculations**

The dry aerosol concentration (just Ag, see Figure 4.2-15) of both ASTEC calculations is in good agreement with the experimental measurement. There are differences in the starting phase between the measured data and the theoretical curve, because aerosol injection in ASTEC started at  $t = 105400$  s while the experimental aerosol injection was switched on at  $t \sim 103600$ s. But the experimental aerosol injection rate was not measured and difficult to calculate from the experimental aerosol concentrations (see /FIR 02/, Appendix provided by GRS). Since the aerosol depletion rate was the objective of the test, the estimation of the aerosol injection rate for the ASTEC input focused rather on reaching the correct starting point of the aerosol depletion at the end of the aerosol injection than on the initial phase. The aerosol depletion rate (slope of the aerosol concentration) is reproduced satisfyingly. For the wet aerosol concentration (Figure 4.2-16, including airborne water, which is present in the vessel due to the steam injection even before aerosol injection), the ASTEC results are in the correct order of magnitude. The reproduction of the wet aerosol concentration by the simulation turned out to be a major, unsolved challenge for almost all codes participating in ISP44. Nevertheless, the respective photometer measurement is not very accurate, especially the decay (after 110,000s) is uncertain /FIR 02/.

The mean diameters are given in Figure 4.2-17 and Figure 4.2-18. The two ASTEC calculations do not deviate from each other. The calculated mean diameters are larger than measured in K148 experiment. But the photometric measurement of the sizes is not very accurate and the measured sizes ( $1\mu\text{m}$ - $2\mu\text{m}$ ) are definitely too small (acc. to /FIR 02/). Hence the comparison of the calculated aerosol / droplet sizes with the measured sizes is not fruitful.

To conclude: There are no differences between ASTEC V2.0r1 and V2.0r2 for the KAEVER K148 test calculation. Since some measurements are not very accurate, the comparison with the experimental results should focus mainly on the dry aerosol concentration and its depletion rate (Figure 4.2-15). Concerning this quantity, satisfying agreement is achieved between calculations and experiment.

KAEVER K148 Experiment

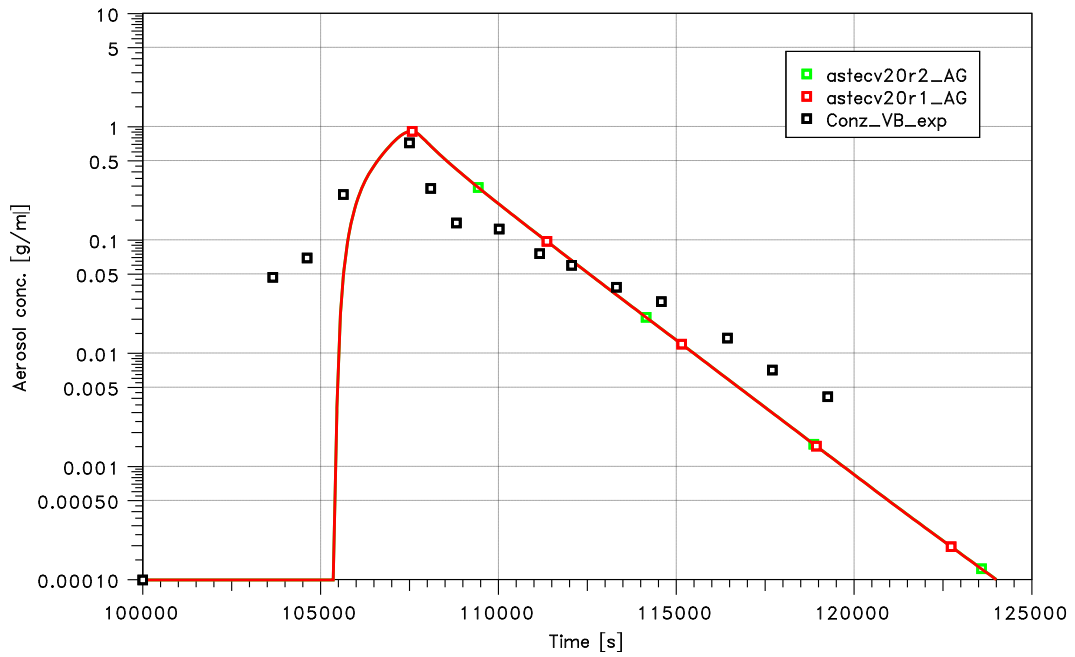


**Figure 4.2-15 Dry aerosol concentration in K148**

KAEVER K148 Experiment

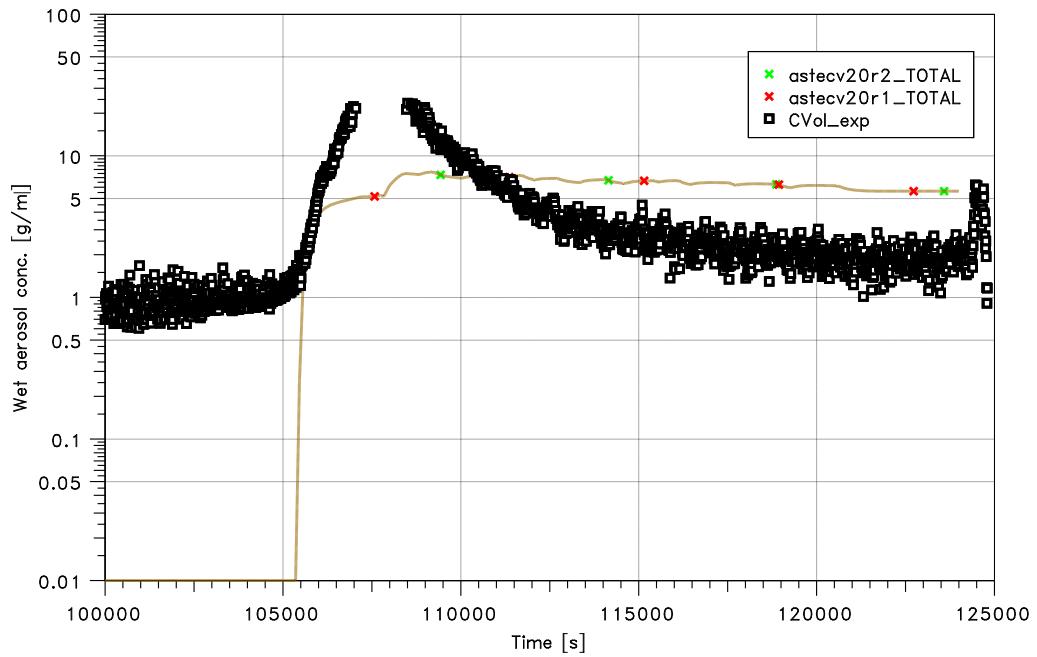


**Figure 4.2-16 Wet aerosol concentration in K148**

KAEVER K148 Experiment

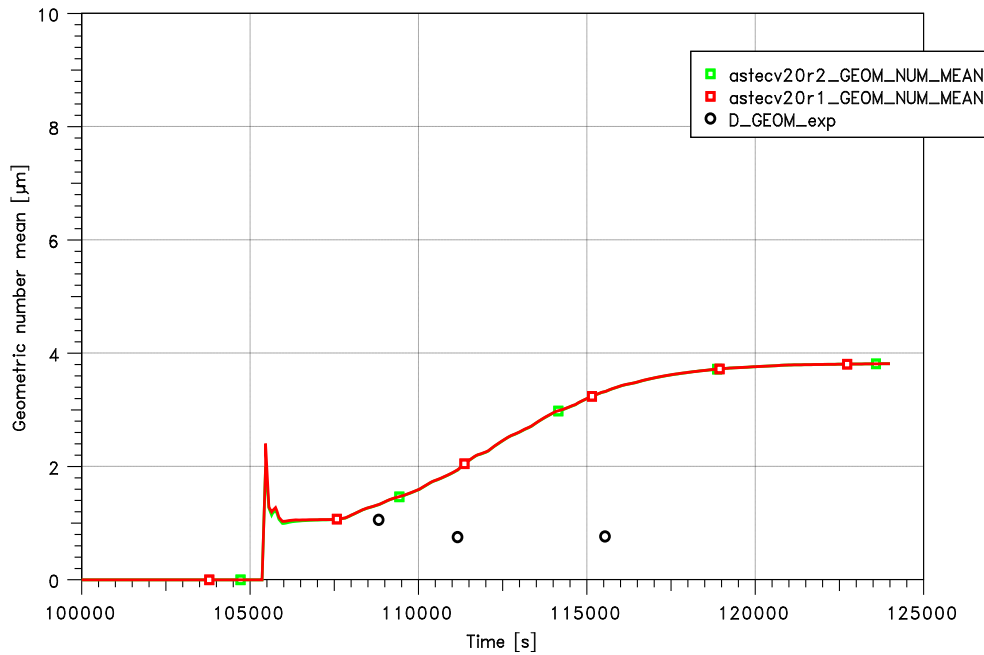


**Figure 4.2-17 Geometric number mean diameter of the aerosol**

KAEVER K148 Experiment

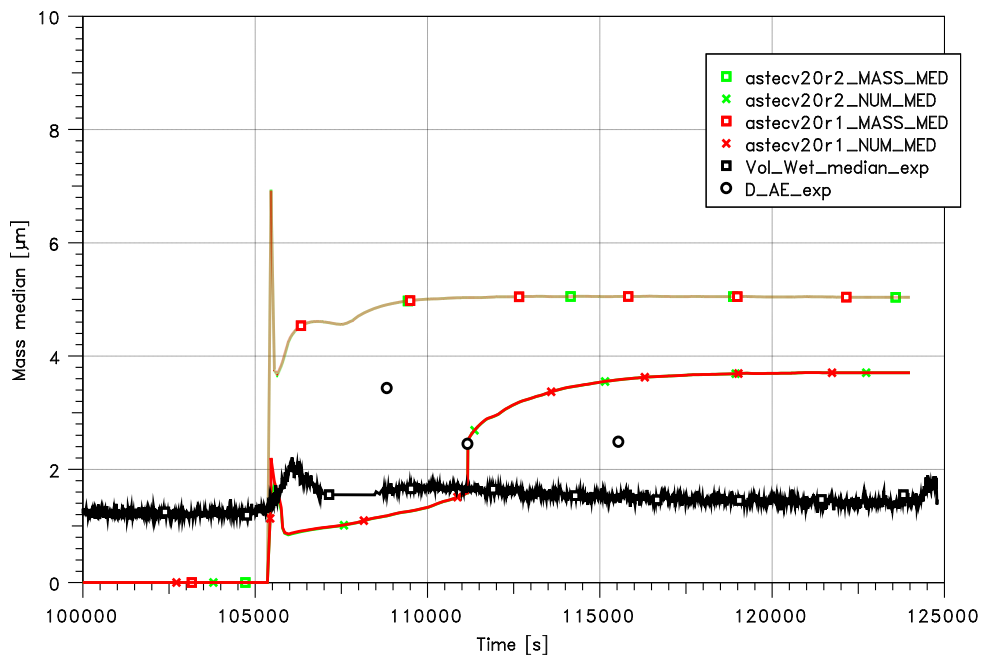


**Figure 4.2-18 Volumetric /mass median diameter of the aerosol**

**4.2.2.4.2 K187: Well-mixed aerosol**

As for K148, the thermodynamic behaviour is reproduced quite well by ASTEC, and there are no deviations between the two ASTEC versions (Figure 4.2-19 - Figure 4.2-22).

The total and the specific dry aerosol concentrations and its depletions are as well satisfyingly matched by both calculations which do not differ much from each other (Figure 4.2-23 - Figure 4.2-26). The three components behave very similarly in the experiment (the mass fraction of the components is the same for injection and for the two measurement points): The aerosols are definitely well-mixed, and hence it was suitable to give identical density and other aerosol input parameters for the three components in ASTEC (see Table 4.2-3).

The wet aerosol concentration measurement (Figure 4.2-27) is not very accurate. Especially the decrease about two orders of magnitude cannot be explained /FIR 02/. Nevertheless, the ASTEC calculations give an appropriate order of magnitude and the same maximal wet aerosol concentration as the experiment.

The particle (droplet) diameters are given in Figure 4.2-28 and the measured distribution is given in Figure 4.2-29. The measured diameters are assumed to be too small /FIR 02/.

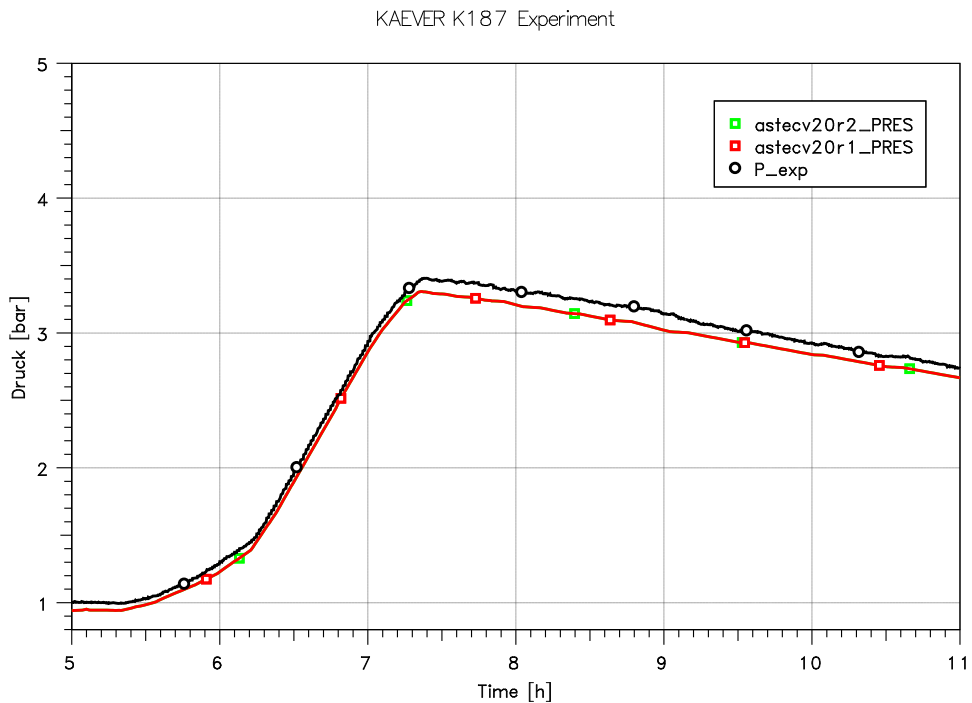


**Figure 4.2-19 Pressure evolution in K187 experiment**

KAEVER K187 Experiment

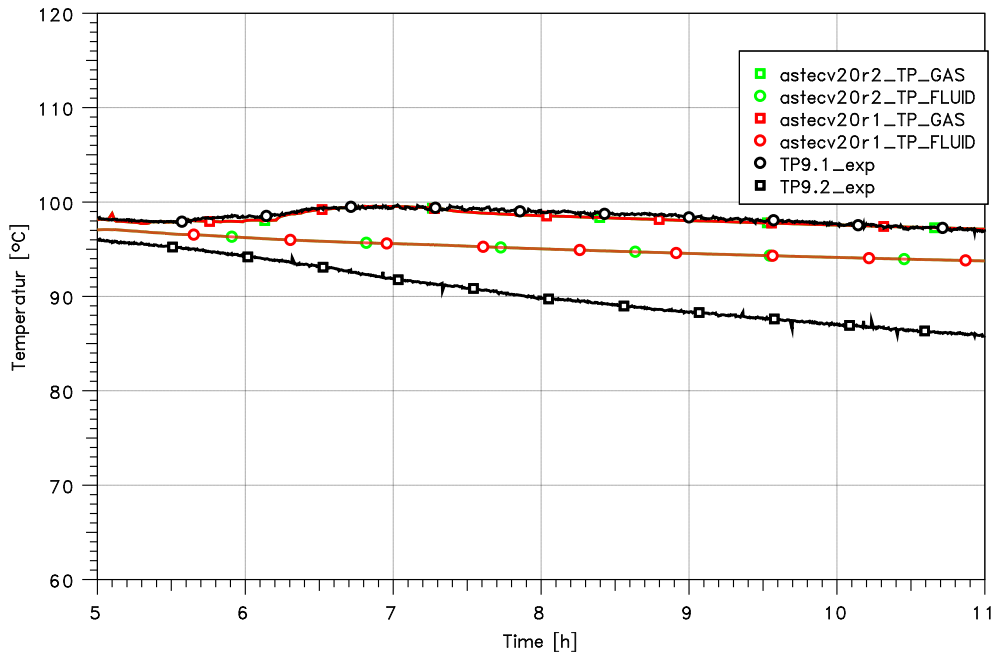


Figure 4.2-20 Gas temperature in KAEVER test vessel in K187 experiment

KAEVER K187 Experiment

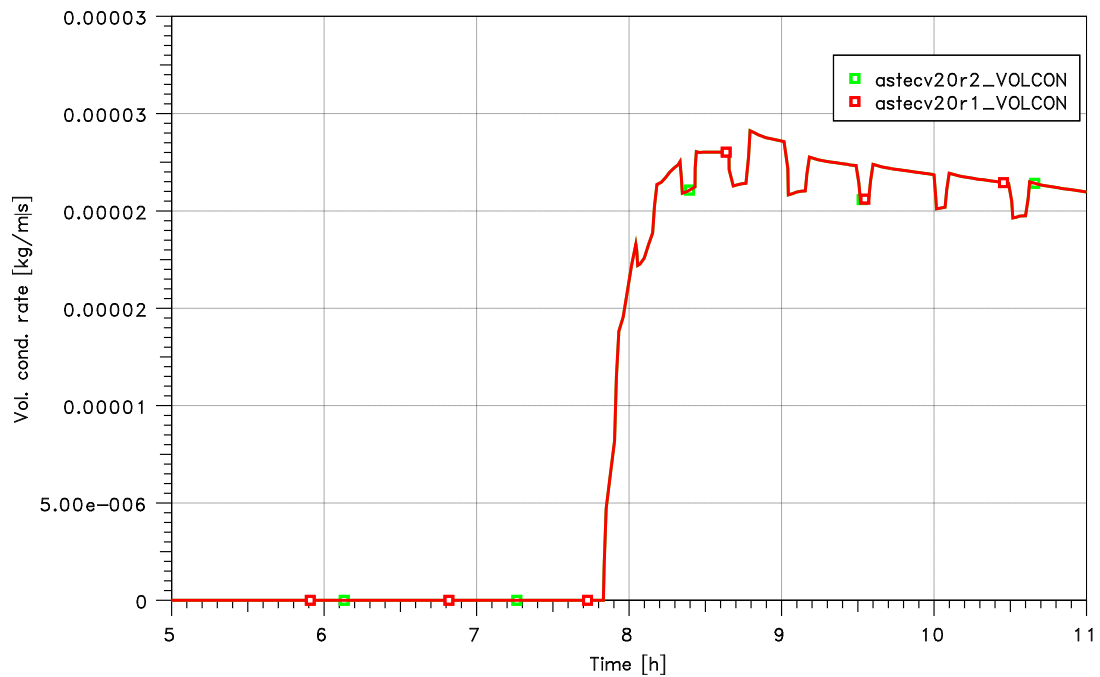


Figure 4.2-21 Volume condensation rate in K187 experiment

KAEVER K187 Experiment

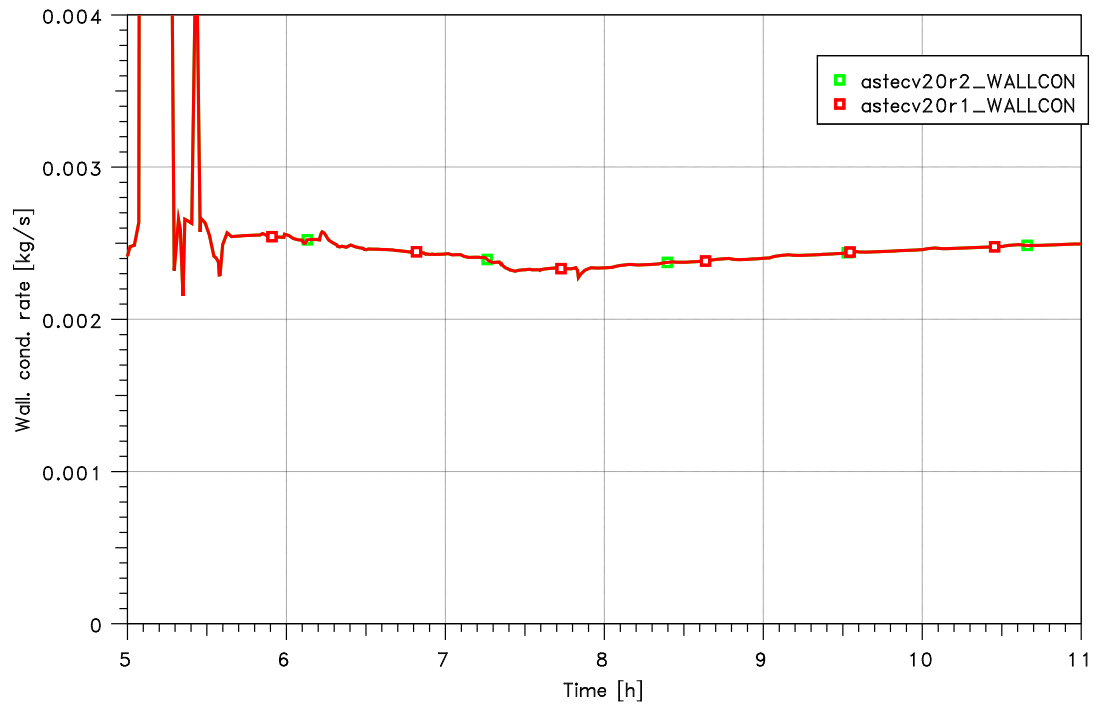


Figure 4.2-22 Wall condensation rate in K187 experiment

KAEVER K187 Experiment

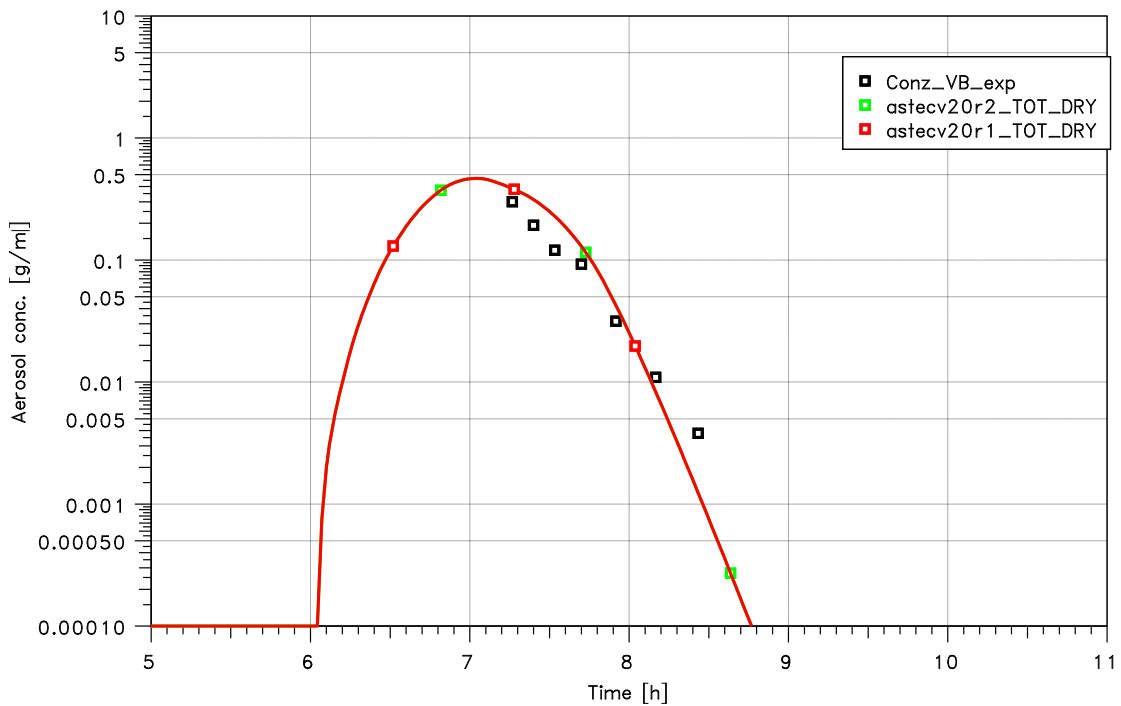


Figure 4.2-23 Total dry aerosol concentration in K187

KAEVER K187 Experiment

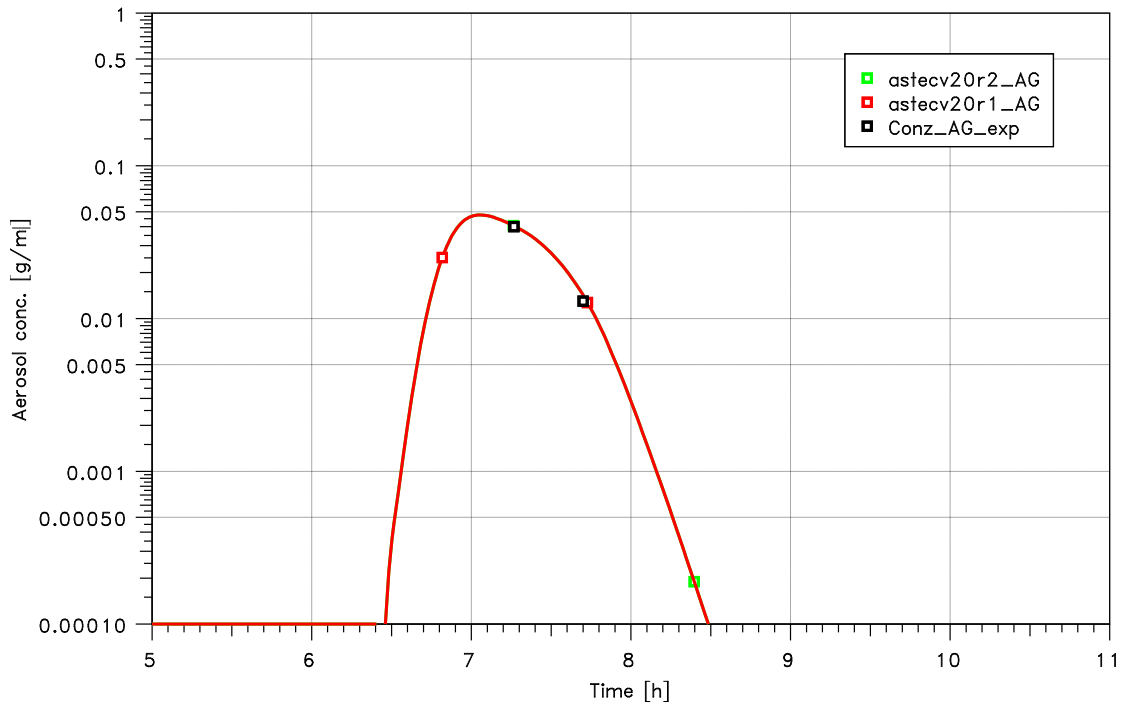


Figure 4.2-24 Dry aerosol concentration of Ag in K187

KAEVER K187 Experiment

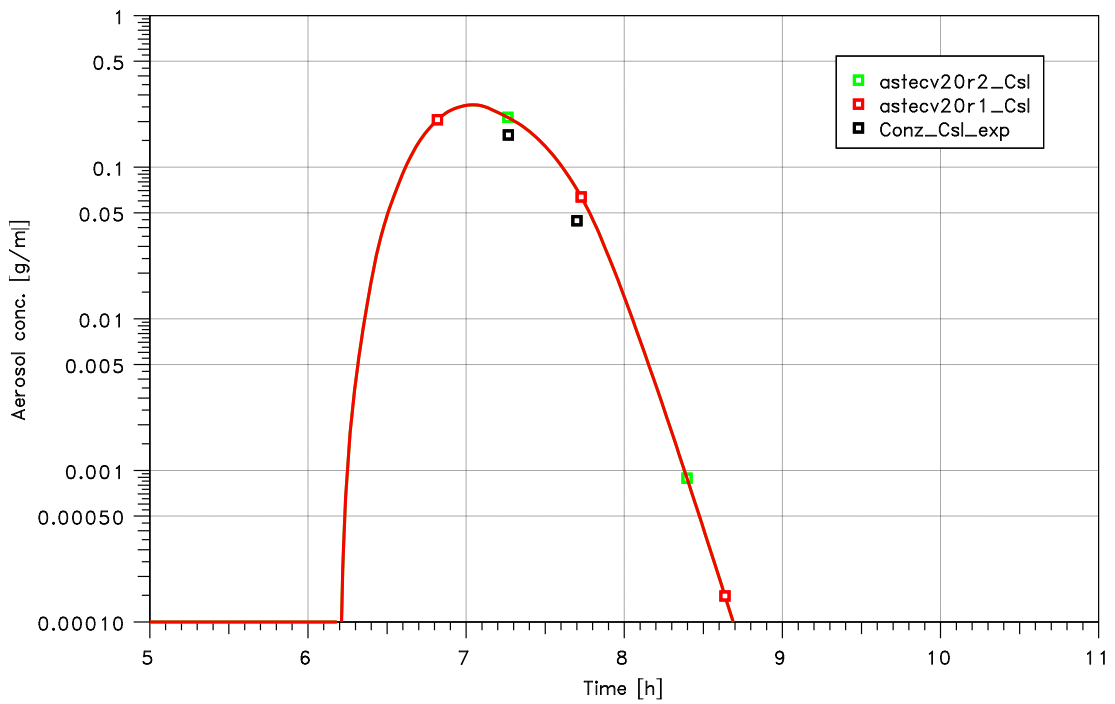


Figure 4.2-25 Dry aerosol concentration of CsI in K187

KAEVER K187 Experiment

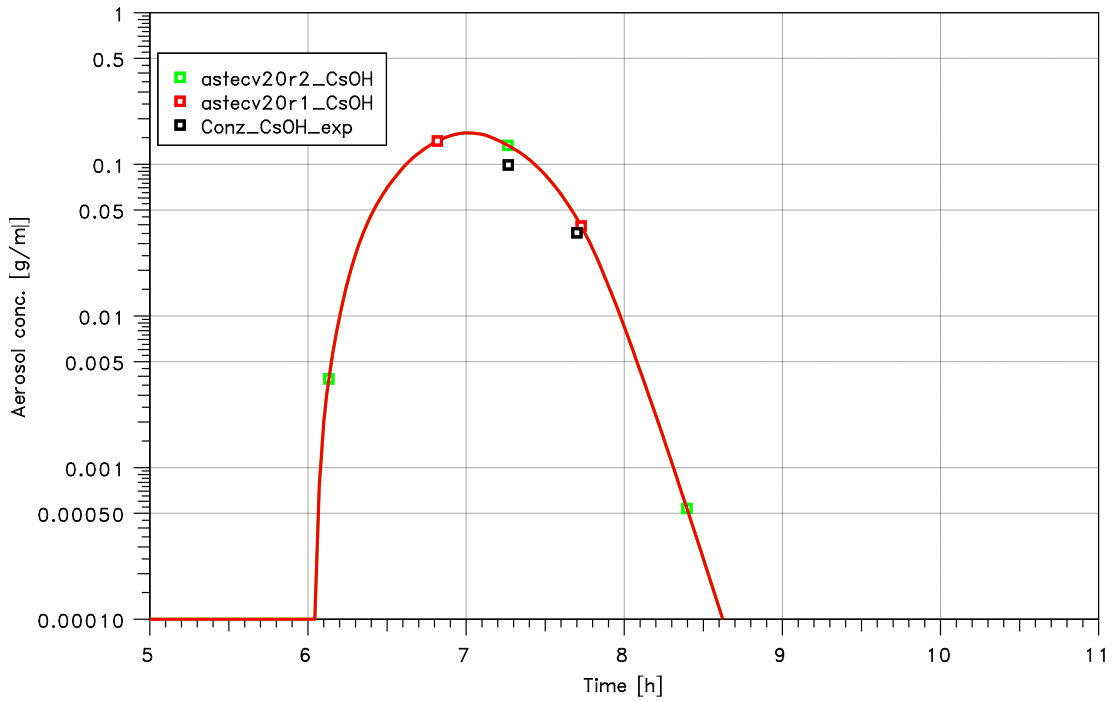


Figure 4.2-26 Dry aerosol concentration of CsOH in K187

KAEVER K187 Experiment

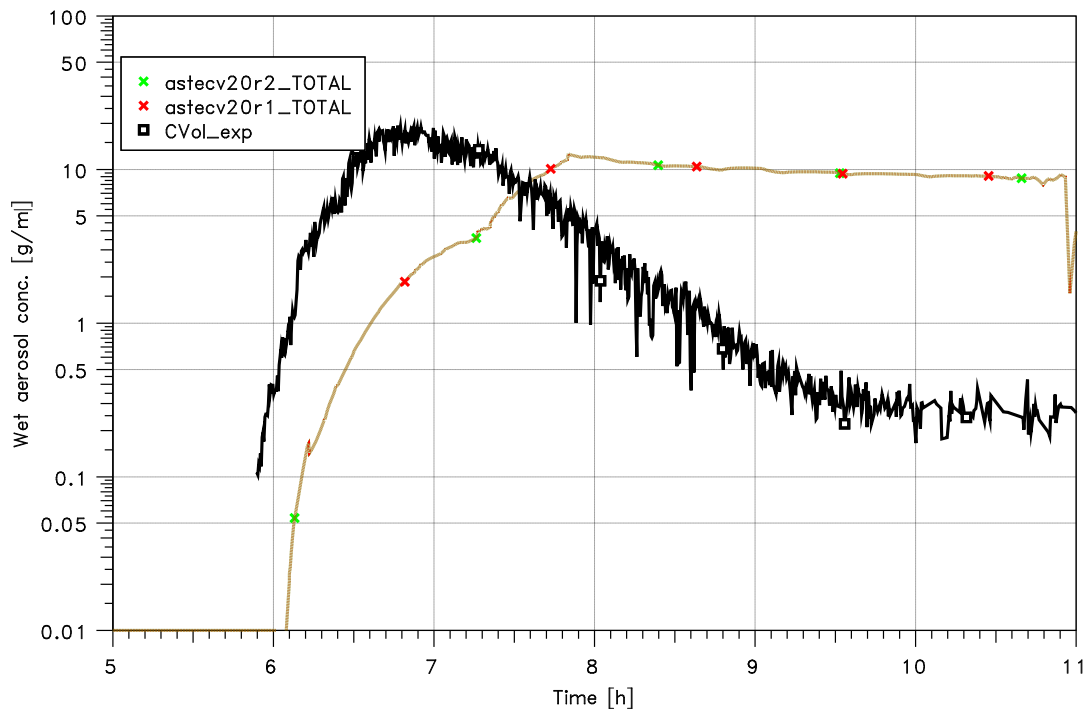


Figure 4.2-27 Total wet aerosol concentration in K187

KAEVER K187 Experiment

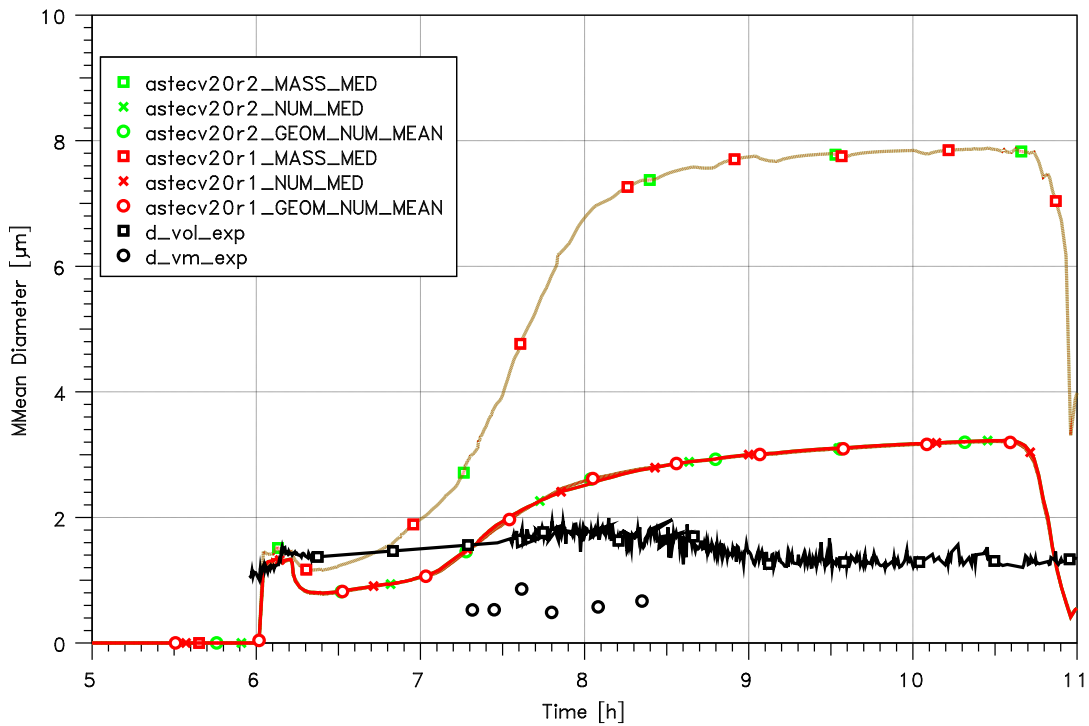


Figure 4.2-28 Mean aerosol particle diameters for K187

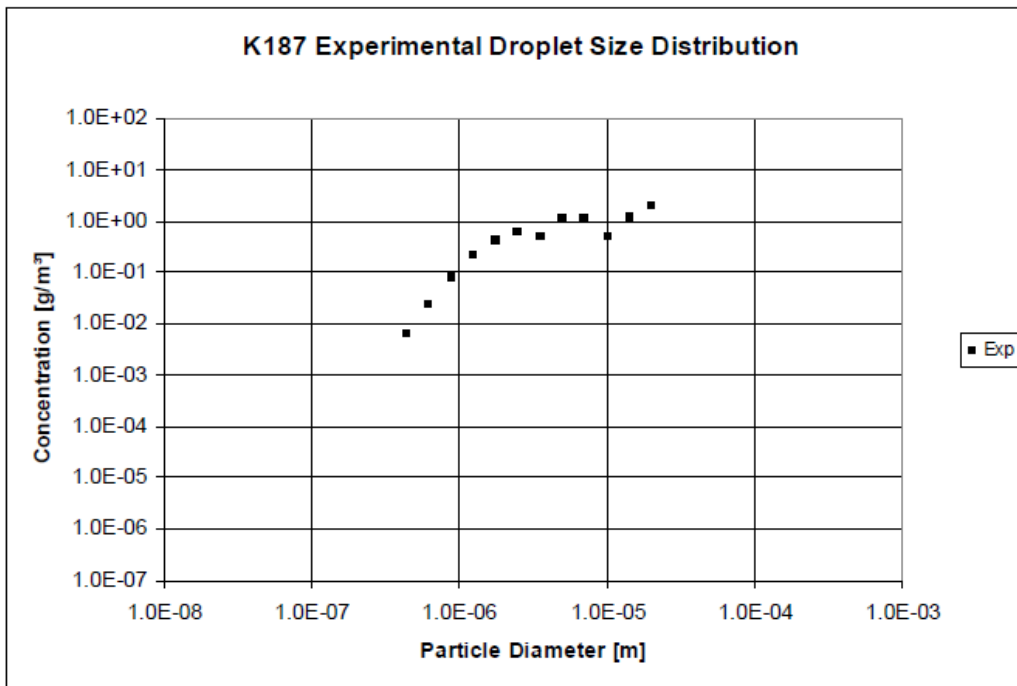


Figure 4.2-29 Experimental measured particle (droplet) size distribution 1 000s after end of aerosol injection (at 7.5h) /FIR 02/.

To conclude: ASTEC sufficiently takes into account the two main important effects for aerosol behaviour at condensing conditions - solubility and Kelvin-effect. There are almost no differences between the two investigated ASTEC versions.

## 4.3 Iodine behaviour

### 4.3.1 THAI lod-11

For the regression testing the THAI iodine test lod-11 was selected. This particular test is assessed to be more suitable than the tests lod-6, 8 or 10. In test lod-11 a non-homogeneous iodine concentration in the atmosphere was established, which is hard to post-calculate. After this test the reaction constants for adsorption and desorption of gaseous iodine onto/from steel walls were measured more precisely in other THAI tests. By use of these data the iodine/steel reaction in the COCOSYS iodine model AIM was improved. In contrast to that ASTEC uses the iodine model IODE.

#### 4.3.1.1 THAI test facility

In 2004, three multi-compartment tests (lod-10, -11, and -12) were performed on the transport behaviour of molecular iodine ( $I_2$ ). The main processes investigated in these THAI multi-compartment tests are /WEB 06/:

- Iodine transport with gas and water flows,
- $I_2$  adsorption on and desorption from a steel surface without and with wall condensation,
- $I_2$  mass transfer between atmosphere and sump.

As all THAI tests have been performed without a radiation source, the transport processes of molecular iodine have been undisturbed by radiolytical reactions. The configuration during these tests was as shown in Figure 4.3-1.

The test number 11 was separated into different experimental phases that are:

(1) **Preparation phase:** A special wall heating and cooling procedure established a stable gas and temperature stratification. At the end of this phase the atmosphere temperature in the dome compartment was about 90 °C and that in the lower compartments between 50 °C and 18 °C, which was the sump water temperature. The pressure was somewhat higher than the ambient pressure.

(2) **Stratification phase:** A stable atmospheric stratification was maintained. At the beginning about 1 g of molecular iodine ( $I_2$ ) was released into the dome by a puff of carrier gas. The beginning of the release marks the start of the experimental time ( $t = 0$ ). A significant portion of the released  $I_2$  was adsorbed at the steel surfaces in the dome.

(3) **Transition phase:** Transition to a mixed vessel atmosphere. In lod-11 the two lower jackets were heated and helium was injected into the bottom compartment. The gas temperatures varied between 70 °C and 80 °C.  $I_2$  was transported from the dome to the upper annulus and from there further down.

(4) **Well-mixed phase:** Long term phase with quasi steady state conditions. Only little heat was injected to maintain natural convection and mix the atmosphere.  $I_2$  was continuously desorbed from the dome structures and transported into the lower compartments. The atmospheric temperature differences were relatively small.

The relative humidity was high (90 % in the dome) during this test but without wall condensation.

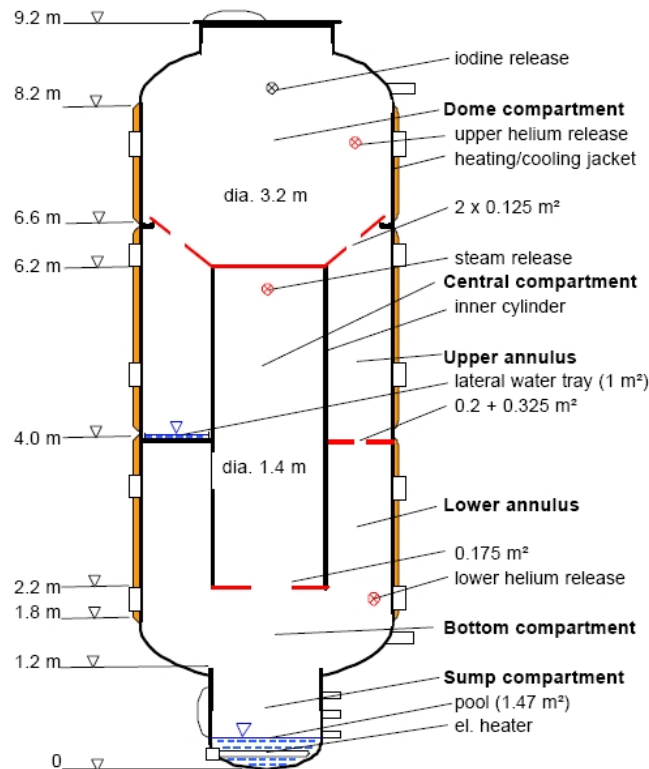


**Figure 4.3-1 Multi-compartment configuration of the THAI-facility for the Iodine tests**

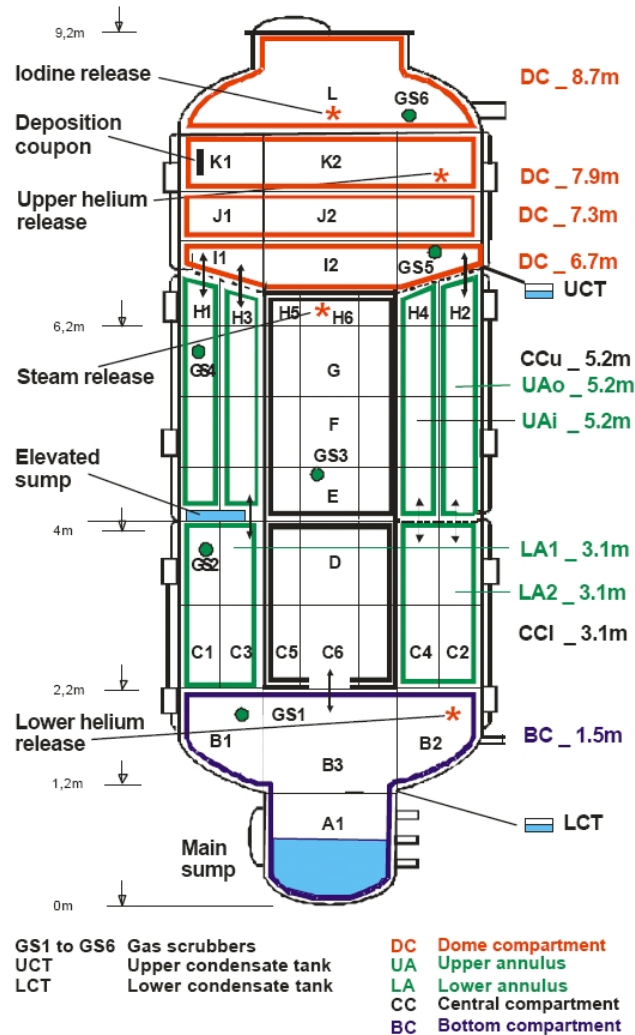
#### 4.3.1.2 CPA input deck

Figure 4.3-2 depicts the nodalisation of the THAI vessel used for the ASTEC-CPA calculations. This dataset was automatically developed from the same COCOSYS dataset using the COC2AST tool /DEI 03/.

The 46 zones (A1 to L) representing the vessel volume are interconnected by 73 atmospheric junctions. The dome compartment (DC) is subdivided into seven zones to simulate stratification processes there. The lower and the upper annulus (LA, UA) are subdivided axially to calculate counter current flows. Two zones model the external tanks (LCT, UCT), which collect the wall condensate, and two other zones represent the environment. The thermodynamic non-equilibrium model (which is applied for all zones) was used in the sump zones in order to simulate the different gas and water temperatures. 58 heat-conducting structures model the vessel walls and internal structures.

Within the corresponding COCOSYS iodine calculation the thermal hydraulic nodalisation was condensed to 13 so-called iodine compartments (BC\_1.5 m to DC\_8.7 m) by combining several zones to one iodine compartment. This COCOSYS-AIM feature takes into account the different spatial accuracy requirements of the modules and reduces the calculation time. In Figure 4.3-2 both nodalisations are indicated (iodine compartments marked by red, green, blue, and black perimeters). The CPA dataset

uses IODE instead of AIM and so the iodine compartments are the same as the thermal hydraulic zones.



**Figure 4.3-2 THAI Iod-11, CPA and COCOSYS-AIM nodalisation of the THAI-facility**

### 4.3.1.3 Results

In the following graphics a comparison between the experimental measurements (black line), the ASTEC version V2.0r2 (green line), the previous version V2.0r1 (red line), and COCOSYS (blue line) is given for some relevant parameters.

Figure 4.3-3 shows the total pressure in the facility. In the beginning the pressure is in the range of 1.5 bar. This behaviour is well calculated by both ASTEC versions and COCOSYS until the transition phase starts with heating at 4.4 h and injection of helium at 5.32 h. During that transition phase the pressure raises up to 1.85 bar. This is underestimated by the COCOSYS calculation by about 0.1 bar at 9 h. The old ASTEC version V2.0r1 shows a completely different behaviour. In contrast to COCOSYS and V2.0r2 the pressure is decreasing after 6 h. The reason for the difference between V2.0r2 and COCOSYS compared to the experiment is wall condensation calculated on the cold structures at the bottom of the vessel which was not observed in the experi-

ment. The occurrence of wall condensation in the calculation is due to uncertain relative humidity and temperatures simulations (s. below). The totally different behaviour of V2.0r1 is due to an error in the subroutine for the injection of heat into wall structures within CPA (made during modification of this subroutine for coupling with other ASTEC modules). This error is fixed in the new ASTEC version V2.0r2 and the results are similar to COCOSYS again.

ThAI lod-1 1

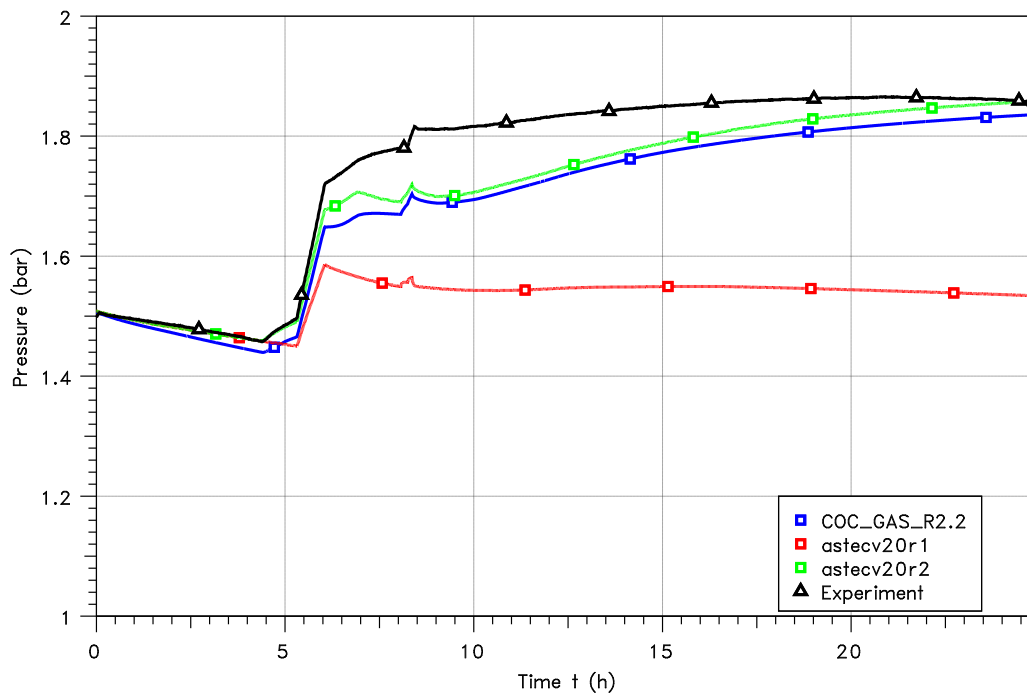


**Figure 4.3-3 THAI lod-11, pressure in the facility**

The measured temperature trends at 2.1 m and 8.4 m height are shown in Figure 4.3-4. The zone centres of the corresponding nodalisation zones differ and are at 1.7 m and 7.9 m. In the upper zone the temperature starts at about 96 °C and slightly falls during the experiment. At 25 h the temperature is at 80 °C. Both, the COCOSYS and the ASTEC V2.0r2 calculations delivers good results for this position. The lower point starts with a temperature of 26 °C and rises due to the heat supply during the transition phase after 4.4 h. After 25 h an almost homogenous temperature field is reached with a temperature of 80 °C at 2.1 m elevation. This experimental value does not correspond to the COCOSYS and V2.0r2 values at 1.7 m height of only 65 °C at 25 h. An explanation for this deviation can be given. The lower edge of the lowest heating jacket is at 1.8 m. Below this height the atmosphere is stratified throughout the whole mixing phase. The measured temperature difference between the heights 1.2 m and 2.1 m is about 10 K. The calculation delivers a higher temperature difference of 14 K between 1.7 m and 2.6 m. With a more detailed nodalisation of this vessel part the stratification can be simulated more accurately. But this local stratification has a minor influence on the global iodine distribution which is the main objective in this test. The old ASTEC version V2.0r1 calculates no heat injection into the wall jackets and thus the temperature is much lower during the mixing phase. This explains the large differences to the COCOSYS and V2.0r2 calculations.

ThAI lod-11

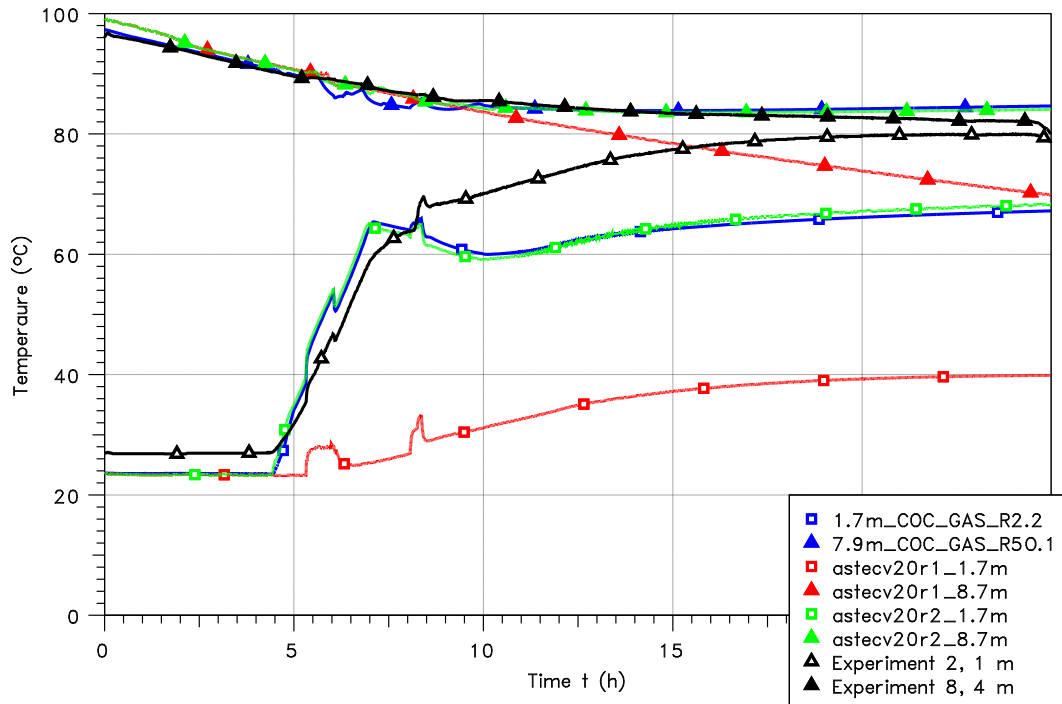


**Figure 4.3-4 THAI lod-11, temperature in a lower and a upper zone**

An important parameter in the lod-11 experiment is the concentration of helium, as it serves as a tracer medium that indicates the mixing velocity of the atmosphere. Figure 4.3-5 shows the helium concentration at 1.7 m and 8.7 m. The injection starts after 5.32 h in the lower part of the THAI facility, thus the helium concentration reaches a maximum of about 13 % at 1.7 m elevation after 6 h. At 8.7 m elevation the concentration rises over a period of 3 h. At 8 h an almost homogenous mixing of helium is reached with an overall concentration of 10 %. The ASTEC V2.0r2 and COCOSYS calculations are in very good accordance with the measurement. Due to the missing heat injection within ASTEC version V2.0r1 no real mixing phase is established. Therefore, the iodine concentrations in the lower and upper part have different values during the whole calculation time.

ThAl lod-11

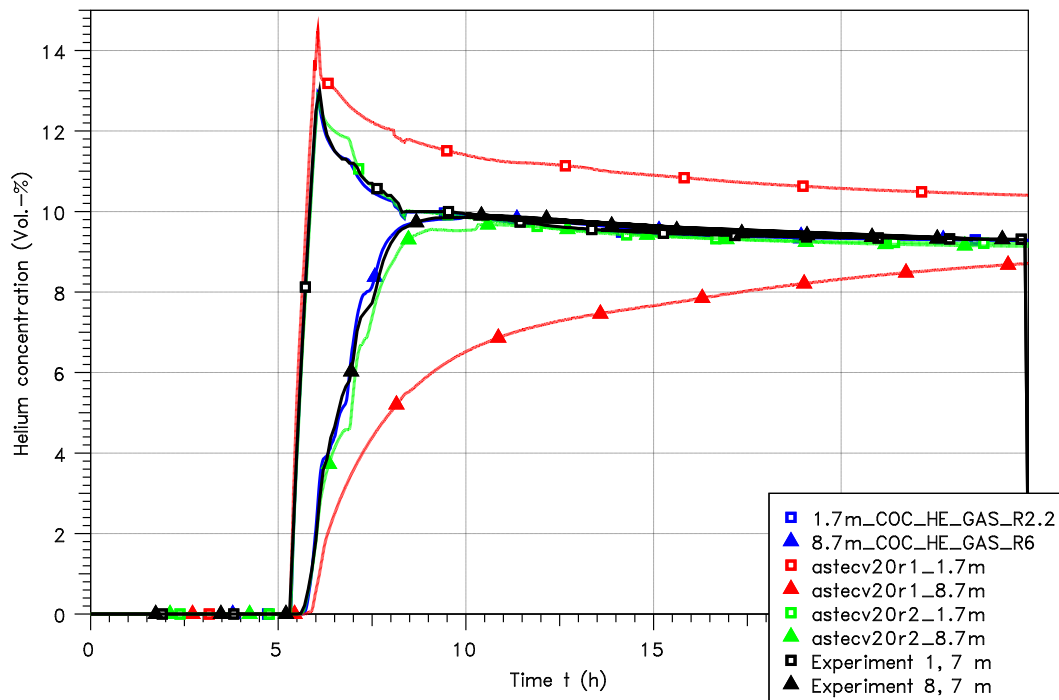


**Figure 4.3-5 THAI lod-11, helium concentration in a lower and a upper zone**

The behaviour of gaseous iodine  $I_2$  is illustrated in Figure 4.3-6. Until the beginning of the transition phase the iodine is stratified with about  $10^{-5}$  g/l at 8.3 m height and only  $3 \cdot 10^{-8}$  g/l at 1.8 m elevation. At  $t = 4.35$  h the heating of the lower and the middle heating jackets starts. One hour later helium is injected at the bottom of the vessel enforcing the convective mixing. After further 5 hours the helium is homogeneously distributed in the vessel whereas a significant iodine concentration difference between the dome and the lower rooms remains during the whole mixing phase. After 7 h the concentration is  $3 \cdot 10^{-6}$  g/l at 7.9 m and only  $3 \cdot 10^{-7}$  g/l at 1.8 m. After 10 h it is  $8 \cdot 10^{-7}$  g/l at 7.9 m and  $10^{-7}$  g/l at 1.8 m. After that no measurements have been taken until 23 h. At his time the mixing of the iodine is proceeded and the difference of the iodine concentration between both positions is reduced to a factor of 2. The concentration has decreased to about  $10^{-7}$  g/l in the whole facility. The calculation with COCOSYS does not show any reduction in the airborne iodine concentration after the transition phase. It gains a constant iodine concentration. The ASTEC calculations show a much higher iodine concentration. Also in the iodine concentration the missing heat injection within version V2.0r1 is visible. Due to the weak mixing this version calculates a high iodine stratification up to the end of the experiment.

ThAI lod-11

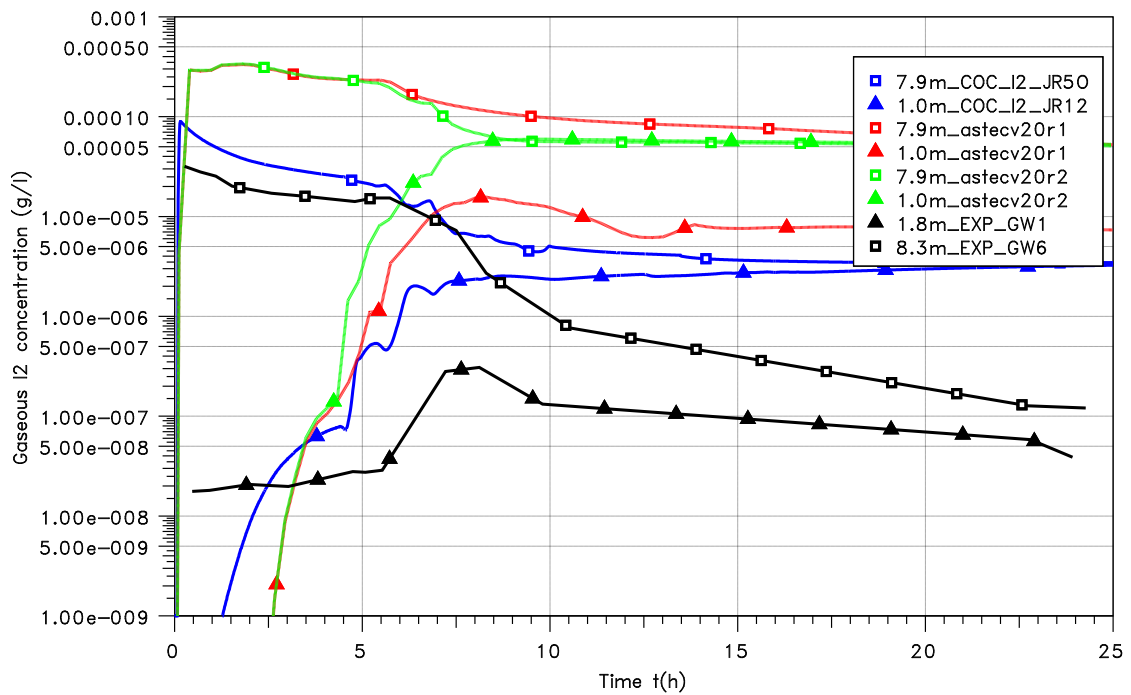


**Figure 4.3-6 THAI lod-11, gaseous iodine concentration in different levels of the facility**

The calculation effort of COCOSYS and both ASTEC versions is shown in Figure 4.3-7. The real time factor, which is defined as the quotient of the simulated process time and the CPU time required for the calculation, is in the range of 22.5 for COCOSYS and in the range of 125 for ASTEC V2.0r2. The CPA calculation is much faster than COCOSYS, but they are not fully comparable as both calculations have been performed on two different machines. More important is the large difference between both ASTEC versions. In the old version the real-time factor was wrong calculated and is very low. This bug is corrected in the new version.

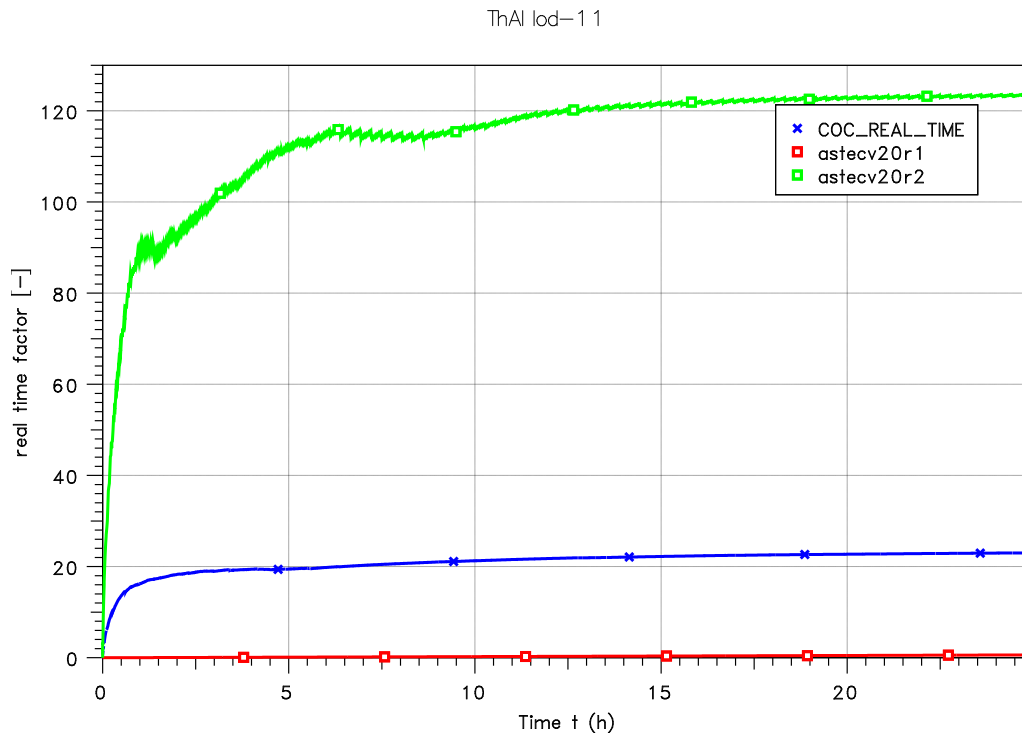


**Figure 4.3-7 THAI lod-11, calculation effort**

#### 4.3.1.4 Summary

The results show that there was a bug in ASTEC version V2.0r1. The analysis showed that this was due to a missing heat injection into CPA wall structures in this version. This mistake was found during regression testing and is solved in the recent ASTEC version. Furthermore the real time factor delivers wrong values in the ASTEC CPA calculation with version V2.0r1. This is also corrected in the recent version.

Still significant differences exist between IODE used in ASTEC and AIM used in COCOSYS related to the iodine behaviour. To reduce the differences as well in comparison to experiments needs more work on code validation.

#### 4.3.2 PHEBUS/RTF-1

The PHEBUS/RTF-1 test is the second iodine test chosen for regression testing. It is a well investigated laboratory scale experiment and it is part of the International Standard Problem ISP-41.

##### 4.3.2.1 Test facility

The Radioiodine Test Facility (RTF /GLO 08/) was built at AECL's Whiteshell Laboratories in order to study multi-effect iodine behaviour. The effects of radioactivity could be investigated by a <sup>60</sup>Co radiation source. Important parameters like temperatures and pH could be adjusted. Iodine behaviour in the liquid and gaseous phase as well as

deposition on steel and painted surfaces was examined under dry and wet conditions. The RTF experimental setup is shown in Figure 4.3-8. The vessel itself has a volume of 340 l. In the PHEBUS/RTF-1 test a liquid pool of 30 l is present inside. The instrumentation and measurement lines are displayed in the figure.

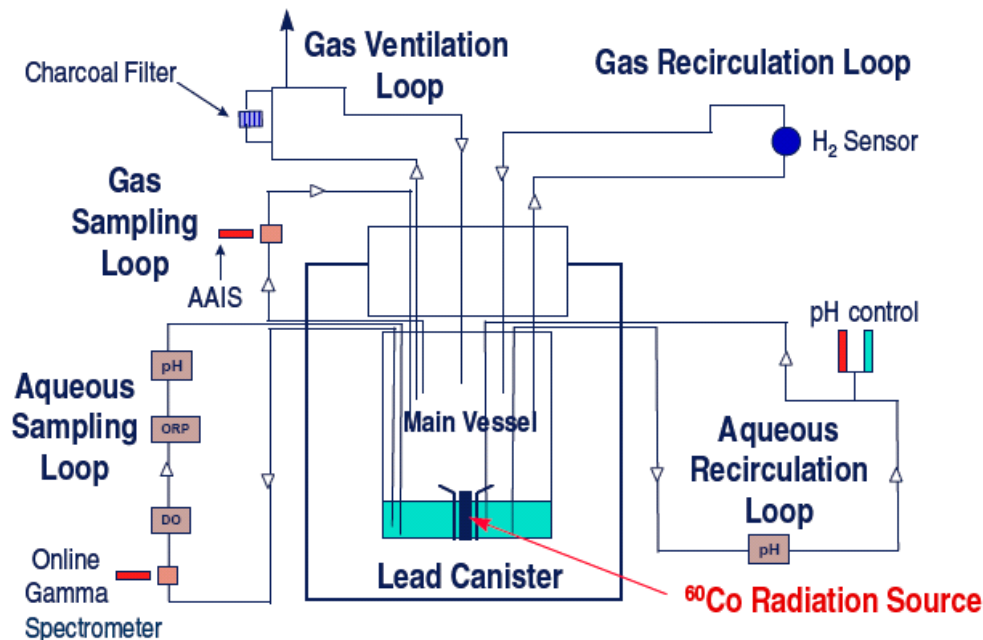


Figure 4.3-8 Schematic of the PHEBUS/RTF Facility from /GLO 08/

#### 4.3.2.2 ASTEC input deck

The used ASTEC input deck is an IODE stand-alone dataset that is available under the validation directory of ASTEC V2.0r1. For the version ASTEC V2.0r2 the used reaction names in the input have changed and so the dataset was updated to that delivered in the validation directory of that version. The dataset consists of a single containment compartment 'COMP1' with a volume of 0.34 m<sup>3</sup> and a 0.03 m<sup>3</sup> liquid part inside. A painted surface of 0.015 m<sup>2</sup> in the wet part and 0.072 m<sup>2</sup> in the dry part is modelled. The steel surfaces are 2.207 m<sup>2</sup> in the dry part and 0.523 m<sup>2</sup> in the wet part. A continuous pH of 4.9 is adjusted in the water sump with a temperature of 90 °C. The atmosphere temperature is 110 °C. The pH is controlled to 4.9 during the whole experiment. In both the sump and the gas phase a dose rate of 0.294 Gy/s is adjusted. In the beginning of the experiment a mass of 3.81\*10<sup>-5</sup> kg I<sup>-</sup> is present in the sump. This corresponds to a concentration of 10<sup>-5</sup> mol/l in the liquid phase. In the course of the experiment this amount of iodine forms different chemical compounds, settles on surfaces, and is released into the atmosphere part. The COCOSYS input is a modified dataset of an open post-calculation with the AIM model available in COCOSYS. This was originally calculated with COCOSYS V2.0AA including AIM-F1 and is now calculated with the version V2.4(dev) including AIM-F3. The latest description of the AIM model is available in a GRS-A report /WEB 09/. Information on the used COCOSYS dataset is available in /BAL 04/.

### 4.3.2.3 Results

In the following a comparison between the ASTEC versions V2.0r1 (red) and V2.0r2 (green) as well as with COCOSYS V2.4(dev) (blue) and experimental measurements (black) is given. A comparison between the iodine models IODE in ASTEC and AIM-F3 in COCOSYS has to be done with care. In difference to the thermal hydraulic models these models are not directly related to each other. Nevertheless, a comparison is performed in order to keep the same procedure as in the thermal hydraulic experiments. Figure 4.3-9 shows the total iodine concentration in the sump. The measurement curve decreases during the experimental time of 72 h from  $10^{-5}$  to  $5 \cdot 10^{-6}$  mol/l. The principle behaviour is well calculated by both ASTEC versions as well as by COCOSYS. In this logarithmic plot the COCOSYS concentration decreases with a straight line and reaches a concentration of  $5 \cdot 10^{-6}$  mol/l after 72 h. ASTEC V2.0r1 calculates a slightly lower concentration and reaches  $4.5 \cdot 10^{-6}$  mol/l at the end of the calculation. The new ASTEC version V2.0r2 calculates first lower concentrations and after 45 h higher concentrations than COCOSYS. In the end  $5.5 \cdot 10^{-6}$  mol/l are reached.

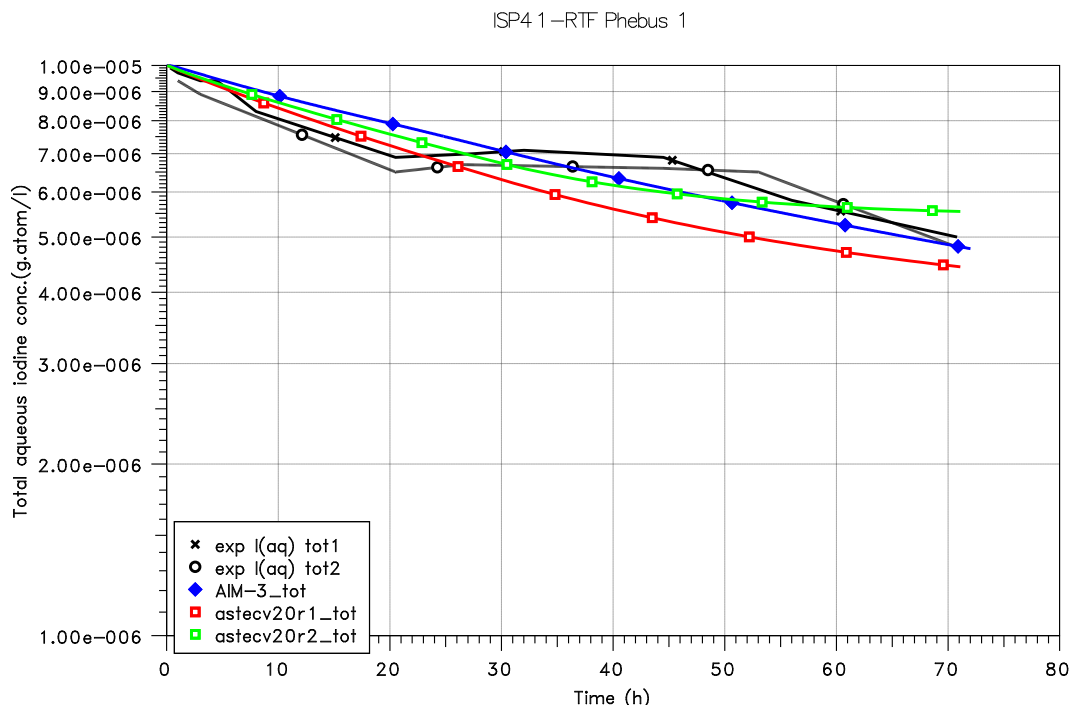


**Figure 4.3-9 RTF-1, Total liquid iodine concentration**

The concentrations of the different chemical compounds in the sump are displayed in Figure 4.3-10. In the experiment only the total sump concentration was measured, so the figure gives only a comparison between COCOSYS and both ASTEC versions. Almost all iodine stays in the form of iodide I<sup>-</sup>. ASTEC calculates an I<sub>2</sub> concentration with a maximum of  $5 \cdot 10^{-8}$  mol/l. This is in good accordance to COCOSYS. The HOI concentration is in the beginning at  $1 \cdot 10^{-8}$  mol/l. After 30 h it rises a little. This is also in accordance with COCOSYS. The CH<sub>3</sub>I concentration is up to  $5 \cdot 10^{-10}$  for ASTEC and  $10^{-10}$  mol/l for COCOSYS in the beginning. At the end both codes calculate  $2 \cdot 10^{-10}$  mol/l. A large difference between COCOSYS and ASTEC is the concentration of iodate in the sump. While ASTEC calculates a fast rise to  $3 \cdot 10^{-7}$  mol/l, COCOSYS calculates only a concentration of  $5 \cdot 10^{-11}$  mol/l after 72 h. There are some differences between both ASTEC versions especially after 30 h and later. The differences in the I<sup>-</sup>

concentration are relevant for the different total iodine concentration in Figure 4.3-9 as this is the dominant species in the water pool.

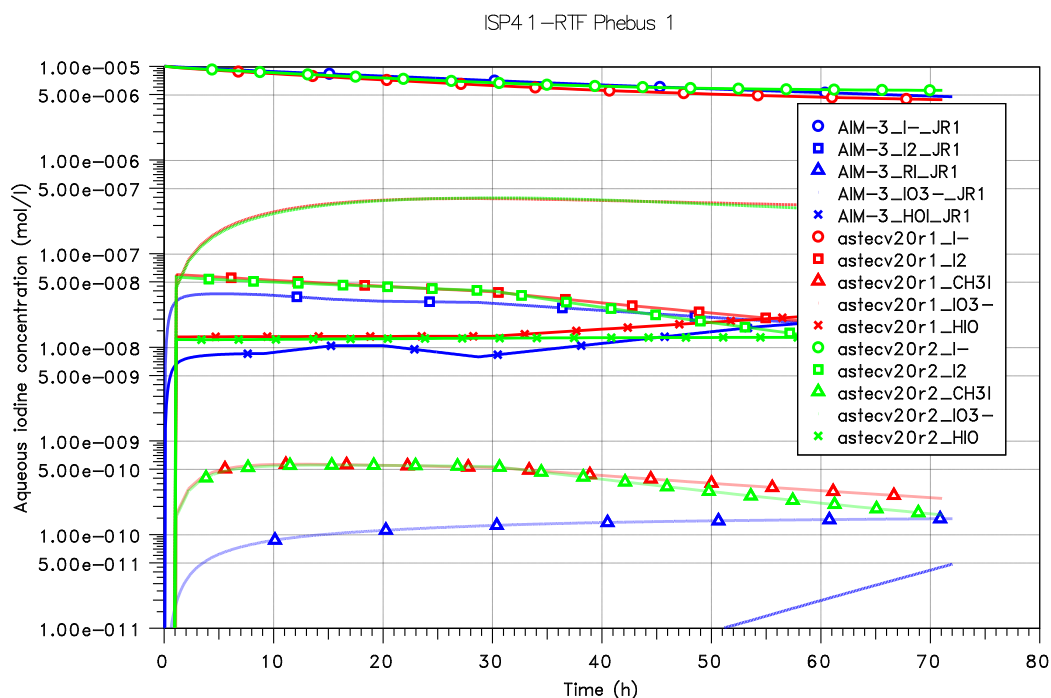


**Figure 4.3-10 RTF-1, Liquid compound concentration**

The iodine depositions on steel and painted wall structures inside the sump volume are shown in Figure 4.3-11. Overall ASTEC calculates a higher wall deposition in the sump area. The iodine concentration on paintings is  $7 \times 10^{-4}$  mol/m<sup>2</sup> after 70 h. COCOSYS calculates only  $10^{-4}$  mol/m<sup>2</sup> of molecular iodine and  $6 \times 10^{-6}$  mol/m<sup>2</sup> of iodide. On steel surfaces ASTEC calculates up to  $5 \times 10^{-5}$  mol/m<sup>2</sup> and COCOSYS calculates no steel deposition at all. In AIM it is assumed that I<sub>2</sub> deposited on steel surfaces is converted to I<sup>-</sup>, which is dissolved in the water. Both ASTEC versions show only minor differences.

The total gaseous iodine concentration is presented in Figure 4.3-12. Both codes deliver results in the range of the experimental measurements of  $10^{-9}$  to  $5 \times 10^{-9}$  mol/l. The ASTEC concentrations are slightly higher than the COCOSYS results. A maximum is reached after about 5 h. Later the concentration decreases due to settling on the walls inside the RTF. The recent ASTEC version calculates first a higher and after 53 h a slightly lower concentration compared to version V2.0r1.

A separation into the species I<sub>2</sub> and CH<sub>3</sub>I is given in Figure 4.3-13. ASTEC calculates a higher iodine concentration than COCOSYS, but the results of the old version are closer to COCOSYS. The new version also calculates a higher iodomethane (CH<sub>3</sub>I) concentration compared to COCOSYS. In the beginning the old ASTEC version is closer to COCOSYS and in the end the new version is closer to the COCOSYS results.

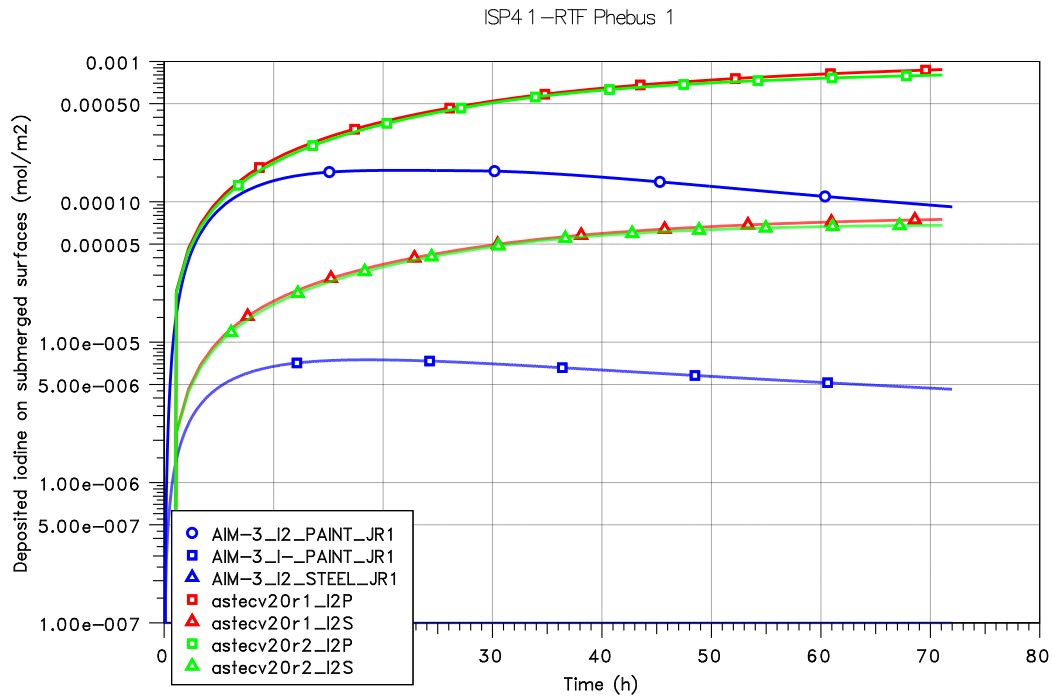


Figure 4.3-11 RTF-1, Wall deposition in liquid phase

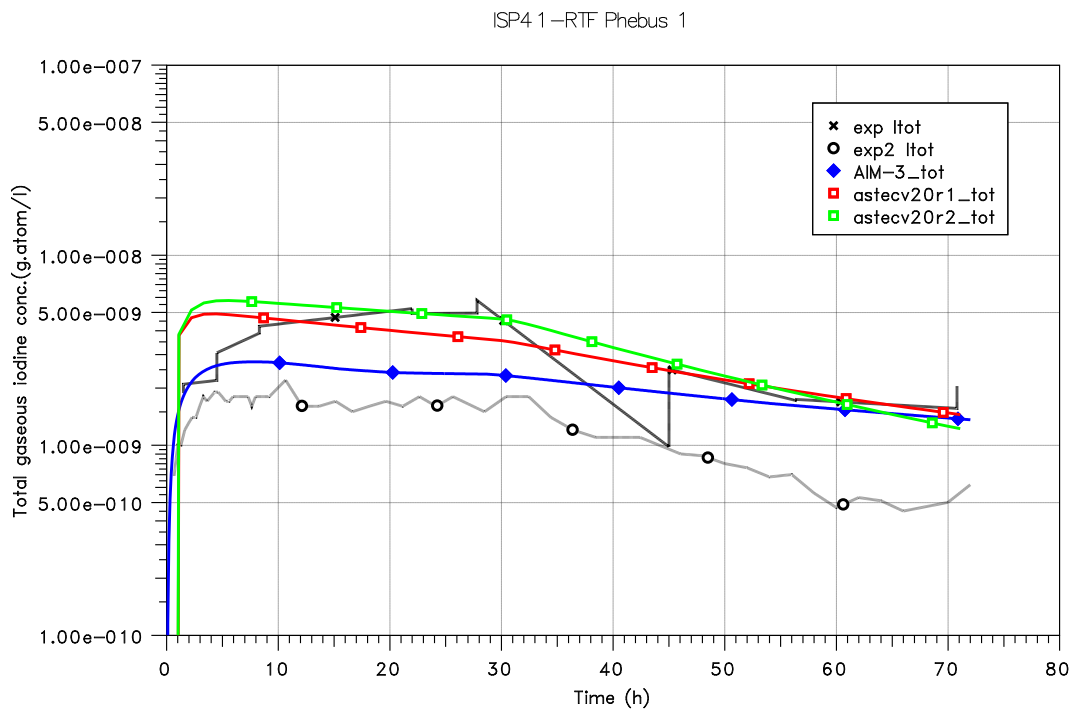
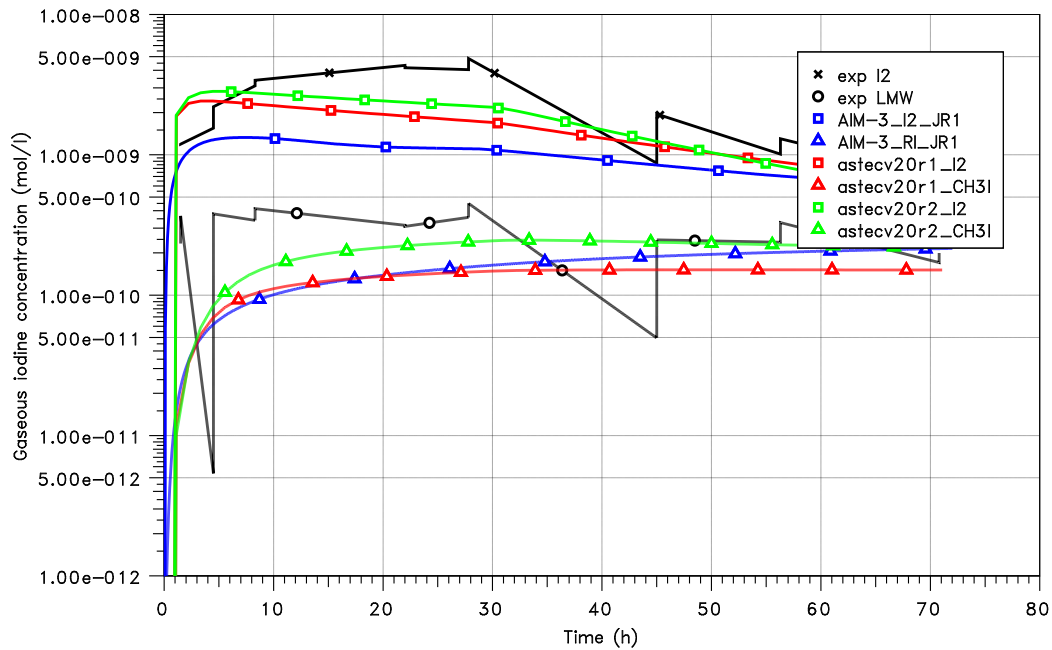


Figure 4.3-12 RTF-1, Total gaseous iodine concentration

ISP4 1 –RTF Phebus 1



**Figure 4.3-13 RTF-1, Gaseous compound concentration**

In comparison to ASTEC, COCOSYS calculates a higher deposition on walls in the gaseous region. This behaviour is shown in Figure 4.3-14 (no experimental values for comparison available). COCOSYS calculates a total iodine deposition of 0.001 mol/m<sup>2</sup> on painted surfaces. The old ASTEC version result is only a third of the COCOSYS result. V2.0r1 calculates a concentration that is closer to the COCOSYS result. Concerning the deposition on steel surfaces, COCOSYS distinguishes between the desorption of iodine and the subsequent chemical reaction to FeI<sub>2</sub> that has an increased bounding to the surface. Overall COCOSYS calculates an iodine concentration of 5\*10<sup>-6</sup> mol/m<sup>2</sup> on steel surfaces. ASTEC does not treat the formation of FeI<sub>2</sub> explicitly. The maximum concentration is only 5\*10<sup>-8</sup> mol/m<sup>2</sup>. The RTF Phebus1 results for COCOSYS show a stronger deposition on the surfaces in the gaseous part of the RTF compared to ASTEC. Therefore, the iodine concentrations in the gaseous region are lower compared to ASTEC.

ISP4 1 –RTF Phebus 1

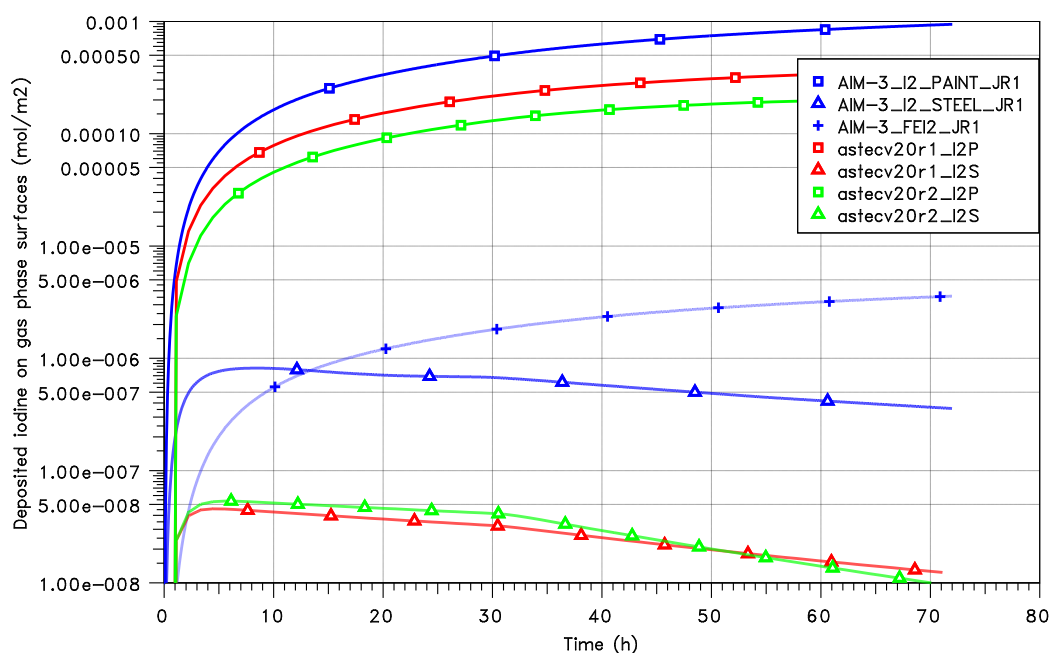


Figure 4.3-14 RTF-1, Wall deposition from gaseous phase

#### 4.3.2.4 Summary

Concerning the comparison between ASTEC and COCOSYS, the overall liquid and gaseous iodine concentrations calculations of both codes are in good accordance with the experiment. The calculation of different species on surfaces, in the liquid phase and in the gaseous phase show partly strong deviations between COCOSYS and ASTEC. These differences are not surprising as the iodine models in both codes deviate from each other. A detailed comparison of different iodine species with the experiment is not possible as they were not measured in the experiment. Concerning both ASTEC versions, large differences in the IODE calculations occur that can be explained with the improvements of the IODE model that were conducted between both ASTEC versions investigated. Details of the IODE modelling improvements are given in chapter 3 as it is described in /CHA 11/.

### 4.4 Hydrogen combustion

#### 4.4.1 ENACCEF RUN 153

Since version V2.0, ASTEC is capable to calculate hydrogen combustion without much additional effort by using the FRONT model. Two respective experiments are incorporated in ASTEC regression testing: In the small scale ENACCEF facility, the flame acceleration during hydrogen deflagration due to obstacle passing is investigated. The Hx23 experiment in the BMC model containment (ch. 4.4.2) represents a large (real) scale scenario.

#### 4.4.1.1 Test facility

The ENACCEF (Eneinte d'Accération de Flamme) facility is situated at Orleans (France) and operated by CNRS with the purpose to study hydrogen deflagration. It is a vertical facility made of steel (62 l volume) consisting of a 3.3 m long and narrow “acceleration tube” (inner diameter: 0.154 m), where the ignition and flame acceleration takes place, and of a large 1.7 m long vessel (called “dome”) for the burn-out of the flame (Figure 4.4-1).

The hydrogen-gas mixture is ignited at the bottom of the acceleration tube by a spark. In the middle of the acceleration tube, up to nine annular “obstacles” might be inserted (distance between each obstacles: 0.154 m). The first obstacle is 0.638 m from the ignition point.

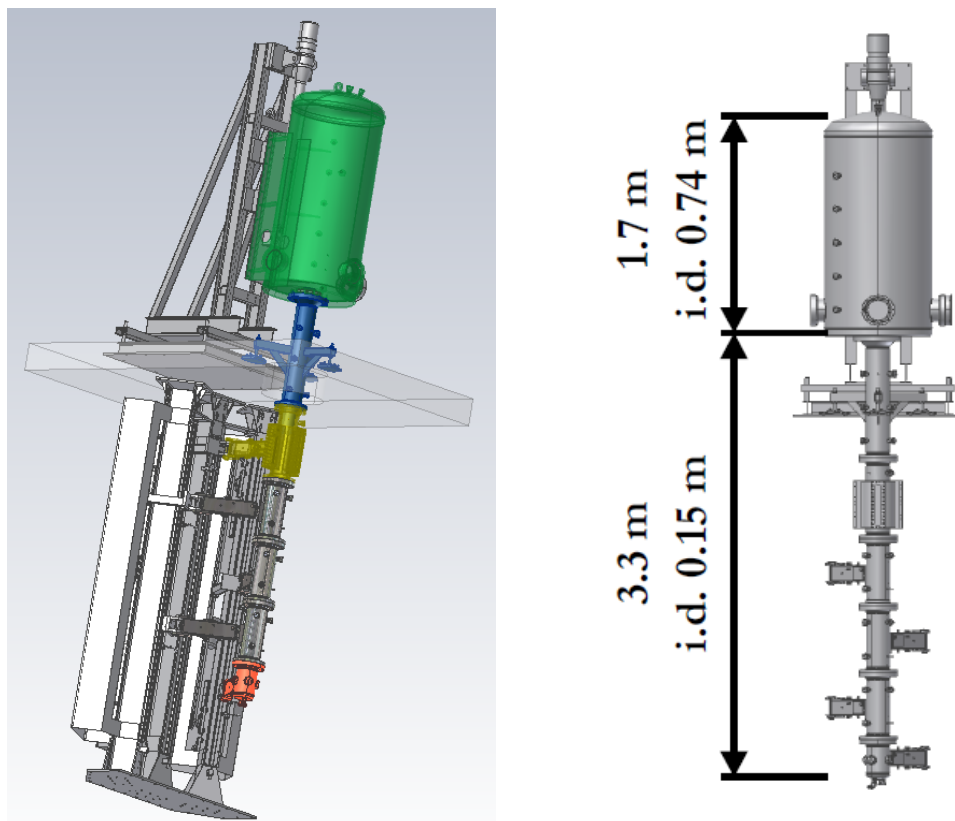
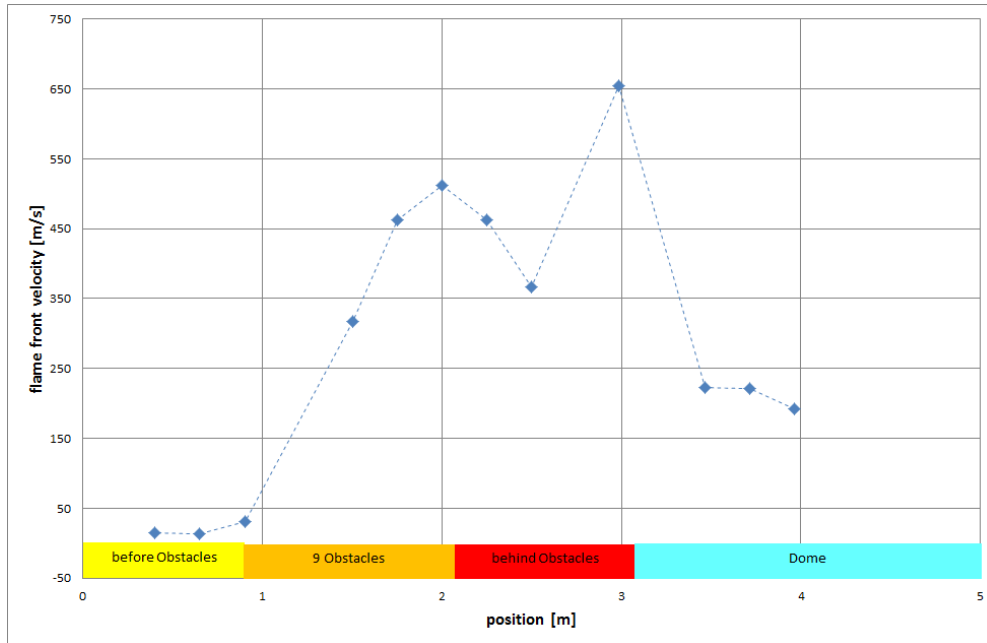


Figure 4.4-1 Overview and sketch of the ENACCEF facility /CHA 10/.

#### 4.4.1.2 Experiment ENACCEF Run153

For the ENACCEF run 153, which were used in SARNET-2 WP 7.2 Benchmark Exercise, nine obstacles with a blockage ratio of 0.63 were inserted in the acceleration tube. The facility was filled with 87 vol% air and 13 vol% hydrogen /BEN 10/.



**Figure 4.4-2 Measured flame front velocities**

The measured flame front velocities are given in Figure 4.4-2. After ignition, the flame front accelerated up to 500 m/s in the obstacle path. The experimental uncertainty of the velocity measurement could not be quantified by the experimentalists and is assumed being large /CHA 10b/. Repetitions of the respective experiment gave flame front velocities up to 650 m/s at the end of the obstacles. Especially the evaluated velocity at the dome entrance varied largely from 300 – 900 m/s.

**4.4.1.3 Nodalization and ASTEC input**

The nodalization in ASTEC for the ENACCEF facility is shown in Figure 4.4-3. The dome is divided in inner cylinder zones and outer ring zones. The zone geometry and junction lengths are exactly taken from the real geometry /HOE 10/. The hydrogen-air mixture is ignited at 1s in zone R2.

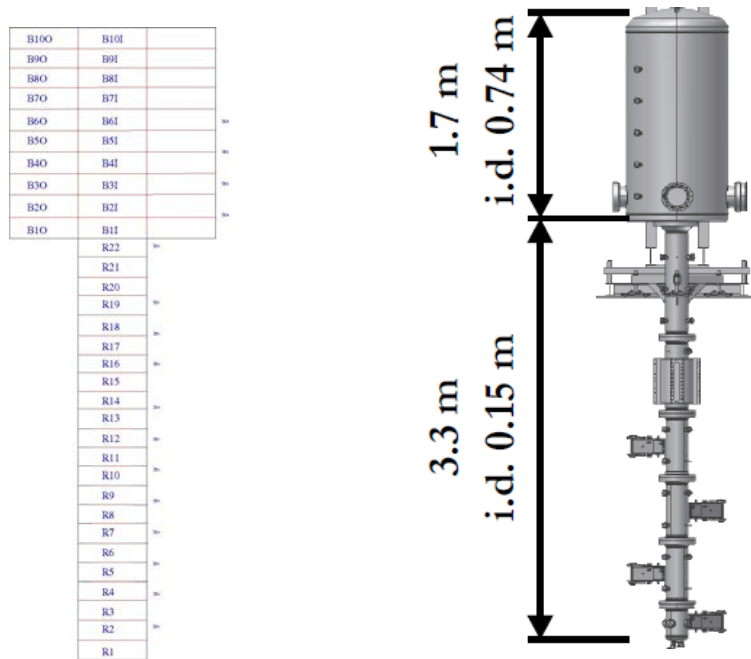


**Figure 4.4-3 ASTEC nodalization for ENACCEF facility**

The input parameters for the FRONT model, which are used in the hydrogen deflagration calculation, are given in Table 4.4-1. Since the calculation of the turbulent flame front velocity is changed from version V2.0r1 to V2.0r2, another choice of the correlation parameters was necessary /ERD 11/. The signification of the parameters is explained in /DEI 03/Deitenbeck, H. ASTEC - Konvertierung von COCOSYS (V1.2) Eingabedaten in ASTEC (V1.0) Eingabedaten und umgekehrt Technische Notiz, GRS, 10.3.2003

/ECK 11/.

**Table 4.4-1 Input parameters for FRONT module for ENACCEF**

| Parameter      | V2.0r1              | V2.0r2 |
|----------------|---------------------|--------|
| H2OUT          | 0.                  | 0.     |
| REYEXP         | -0.12               | -0.12  |
| REYFAC         | 1.5                 | 0.34   |
| TURW           | 0.9                 | 0.9    |
| DTRL           | <i>Not existing</i> | 0.0125 |
| TURLEN_H       | <i>Not existing</i> | 0.     |
| FBURN          | <i>Not existing</i> | 1.0    |
| IZENT (option) | 2                   | 3      |
| COMO (option)  | EXPO                | EXPO   |

**4.4.1.4 Results**

The ASTEC calculated flame front velocities are given in Figure 4.4-4. For V2.0r1, the flame front velocity is no output quantity. The order of magnitude of the calculated

flame front velocities is in agreement with the experimental values (Figure 4.4-2), especially considering the experimental uncertainties.

The calculation of the turbulent flame front velocity in V2.0r1 turned out to model the flame acceleration in the part of the tube *without* obstacles not appropriately (also in experiments completely without obstacles) /HOE 10/: The model in V2.0r1 always assumed the presence of turbulence eddies of the size of the junction's cross diameters. Hence more turbulence was created in parts *without* obstacles than in parts *with* obstacles.

A corresponding improvement of the model was carried out for version V2.0r2, which finally gives slower flame front velocities in parts without obstacles. It was necessary to introduce respective new user given input parameters – the size of the turbulence eddies in absence of obstacles (DTRL: for vertical junctions without obstacles and TURLEN\_H for horizontal junctions).

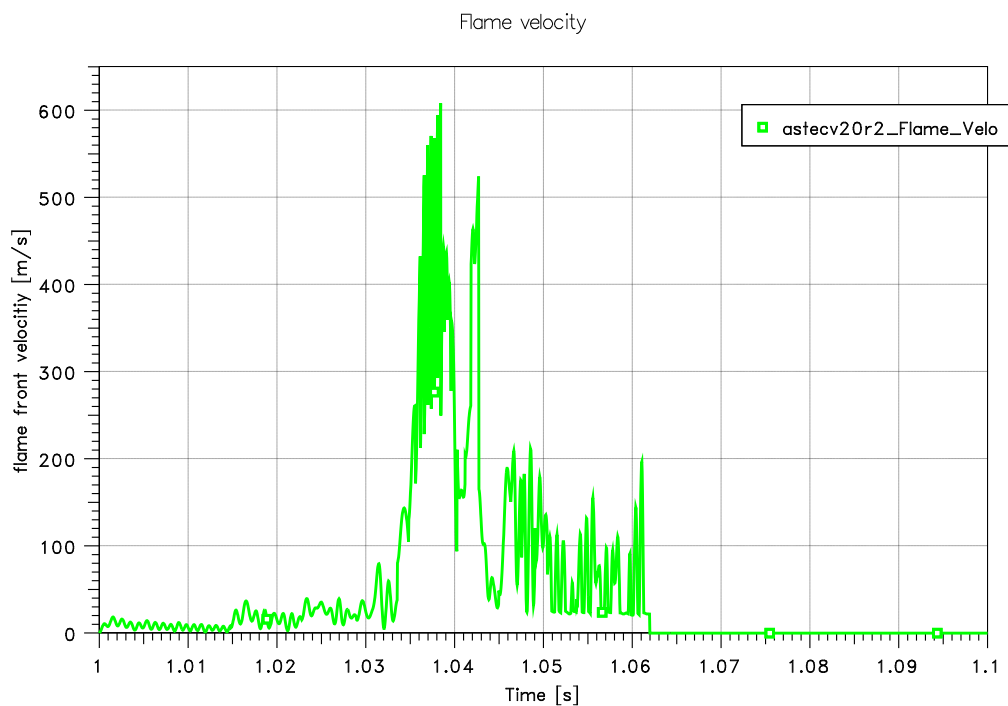


**Figure 4.4-4 Calculated flame front velocity; compare with Figure 4.4-2**

The total pressure increase (Figure 4.4-5) is simulated by ASTEC quite sufficiently. The difference between the two code versions is a changed flame front model and thus changed parameters in Table 4.4-1. The parameters used for the new code version are optimized for the use on the ENACCEF facility. Therefore, the shape of the pressure curve is very well post calculated. But the total pressure increase is also well calculated by the old model with the parameters used for V2.0r1.

Since the exact experimental ignition time is not known (the spark igniter is switched on several times in a row in the experiment because the spark does not ignite directly), the experimental measured pressure is shifted to meet the first pressure peak of the calculations in Figure 4.4-5. This first sharp pressure peak is due to the combustion in the respective zone (pressure build up because of large quantity of burnt gases which do not distribute so fast). It is not clear whether its peak is resolved by the pressure sensor completely.

The “slow” pressure increase up to 4.5 bar within 0.02 s is caused by the combustion in the dome (containing most of the hydrogen present in the facility). The pressure decreases afterwards due to heat losses. Since the thermal material properties of the facility’s steel were not known, these heat losses could not be simulated by ASTEC appropriately.

The gradient of the pressure increase represents the flame front velocity in the dome.

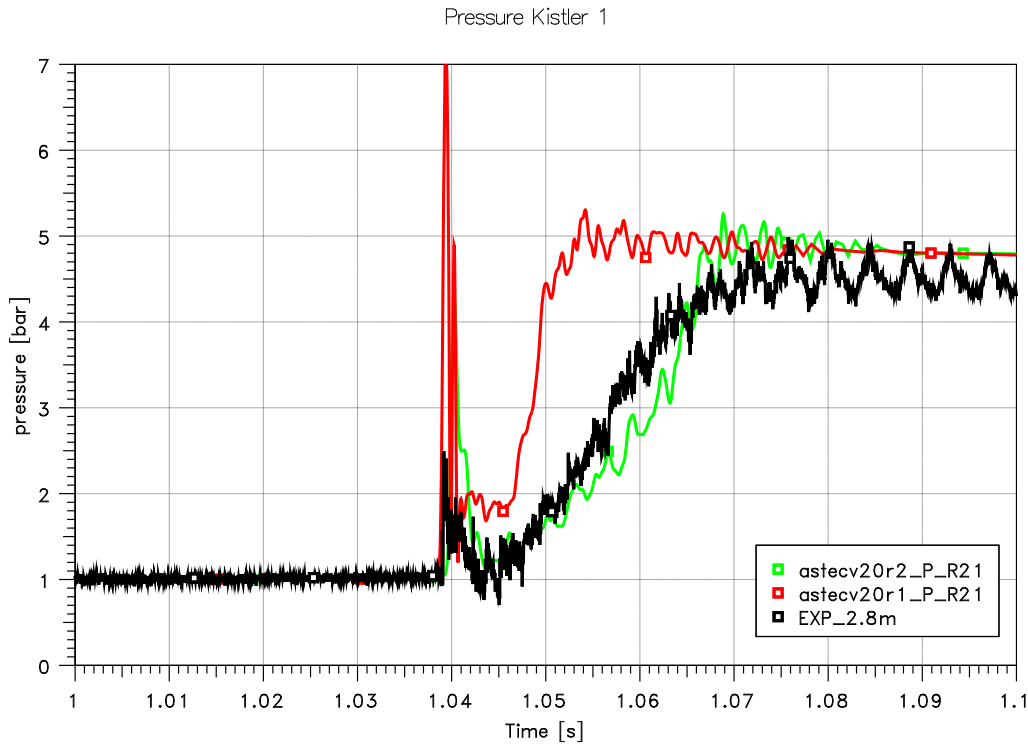


**Figure 4.4-5 Pressure evolution at the dome entrance (2.877m from ignition)**

Figure 4.4-6 shows the calculated gas temperatures between the obstacles, at the end of the acceleration tube and in the dome. When combustion takes place in the respective zone, gas temperature rises very fast. After the dome’s hydrogen is burnt, the heat distribution over the entire facility increases the gas temperatures in the tube again about 200 - 300 °C. The temporal distance between the temperature rises represents as well the flame front velocity.

The same temporal distance can be taken from the hydrogen concentration plot (Figure 4.4-7). The hydrogen in the tube zones is burnt completely. In the dome, the hydrogen deflagration takes place in two directions (lateral and axial) and slows down (Figure 4.4-2). A cloud of un-burnt hydrogen is pushed by the flame front through the dome and reaches already “burnt” zones. Hence in the dome zones, the hydrogen concentration shows an unsteady hydrogen concentration at low level (3 vol% in Figure 4.4-7) after the initial fast decrease.

The starting process of the new code version is a little lower in both graphics. The first ignition peak occurs at the same time, but during the combustion in the dome the temperature rise and hydrogen burn-up is slower in comparison with the old version.

Gas Temperatures

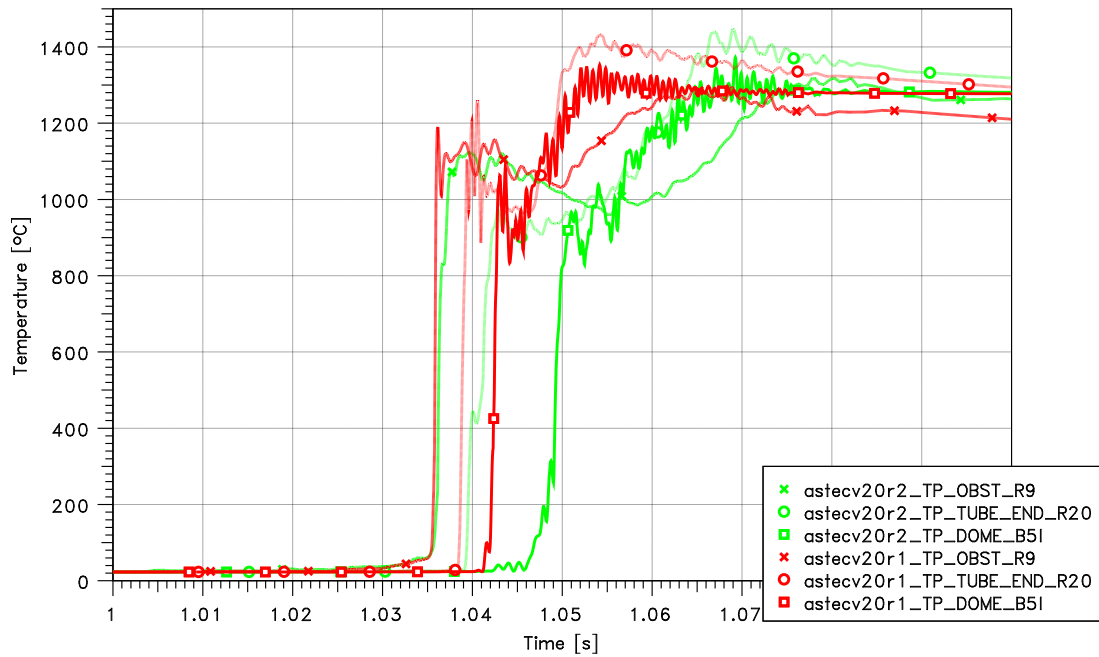


Figure 4.4-6 Gas temperatures in the facility

Hydrogen Concentration

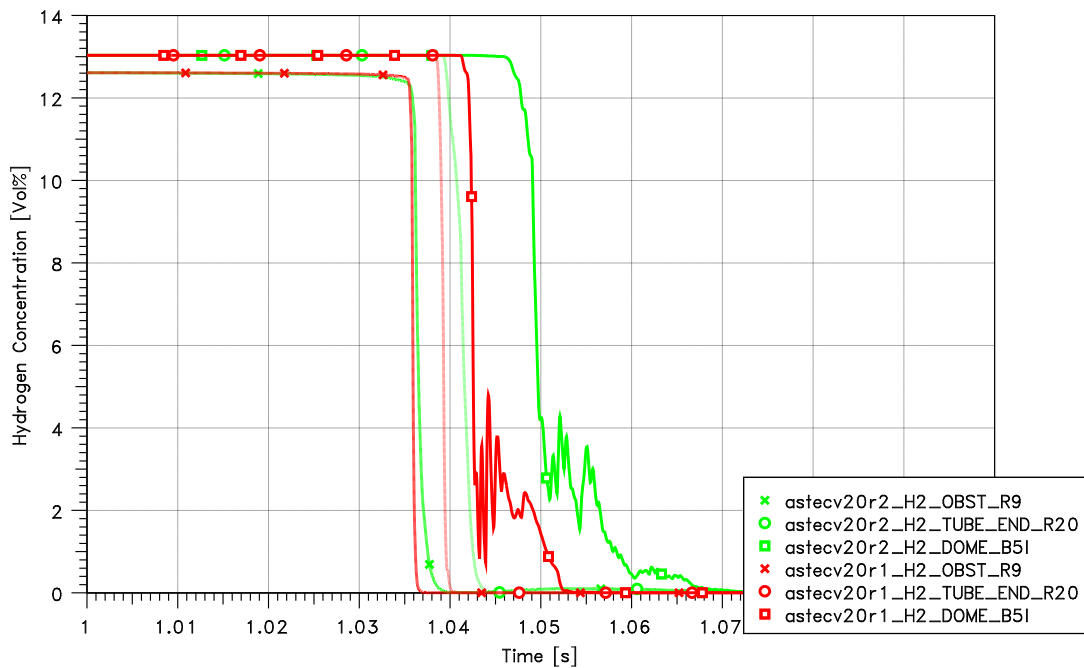


Figure 4.4-7 Hydrogen concentration at different locations in ENACCEF

#### 4.4.1.5 Summary

The essential results of the experiment are reproduced by both ASTEC calculations. Both give flame front velocities in a reasonable order of magnitude and hence an appropriate pressure built up. Just the gas temperature rise and the first peak pressures

seem to be too sharp / fast for V2.0r1. In the V2.0rev1 version, the flame front velocity was overestimated in the absence of obstacles. This inappropriate modeling could be overcome with the V2.0rev2 version. Due to the incorporation of the FRONT model in the differential equation solver FEBE, the numerical behavior is smoother.

#### 4.4.2 BMC Hx23

##### 4.4.2.1 Test facility and description

The Battelle Model Containment (BMC) has a free volume of 626 m<sup>3</sup>. It was built rotationally symmetric of reinforced concrete and is subdivided into several compartments (Figure 4.4-8). Its geometry represents roughly the containment of a PWR.

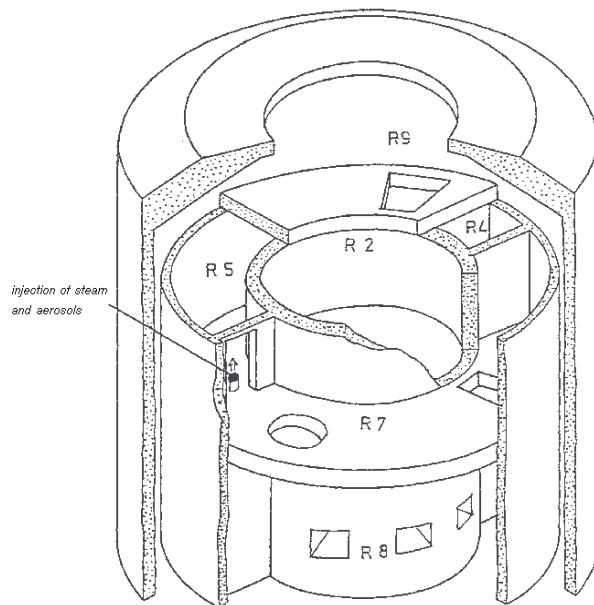
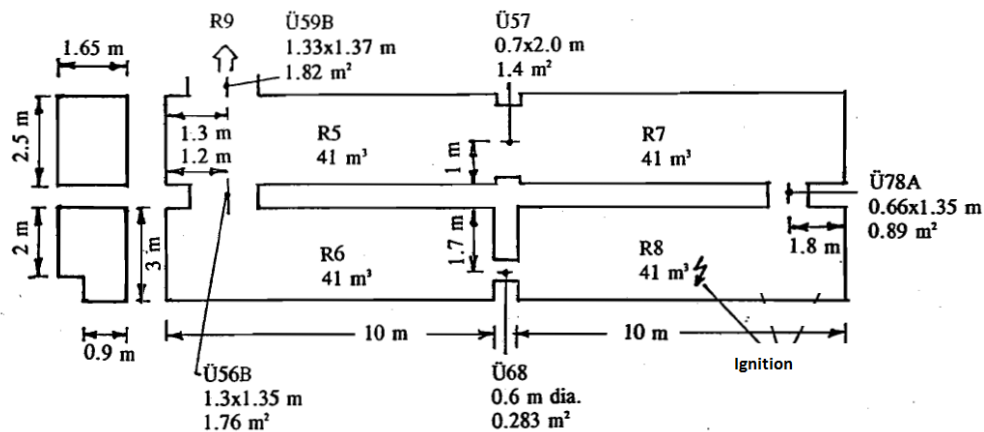


Figure 4.4-8 Battelle Model Containment



centerline curvature radius of compartments nos. R5 to R8: 3.475 m

#### Figure 4.4-9 Five-room geometry for Hx23 experiment

Five rooms of the Battelle Model Containment were used for Hx23 experiment (Figure 4.4-9). The compartments R5 – R8 were filled with 9 vol% hydrogen. The connections between the rooms are displayed in Figure 4.4-9. The gas was ignited in room R8. The flame travelled along two paths (through room right side of R8, R7 and R5 respectively through left side of room R8, R6 and R5). Afterwards, the mixture could leave the system into the huge expansion room R9 (see Figure 4.4-8), which was not filled with hydrogen.

#### 4.4.2.2 Nodalization and ASTEC input

The considered five rooms are nodalized very coarsely (Figure 4.4-10), especially compared to the very detailed nodalization for the small scale ENACCEF facility (ch. 4.4.1.3).

In the past calculations with ASTEC V2.0r1 have been performed by Luther /LUT 09/ and with the development version which included the improvements for V2.0r2 version by Erdmann /ERD 11/. For both the V2.0r1 model and the improved V2.0r2 version, input parameters different from the ones used for the ENACCEF facility had to be used (Table 4.4-2 in comparison with Table 4.4-1).

In the V2.0r1 calculation /LUT 09/, “COMO=LINEAR” was used giving a “slower” start of the hydrogen combustion in the ignition zone. /ERD 11/ chose different factors REYFAC and REYEXP for the turbulence correlation and a different eddy size in absence of obstacles (DTRL) in comparison to the respective ENACCEF calculation.

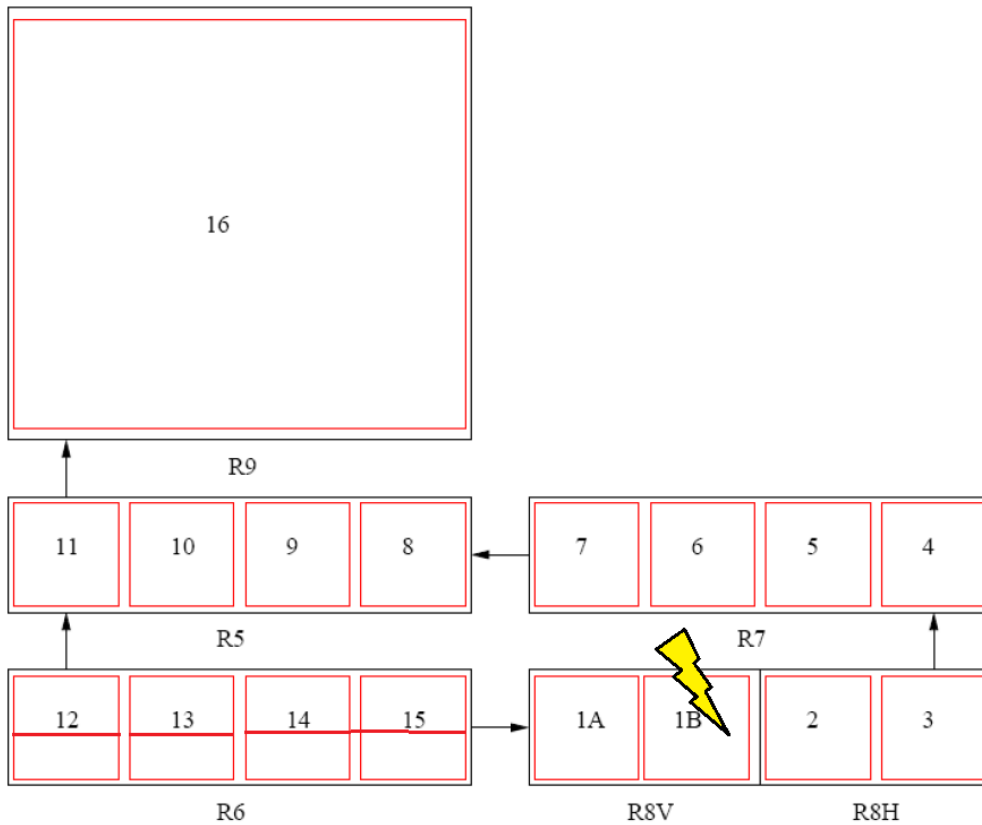


**Figure 4.4-10 ASTEC nodalization for Hx23 \*)**

\*) - Rooms R5-R8 are divided in four zones horizontally, room R6 additionally in two vertical layers. The ignition zone R1B is indicated with a lightning bolt.

**Table 4.4-2 Input parameters for FRONT module for Hx23 (for their signification see /DEI 03/Deitenbeck, H. ASTEC - Konvertierung von COCOSYS (V1.2) Eingabedaten in ASTEC (V1.0) Eingabedaten und umgekehrt Technische Notiz, GRS, 10.3.2003**

/ECK 11/)

| Parameter      | V2.0r1              | V2.0r2 |
|----------------|---------------------|--------|
| H2OUT          | 0.                  | 0.     |
| REYEXP         | -0.12               | -0.12  |
| REYFAC         | 1.5                 | 1.5    |
| TURW           | 0.9                 | 0.9    |
| DTRL           | <i>Not existing</i> | 0.001  |
| TURLEN_H       | <i>Not existing</i> | 0.     |
| FBURN          | <i>Not existing</i> | 1.0    |
| IZENT (option) | 2                   | 3      |
| COMO (option)  | LINEAR              | LINEAR |

### 4.4.2.3 Results

The experimental pressure (Figure 4.4-11) and temperature (Figure 4.4-12) curves are shifted 1.8 s to meet the calculated results of the V2.0r1 calculation. The version V2.0r2 calculates a faster deflagration, so this peak is 0.3 earlier than the experiment. Due to the choice of “COMO=LINEAR”, the hydrogen combustion in the ignition zone begins very slowly leading to the “delay” of pressure and temperature increase compared to the experimental values. The new code version starts faster and the largest pressure peak is reached about 0.3 s earlier compared to V2.0r1. The initial pressure increase has the same shape as in the old version. Afterwards a second pressure increase is more pronounced in the new version. The final pressure is lower with the new version and closer to the experiment.

Hx23 Experiment

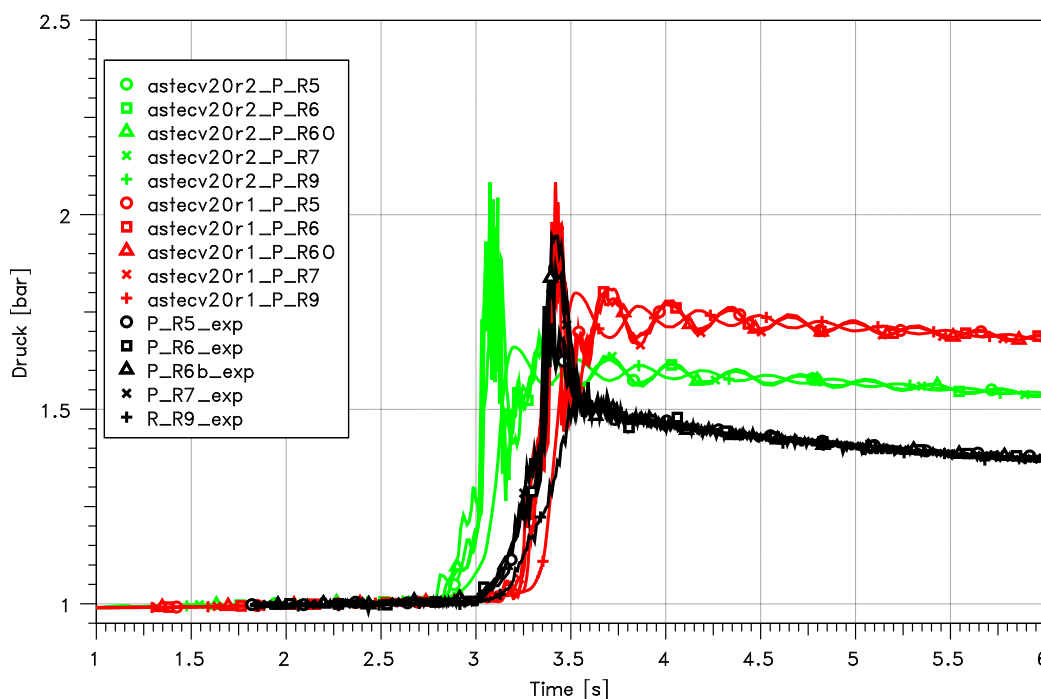


**Figure 4.4-11 Pressure in the BMC Hx23 experiment**

The course of the flame through the five rooms can be reconstructed with the gas temperature measurement (Figure 4.4-12). In the experiment, firstly the temperatures in the ignition compartment begin to rise slowly, followed by R6 (horizontal adjacent room) and – a little later - R7 (vertical adjacent room). But the temperature rise in R7 is faster than in the two other rooms (indicating faster combustion). R5 is of course the last room that is reached by the combustion. The new ASTEC version shows an earlier temperature rise due to the faster ignition behaviour. Especially the temperature rise in the ignition zone R8 is much slower compared to the old calculation.

The sequence of the rooms in the calculation is the same as in the experiment, but all temperatures (except the one in the ignition compartment R8) rise very quickly. The combustion in R7 seems not to be faster than in the other rooms. The larger difference between the beginning of temperature rise in R6 and R7 in the calculation is caused by the position of the considered zones no. 6 and 14.

The overestimation of the gas temperatures by both calculations is a reported general inadequacy of FRONT /ERD 11/.

Hx23 Experiment

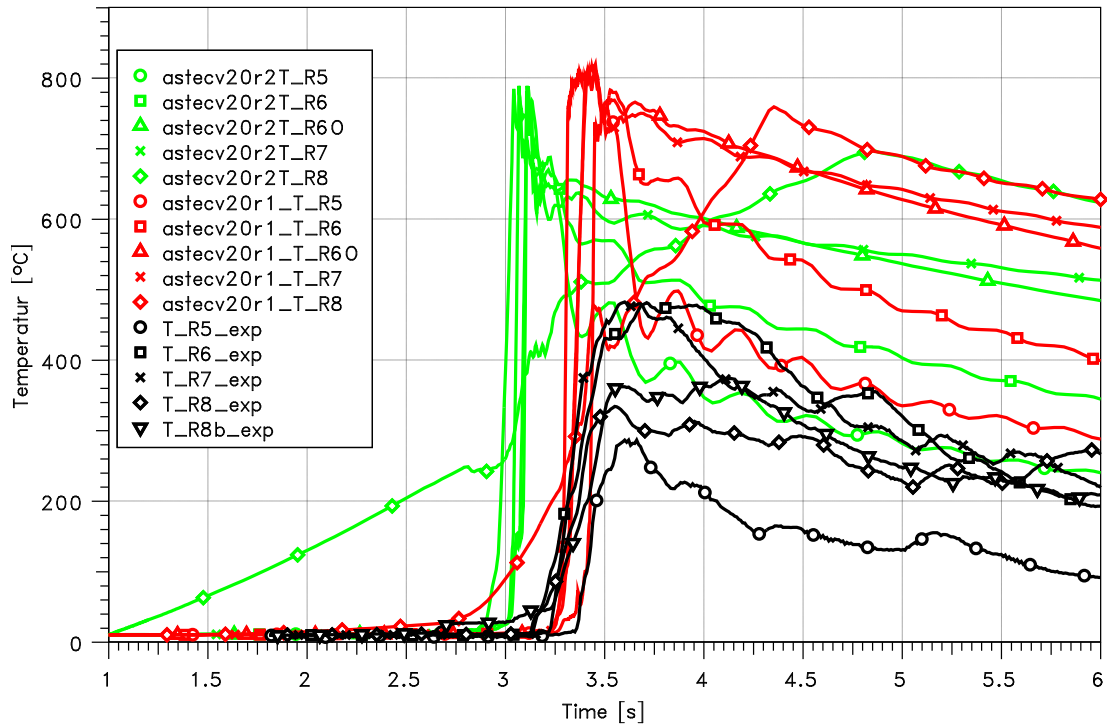


**Figure 4.4-12 Temperature in the BMC Hx23 experiment**

The calculated hydrogen concentrations (Figure 4.4-13) illustrate as well the course of the flame front. Due to the pressure built up caused by combustion, hydrogen is pushed into R9, where it is not burnt in the calculation.

Hx23 Experiment

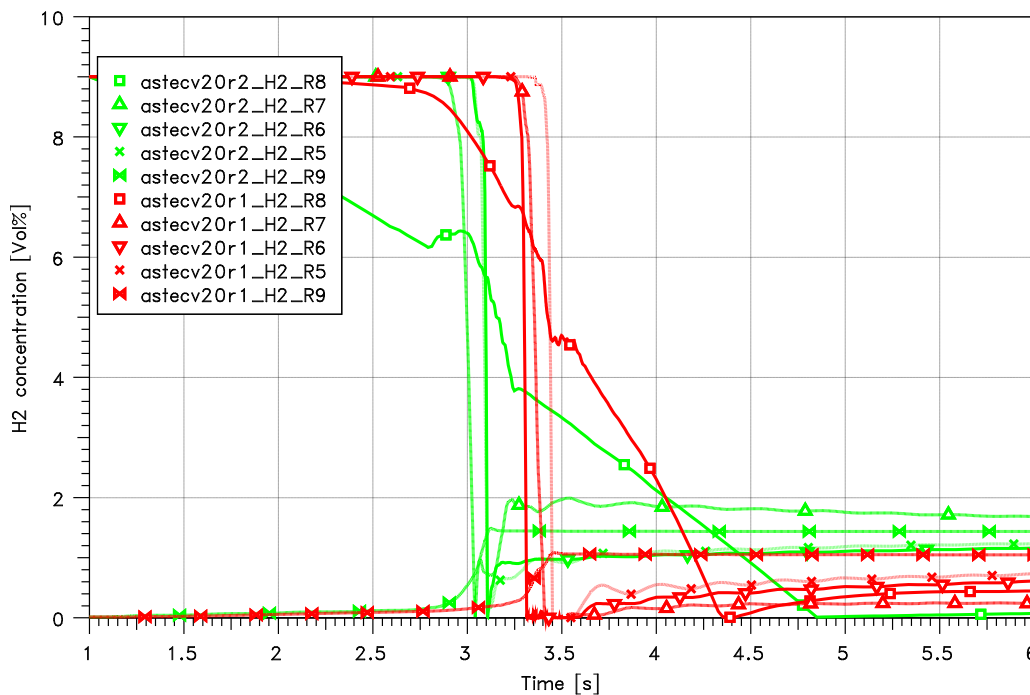


Figure 4.4-13 Hydrogen concentration in Hx23 experiment

4.4.2.4 Summary

The essential results of the experiment are reproduced by both ASTEC calculations. Differences between the two versions are related to the model improvement. The measured maximum pressure is reproduced quite satisfyingly (Figure 4.4-11) while the overestimation of the pressure after the end of combustion is related to the overestimation of temperature.

4.5 Molten corium concrete interaction (MCCI)

Two stand-alone calculations of MEDICIS, the ASTEC module for MCCI, were carried out for regression testing. They use either core melt with stratified oxide and metal layer (COMET-L3) or unstratified mixed core melt with thermal properties similar to plain oxidic melt (OECD-CCI-2). These are the two essential different possible configurations of the core melt which might occur during a severe accident.

Furthermore, both experiments represent the two most important kinds of concrete: While COMET-L3 used siliceous concrete (mainly used in German plants), OECD-CCI-2 investigates limestone concrete (mainly used in USA) which is known to release much more gases (CO<sub>2</sub>, Steam etc.) when MCCI occurs.

In both experiments, concrete is exposed to hot melt generated by thermite reaction. After a phase of undisturbed erosion of the concrete by MCCI, water was poured onto the melt surface (after 10 min (COMET-L3) resp. 5 h (OECD-CCI-2)) while decay heat simulation continued.

4.5.1 OECD-CCI-2

4.5.1.1 Test facility

An overview of the CCI test section at the Argonne National Laboratory (USA) is given in Figure 4.5-1. The melt is prepared by a thermite reaction directly in the cavity surrounded by the investigated concrete. After the thermite reaction, the melt has a temperature of ~2000 °C and covers a surface in the concrete cavity of 0.5 m x 0.5 m.

In order to simulate the decay heat of the molten core material, the melt is now heated directly with electrical current flowing through the melt (DEH: Direct Electrical Heating). The corresponding Tungsten electrodes provide constantly 120 kW input target power and cover a surface of 120 cm width and 91 cm depth (blue in Figure 4.5-2). Hence heating is provided even after the melt has eroded the sidewall concrete and the basemat.

The electrodes are protected by UO<sub>2</sub> pellet layer and backup plates; the respective sidewall consists of MgO. Hence the melt can only erode the concrete of the basemat and the sidewalls which are not covered with the electrodes.

Thermocouple trees are inserted in the concrete of the sidewall and in the initial melt in order to measure melt temperature and arrival times.

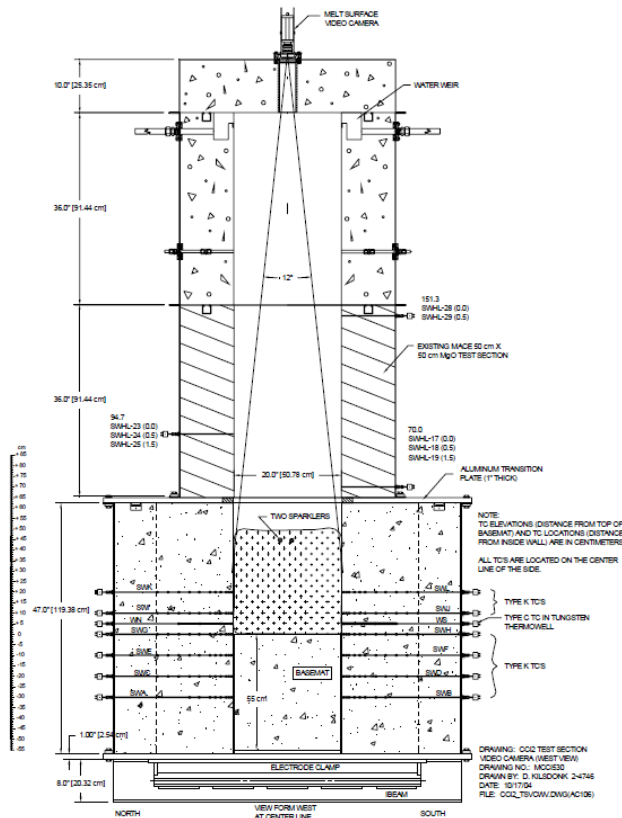
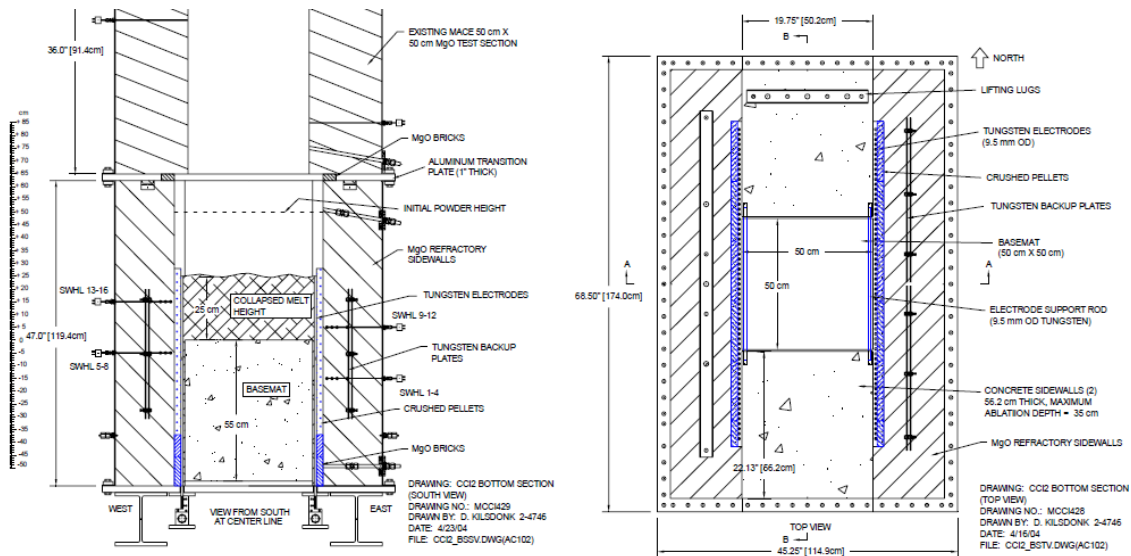


Figure 4.5-1 General view of the OECD-CCI-2 Test Section /FAR 04/



**Figure 4.5-2 Side view (left) and top view (right) of the MCCI-part of OECD-CCI-2 Test Facility (in blue: Tungsten electrodes for direct electrical heating /FAR 04/)**

The used concrete is Limestone/Common Sand (LCS) type. The 400 kg corium melt shall represent 100 % oxidized PWR-corium with 8 weight% of concrete. The detailed composition is given in Table 4.5-1.

**Table 4.5-1 Composition of Corium in OECD-CCI-2**

| Constituent       | Weight%           |
|-------------------|-------------------|
| UO <sub>2</sub>   | 60.62             |
| ZrO <sub>2</sub>  | 24.9              |
| Calcined Concrete | 8.07 <sup>2</sup> |
| Cr                | 6.41              |

#### 4.5.1.2 Experiment OECD-CCI-2

After preparation of the melt (~30 s), undisturbed MCCI was admitted for 5 hours. The melt did not stratify (mixed oxidic melt), but a crust formed at its surface. The melt was heated constantly with 120 kW input target power.

After 5 hours, surface flooding (2 litres/second, 20 °C) was initiated. Power input carried on with constant voltage (i.e. decreasing power). The test was terminated after 7 hours because concrete temperatures had stabilized (no more erosion).

The final erosion profile of the concrete is given in Figure 4.5-3. Lateral and axial (horizontal and vertical) ablation rates turned out to be approximately the same.

<sup>2</sup> Calcined limestone/common sand concrete, consisting of 42.0 / 14.1 / 38.8 / 5.1 wt% of SiO<sub>2</sub> / MgO / CaO / Al<sub>2</sub>O<sub>3</sub>.

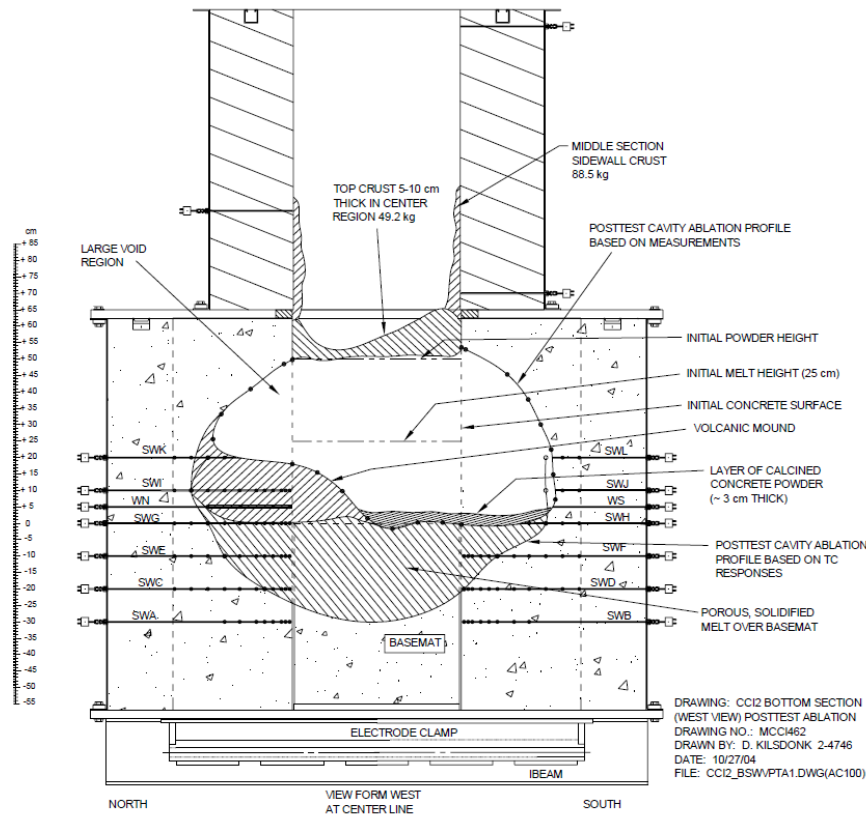


**Figure 4.5-3 Cavity Erosion Profile at the end of OECD-CCI-2 - maximal vertical and maximal horizontal erosion lengths are approximately the same /FAR 04/**

#### 4.5.1.3 ASTEC input

OECD-CCI-2 is calculated with a stand-alone MEDICIS. In concordance with the experimental facility, a not axial-symmetric cavity with initially 150 points was used. The initial temperature is set to 2273 K.

The effective heat transfer coefficient from the melt is set constant ( $HTEFF = 3$ ) to  $HEFF = 200 \text{ W}/(\text{m}^2\text{K})$  at the corium/concrete interface and to  $HEFF = 300 \text{ W}/(\text{m}^2\text{K})$  in vertical upward direction (interface to gas and water). The crust at the melt surface is not modelled as own layer.  $T_{liquidus}$  and  $T_{solidus}$  of the corium are given as user input.

#### 4.5.1.4 Results

The melt temperatures (Figure 4.5-4) before surface flooding (at 18 000 s) are simulated quite well by both ASTEC calculations, which give identical results.

Temperature of oxide layer

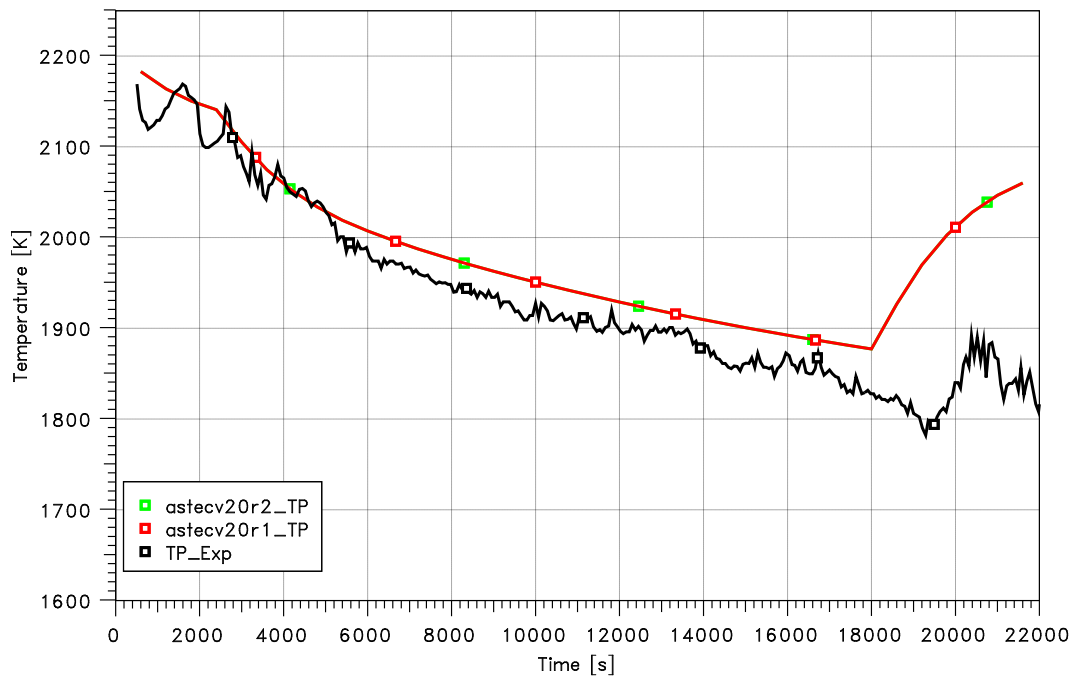


**Figure 4.5-4 Temperature of the melt (single layer)**

In MEDICIS, there is still a lack of models which capture the heat transfer from melt to water at surface flooding appropriately. Hence the melt temperatures after 18 000 s are not calculated satisfyingly.

Both simulations agree as well for the ablation rates (radial Figure 4.5-5 and horizontal Figure 4.5-6). ASTEC reproduces the main effect observed in the experiment: Lateral and axial ablation rates are the same since effective heat transfer coefficients HEFF are given equally for horizontal and downward direction

Horizontal Ablation

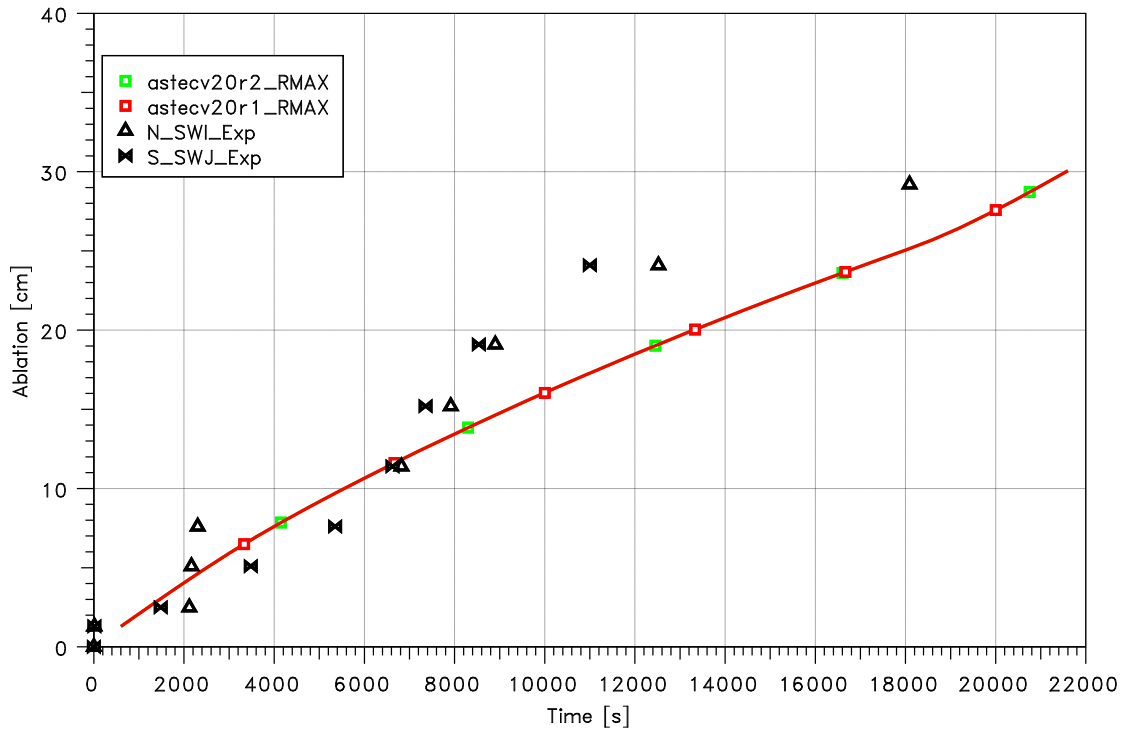


**Figure 4.5-5 Maximal horizontal (lateral) ablation (at +10cm elevation, see Figure 4.5-3)**

Vertical Ablation

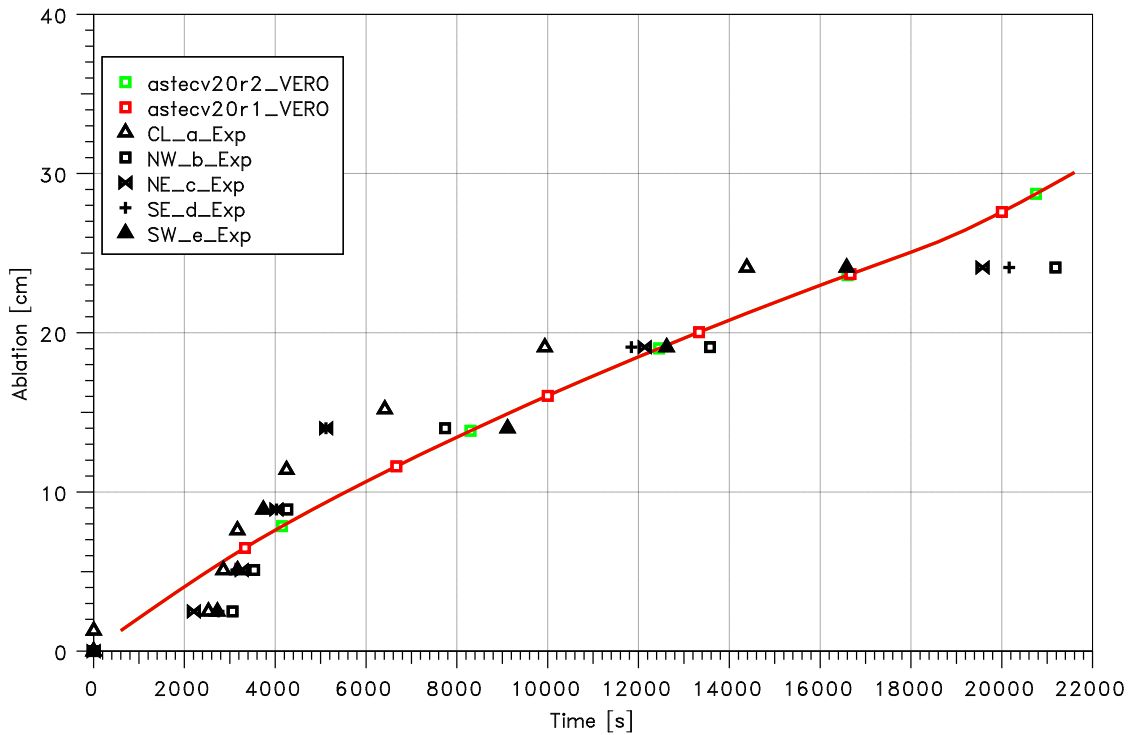


**Figure 4.5-6 Vertical (axial) ablation**

## 4.5.2 COMET L3

### 4.5.2.1 Test facility

An overview of the COMET (Core Melt Test) test section located at Forschungszentrum Karlsruhe (Germany) is given in Figure 4.5-7. The melt is generated by thermite reaction in a separate reaction vessel outside of the main test section (with the concrete cavity). After the thermite reaction (which usually lasts ~ 30 s), the metal and the oxide layers start to separate (usually completed after 1 min). Now the melt is poured into the main test section (Figure 4.5-7). The metal layer is denser than the oxide layer and hence stays at the bottom.

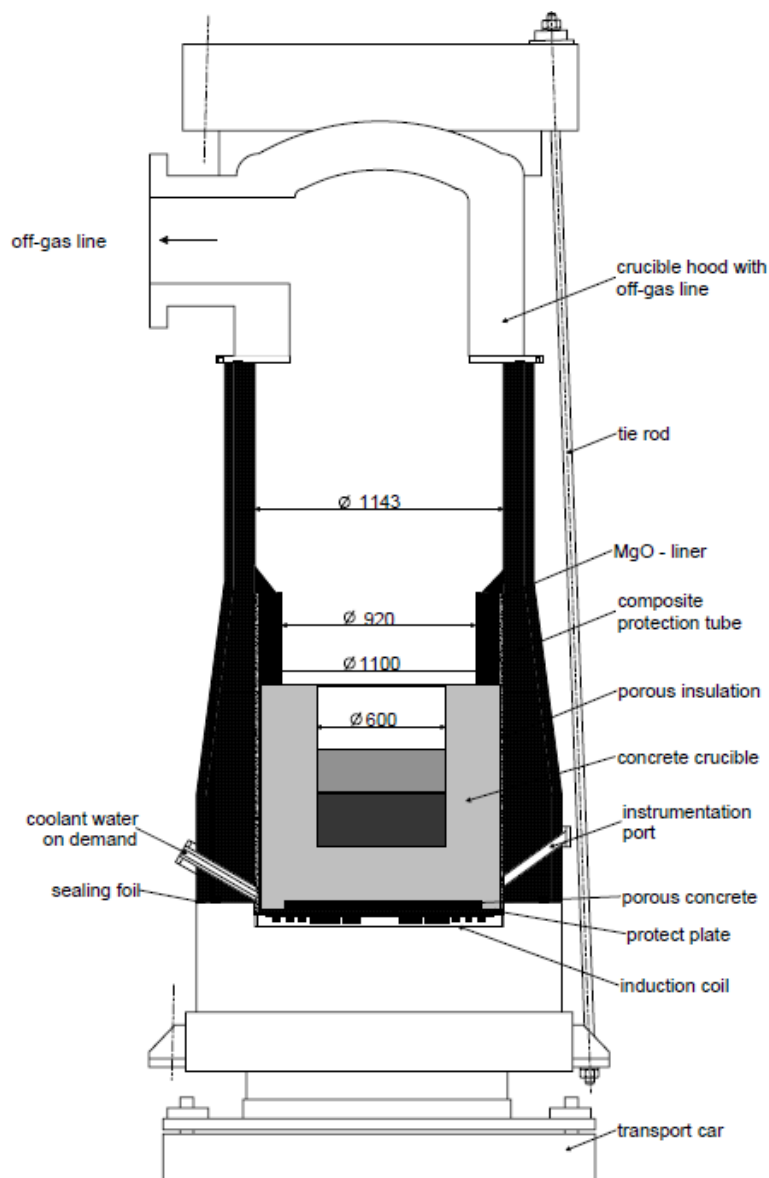


Figure 4.5-7 Overview: COMET test facility /ALS 07/

The concrete cavity is radial symmetric with an initial diameter of 0.6 m. Beneath the concrete cavity, there is a water-cooled induction coil in order to simulate the decay heat: the electromagnetic field created by the induction coil (max. 2600 V, 1200 A) couples to the metallic layer of the melt. The maximal equivalent rated upper heating power is 400 kW. The “net” heating power depends on several parameters like the temperature dependent electrical properties of the metal layer, the distance between induction coil and metal layer (decreases with continuing erosion in downward direction etc.).

When the downward erosion exceeds 90 mm, surface flooding is initiated by a spray system (shower) in the hood of the main test vessel (0.375 litres/s).

Thermocouple trees are inserted into the concrete basemat and sidewall in order to measure the erosion of the concrete: These thermocouples fail when getting in contact with the melt. Hence the melt temperatures are not measured. There is just an infrared camera at the top of the hood which measures the surface temperature of the upper (oxide) layer (resp. of its crust).

#### 4.5.2.2 COMET L3 Experiment

The concrete used in COMET L3 is siliceous concrete type (see Table 4.5-2). The composition of the melt is given in Table 4.5-3. The metal layer consisted of 425 kg melt and the oxide layer of 211 kg. The initial temperature of the metal layer is measured by a W-Re-(Wolfram-Rhenium)-thermocouple (COMET L3: 1664 °C).

**Table 4.5-2 Composition of concrete in COMET facility**

| Constituent                    | Weight% |
|--------------------------------|---------|
| SiO <sub>2</sub>               | 70.3    |
| Ca(OH) <sub>2</sub>            | 13.55   |
| Al <sub>2</sub> O <sub>3</sub> | 6.58    |
| CaCO <sub>3</sub>              | 5.46    |
| Free water                     | 4.11    |

**Table 4.5-3 Composition of the melt in COMET L3 test**

| Constituent                    | Weight%     |             |
|--------------------------------|-------------|-------------|
|                                | Metal layer | Oxide layer |
| Fe                             | 90.0        | -           |
| Ni                             | 10.0        | -           |
| Al <sub>2</sub> O <sub>3</sub> | -           | 56.25       |
| CaO                            | -           | 43.75       |

After preparation, the melt was poured within 254 s into the main test cavity. The decay heat simulation by the induction coil was set to net equivalent heating power  $P_{net} = 200$  kW (slow increase from 180 kW up to 230 kW due to reduced distance between metal layer and induction coil, later reduced manually to 200 kW again).

Dry erosion of the concrete took place until 800 s when the erosion reached 90 mm in vertical direction. Afterwards, top flooding was initiated. The net heating power was

kept at 200 kW until the vertical ablation reached 180 mm (at 1878 s) and was finished afterwards. The final erosion of the cavity is displayed in Figure 4.5-8 and Figure 4.5-9. Axial ablation (vertical downwards) was stronger than lateral ablation (horizontal) – different than in OECD-CCI-2 test (section 4.5.1).

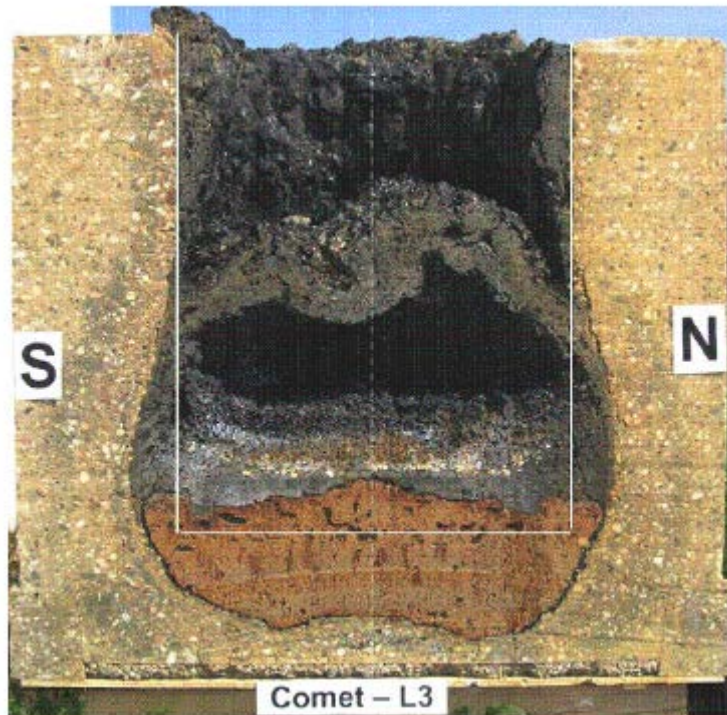


Figure 4.5-8 Picture of the N-S-plane cut of COMET L3 cavity; white lines indicate the initial cavity /ALS 07/

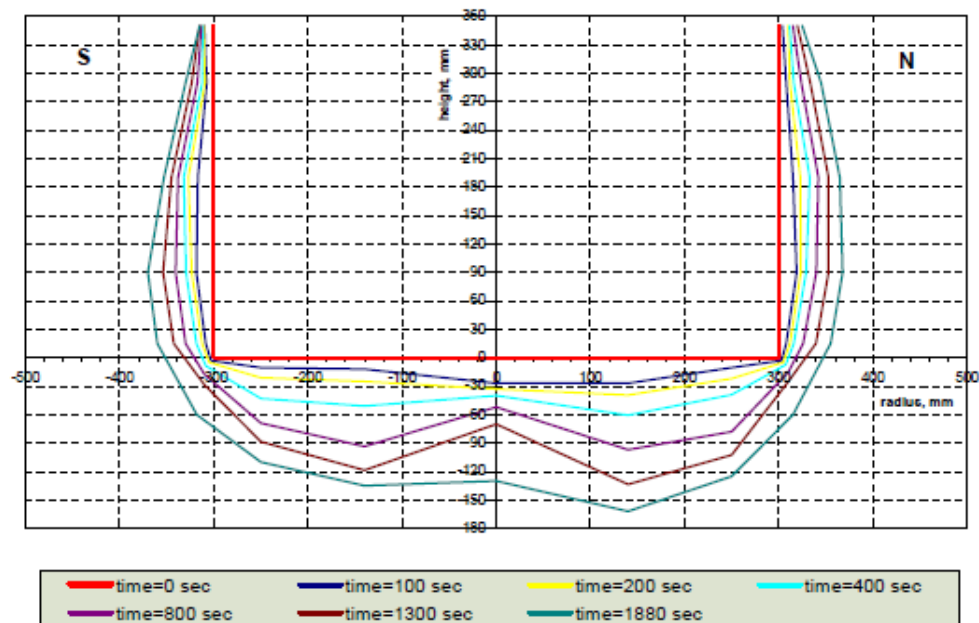


Figure 4.5-9 Time dependent erosion of the cavity in COMET L3 /ALS 07/

### 4.5.2.3 ASTEC input

COMET L3 is calculated with a stand-alone MEDICIS version. The axial-symmetric cavity is simulated with 150 points. The initial temperature of both melt layers is set to 1938 K (=1664 °C).  $T_{liquidus}$  and  $T_{solidus}$  of the corium are given as user inputs (equally for both calculations).

The effective heat transfer is set constant (HTEFF = 3) according to Table 4.5-4. In order to capture the difference between horizontal and vertical erosion rate, the respective heat transfer coefficients are set differently.

**Table 4.5-4 Heat transfer coefficients for the different orientations in W/m<sup>2</sup>K in both calculations**

| Direction  | Metal layer | Oxide layer |
|------------|-------------|-------------|
| downward   | 1600.       | 200.        |
| horizontal | 500.        | 180.        |
| upward     | 2000.       | 200.        |

For the heat transfer between the metal and oxide layer, the Greene correlation is used. The experimental convection coefficient between the two layers is estimated to 2000 W/m<sup>2</sup>K. Hence the scaling factor FGREEN was adjusted in both calculations in order to achieve (approximately) the desired value and was finally set to 0.015.

The corresponding heat transfer coefficients are given in Figure 4.5-10. In the new version the calculated heat transfer is slightly lower compared to the previous version. The crust is not modelled as own layer.

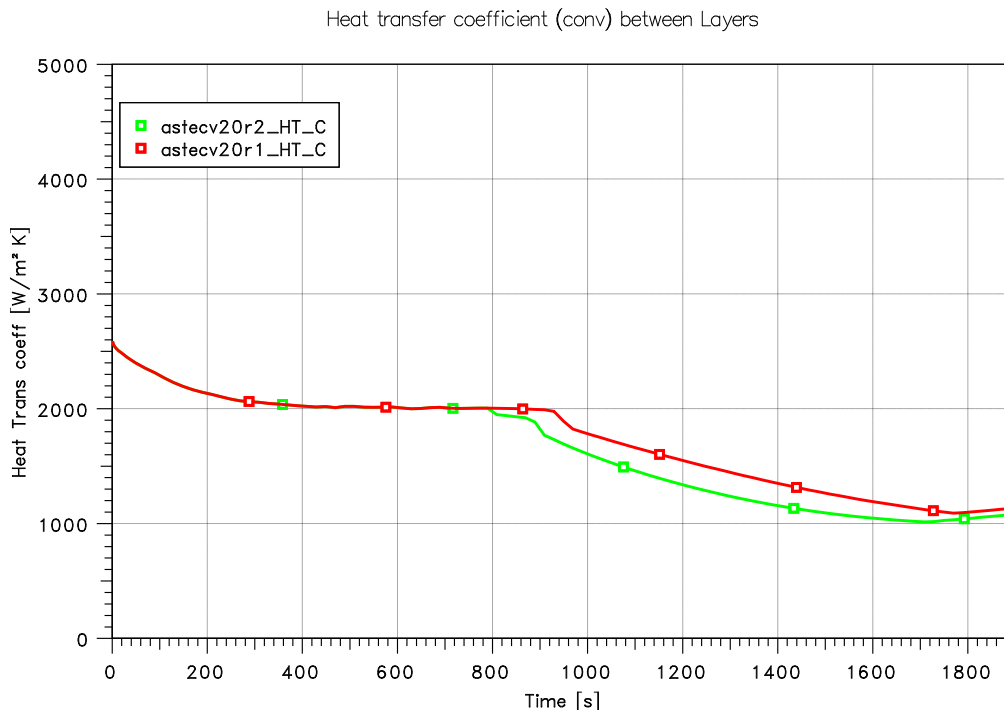


**Figure 4.5-10 MEDICIS calculated heat transfer coefficients between metal and oxide layer**

#### 4.5.2.4 Results

The calculated temperature of the metal (Figure 4.5-11) is exactly the same in both calculation, but the temperature in the oxide layer (Figure 4.5-12) is a little lower in the new version V2.0r2. This is direct consequence of the lower heat transfer coefficient in Figure 4.5-10. Both temperatures decrease jointly while the concrete erosion progresses further. Since the experimental IR-measurements just give the surface temperatures of the oxide layer, not the bulk temperatures, there are no measured temperatures for a comparison.

Due to the differently chosen heat transfer coefficients for the different directions, ASTEC succeeds in reproducing the experimentally observed difference between the axial and lateral ablation rates (Figure 4.5-13 and Figure 4.5-14). The agreement with the experimental measured data is very satisfyingly.

Nevertheless, the total eroded mass of concrete in the experiment after test end is slightly overestimated (Figure 4.5-15). Actually, this mass was determined experimentally after the test end and cool down of the cavity (and not at 1 900s as indicated in Figure 4.5-15). Since the melt was still hot and liquid at 1 878 s (when the heating of the lower metal layer was switched off), the total eroded mass in the experiment exactly at 1 878 s might be a bit less than indicated in Figure 4.5-15.

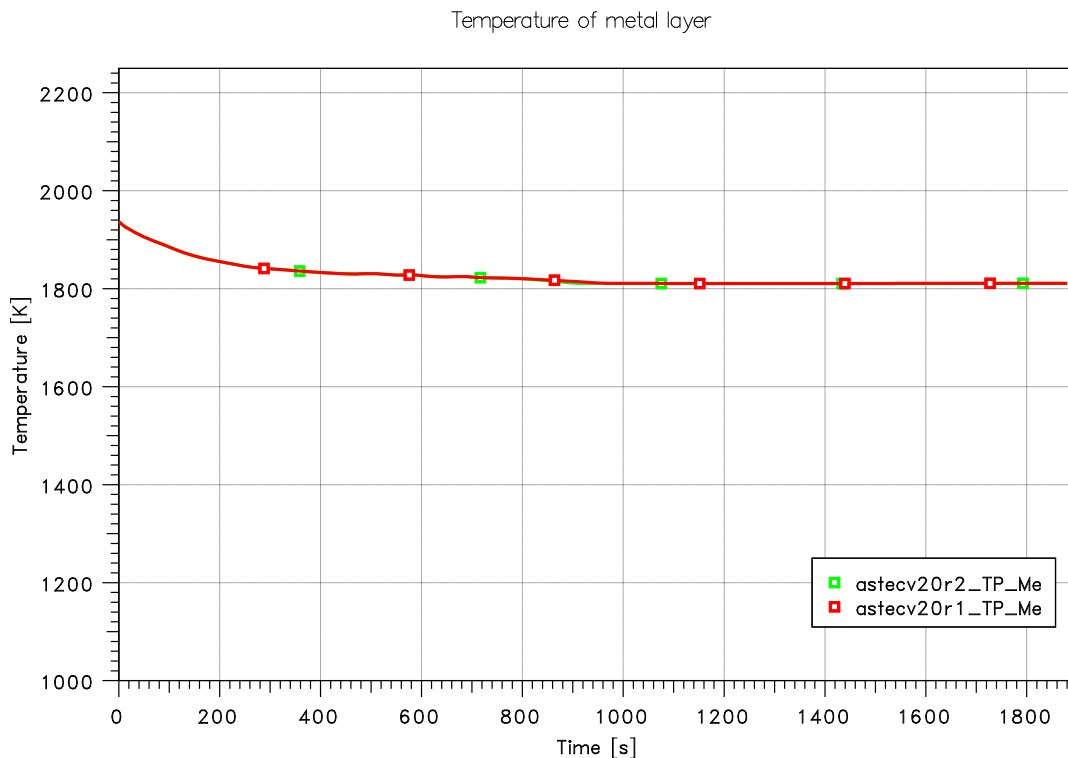


**Figure 4.5-11 MEDICIS calculated temperature of the metal layer in COMET L3**

Temperature of oxide layer

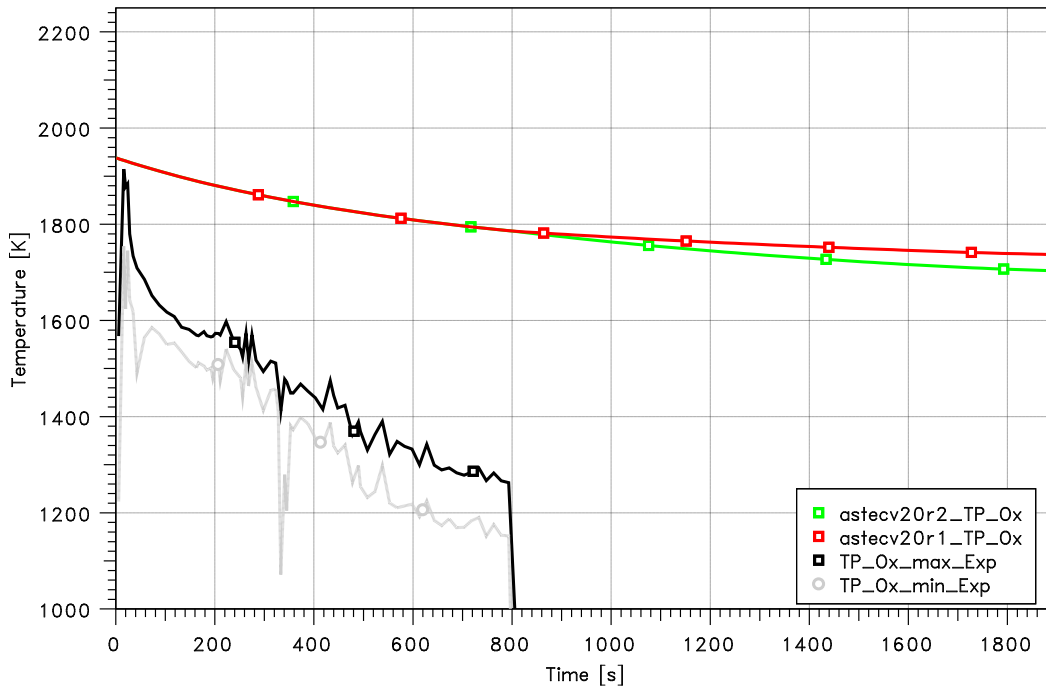


**Figure 4.5-12** MEDICIS calculated temperature of the oxide layer bulk in COMET L3 (red / green). Black/ grey: IR-measured maximal and minimal oxide layer surface temperature.

Axial Ablation

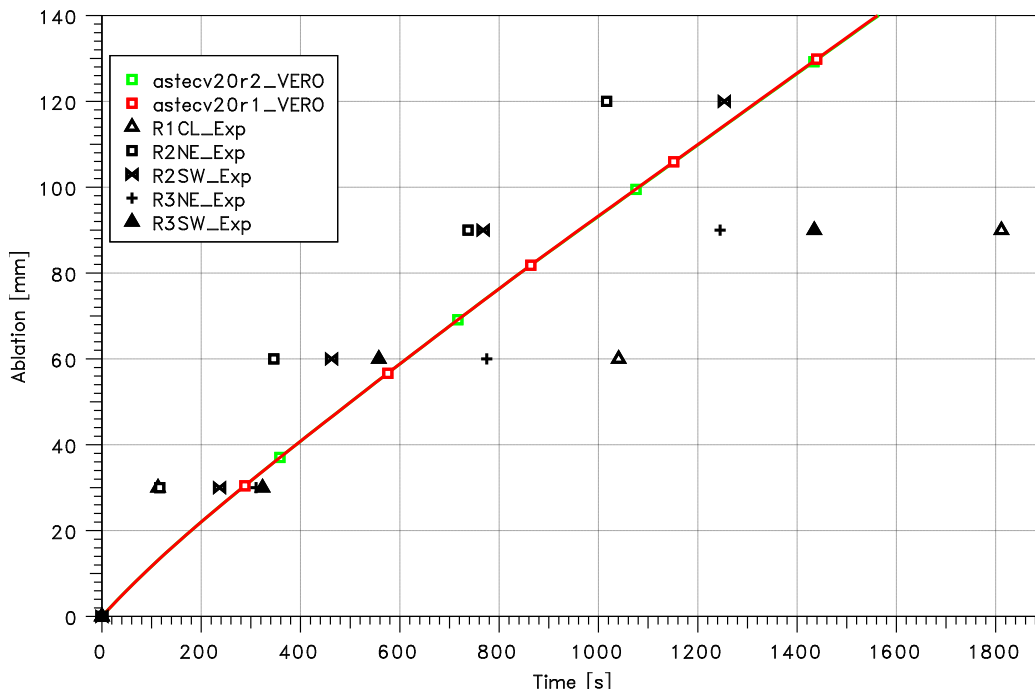


**Figure 4.5-13** Maximal axial ablation

Radial Ablation

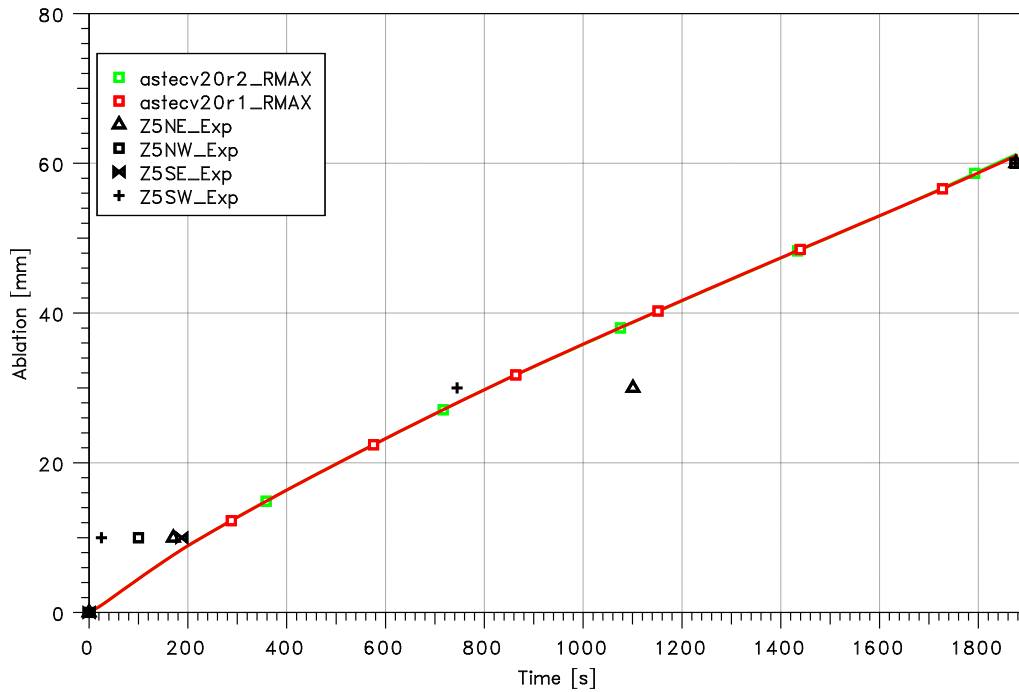


Figure 4.5-14 Maximal radial ablation

Total eroded mass of concrete

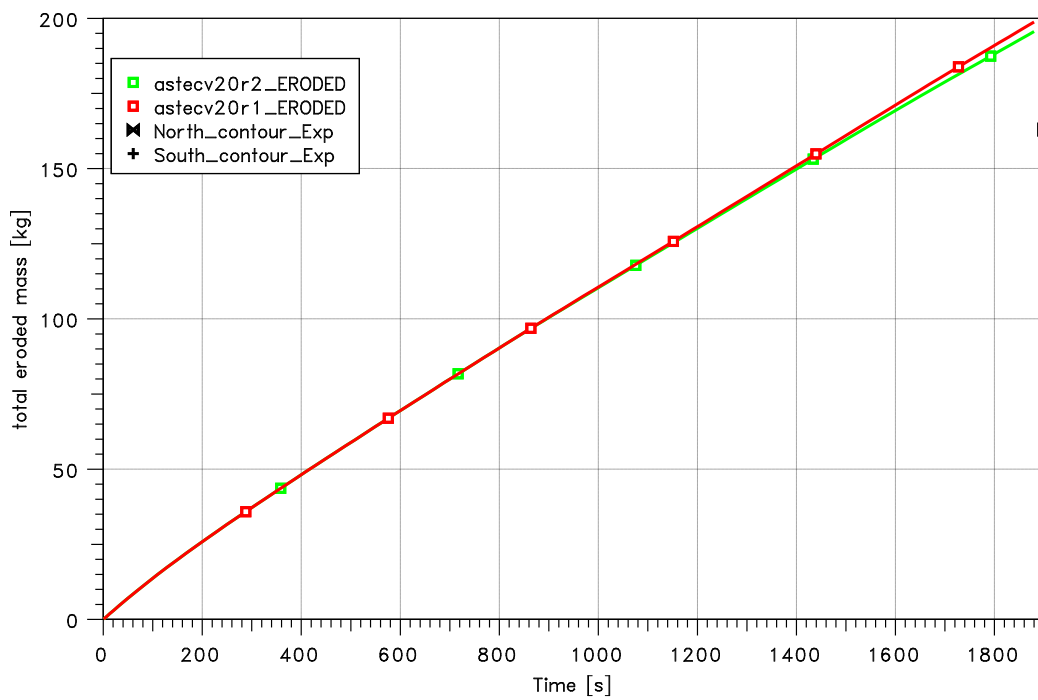


Figure 4.5-15 Total eroded mass of concrete

### 4.5.3 Summary

To conclude: The ASTEC MEDICIS calculations (Stand-alone calculation) give satisfying agreement with the experimental obtained erosion rates and particularly reproduce the difference between axial and lateral ablation. This agreement was achieved by the input of specific, adjusted heat transfer coefficient different for each direction. Concerning the calculated heat transfer between the metal and oxide layer a difference occurs between the versions compared (Figure 4.5-10). The used Greene correlation has not been modified. A further investigation shows also differences in the superficial gas velocity inside the oxide layer and of the viscosity inside the metal layer. At the moment it is assumed that the differences are related to changes in the Stedman correlation for the calculation of viscosity in the metal layer as described in /CHA 11/. This could not be fully resolved, because the version needed for a check could not be linked under Windows operating system.

There are only minor differences between the two ASTEC versions.

## 4.6 Pressure suppression systems

In ASTEC CPA the DRASYS model for the simulation of pressure suppression systems (PSS) is available. The DRASYS zone model is a detailed model describing the fluid dynamics of a PSS.

### 4.6.1 GKSS M1

The main objective of the GKSS M1 /AUS 81/ experiment is the investigation of the air lean and air free steam condensation phase (condensation oscillations and chugging), which occurred in this experiment after about 120 s. During this phase pressure oscillations occur that lead to horizontal forces acting on the vent pipes and significant pressure loads on the wet-well bottom and walls. However, these phenomena are not the main objective of the ASTEC models for pressure suppression systems, i.e. the DRASYS and the simple PSS model using the INSERTION option.

The good measurement of temperature and pressure development makes this experiment a good database for the validation of computer codes in all phases of pressure suppression, especially in a German BWR. It provides data for the vent clearing and pool swell phases as well as for the condensation oscillation and chugging phases. Thus, this experiment is also suitable for a comparison between ASTEC and experimental data in all phases of a pressure suppression event. Also a comparison to COCOSYS results is given

More results on the COCOSYS nodalisation as well as on calculation results and their discussion can be found in /NOW 07/. The nodalisation and dataset are as far as possible the same with ASTEC.

#### 4.6.1.1 Test facility

The principal configuration including some main dimensions of the rig for the GKSS M1 experiment is shown in Figure 4.6-1. This figure is taken from /SCH 84/. Its set-up is illustrated from two different points of view. The high pressure steam vessel used to provide the steam for LOCA simulation is not present in that picture.

The steam is released through a pipe (arrow marked with "DAMPF" in Figure 4.6-1) into the top of the break room (marked with "DRUCKKAMMER", i.e. dry-well). Three vent pipes are leading from the break room into the pool of the PSS zone (termed as "KONDENSATIONSKAMMER", i.e. wet-well). From the atmospheric part of the PSS zone (the wet-well behind the water pool) a pipe is leading to an expansion vessel that can partly be filled with water to adjust the favoured free atmospheric volume.

A more detailed description of the experimental rig design is given in the GKSS M1 report /AUS 81/.

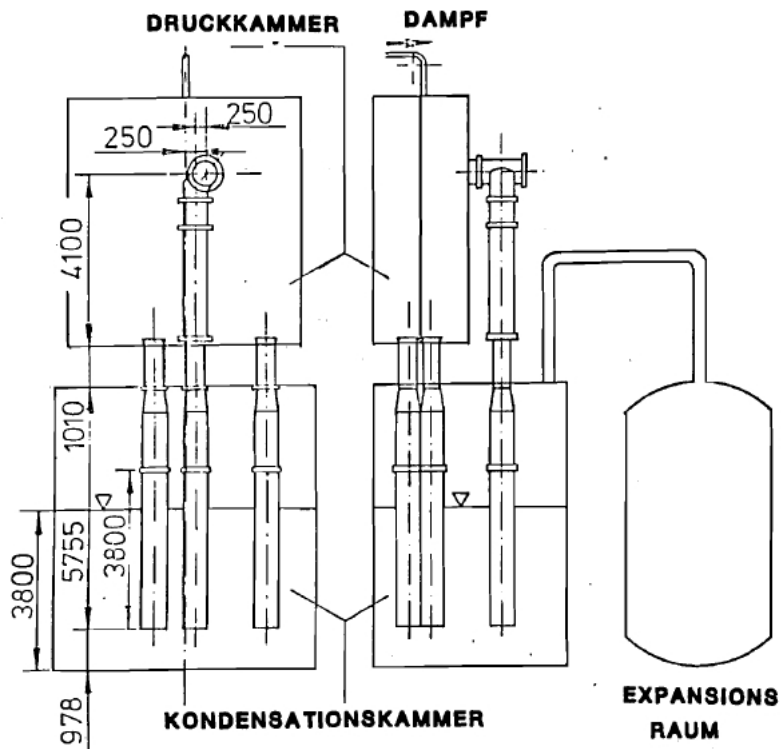


Figure 4.6-1 Schematic configuration of the GKSS experimental facility

#### 4.6.1.2 ASTEC input deck

Within the regression testing for ASTEC the GKSS test case is only run with the DRASYS module. The simple PSS simulation applying the INSERTION option /ARN 07/ is used in the BWR-72 test case (section 4.7.1). For the calculation of the GKSS M1 experiment with ASTEC and the DRASYS zone model a simple four zones nodalisation is used. This nodalisation is illustrated in Figure 4.6-2.

Zone D1-PSS is the DRASYS zone modelling the PSS vent pipe, pool, and the atmosphere above the pool water. All other zones are simulated with the equilibrium zone

model. The steam injection is given into the break room R2-BREAK. This zone is directly connected to the pipe zone part of the DRASYS zone via the junction J1. The expansion room R4-SACK is connected to the GASROOM part of the DRASYS zone via the junction J2. The surrounding of the test facility is modelled by the ENVIRON zone.

Wall heat transfer is simulated by different walls defined in the dataset to the environment zone ENVIRON and between the PIPE and GASROOM zone parts. More results on this nodalisation as well as on calculation results with COCOSYS and their discussion can be found in /NOW 07/.

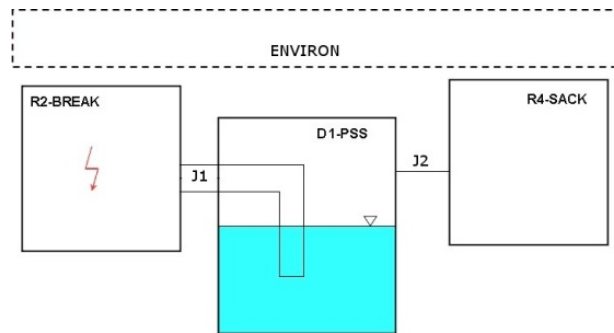


**Figure 4.6-2 Simple 4 zones model of the GKSS M1 experiment with the DRAYS zone D1-PSS**

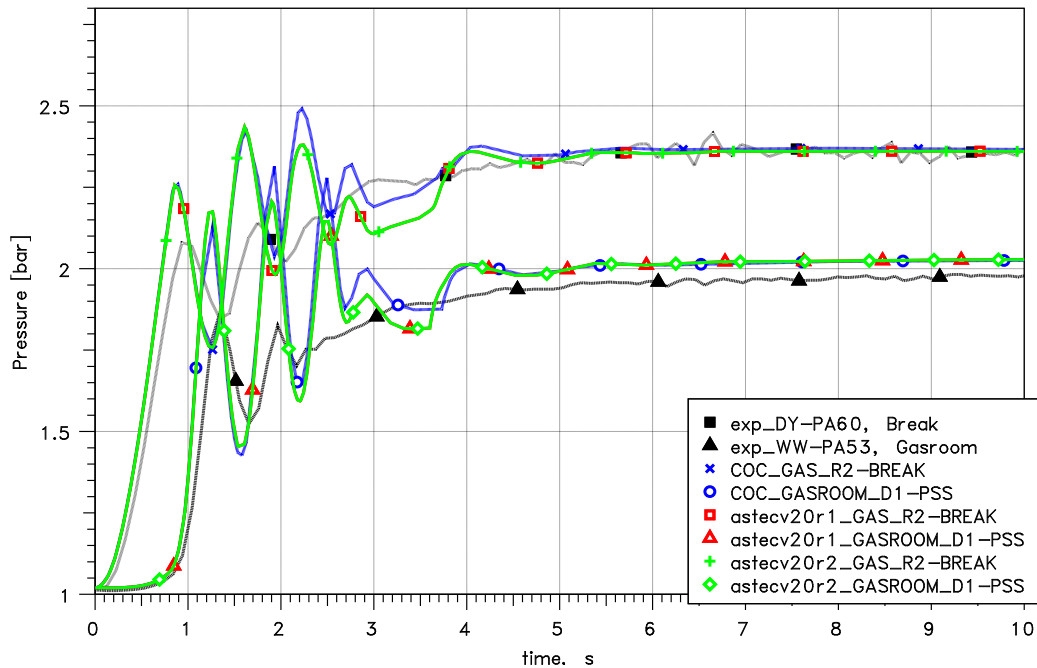
#### 4.6.1.3 Results

In the following the results calculated with COCOSYS are marked with blue colour and that with ASTEC version V2.0r1 with red and version V2.0r2 with green colour. Experimental results are drawn in black.

The pressure rise during the short term phase of the experiment is shown in Figure 4.6-3. In the graphic a comparison between COCOSYS and the ASTEC versions V2.0r1 and V2.0r2 is given.

The vent clearing phase lasts until 0.8 s. Up to this point the pressure in the break room rises continuously. After that phase pressure oscillations occur as a consequence of the pool swell phase. The calculation with DRASYS overestimates the pressure peaks. In the experiment only two peaks are observed, while the calculations gain four. This is mainly caused by the used simple nodalisation. During the DRASYS model validation a more detailed nodalisation with 15 zones, in which each vent pipe was simulated separately, was applied. Thus, better results for the calculated short term pressure behaviour were achieved (more information can be found in /SCH 84/). The pressure after 5 s is well calculated in the break room as well as in the wet-well atmosphere by COCOSYS and both ASTEC versions, the latter producing identical results.

GKSS M1 test



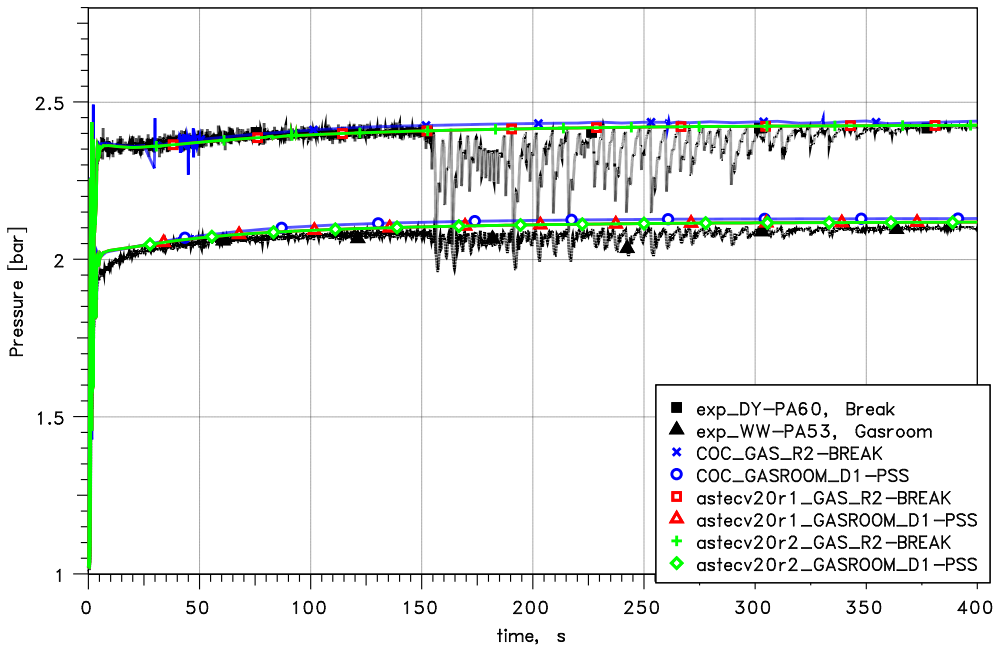
**Figure 4.6-3 GKSS, test M1, short term pressure build-up in break room and wet-well zone (DRASYS zone)**

Figure 4.6-4 shows the long term pressure build up in the wet-well and dry-well zone atmosphere. This is a comparison between both ASTEC versions, COCOSYS and the experiment. The pressure in the dry-well is well calculated with COCOSYS. The ASTEC pressure is almost the same.

The pressure in the wet-well is slightly overestimated by COCOSYS, i.e. the model give conservative values for the maximum pressure during this phase. The deviation in the calculated pressure behaviour between COCOSYS and ASTEC is the same as in the dry-well. The pressure difference between dry- and wet-well is given by the insertion depth of the vent pipes.

The chugging phase from 160 s on is not described by both codes (in fact no code is known which can predict chugging induced pressure oscillations in detail yet).

GKSS M1 test



**Figure 4.6-4 GKSS, test M1, pressure build-up in break room and wet-well zone**

Figure 4.6-5 shows the temperature in the break room. The temperature rise at the beginning is well reproduced by all calculations. The temperature is constant up to 120 s. Then a temperature rise is observed that indicates a transition into superheated conditions that is not reproduced by the calculations. It is attributed to the determination of the enthalpy of the injected steam /NOW 07/. This point was investigated in more details in /ARN 99/ (i.e. with a higher enthalpy the temperature rise can be reproduced principally), but on the basis of the available experimental data no reliable information on the steam enthalpy could be gained.

As seen in Figure 4.6-6 the temperature in the water pool of the wet-well during the first 160 s is well calculated by both codes. The calculated results for pool temperature show a mean value for the whole pool water. From 160 s on a further temperature increase is observed that is not reproduced by the calculations. This is also linked with the above mentioned transition to superheated atmosphere conditions caused by the used specific enthalpies of the injected steam.

GKSS M1 test

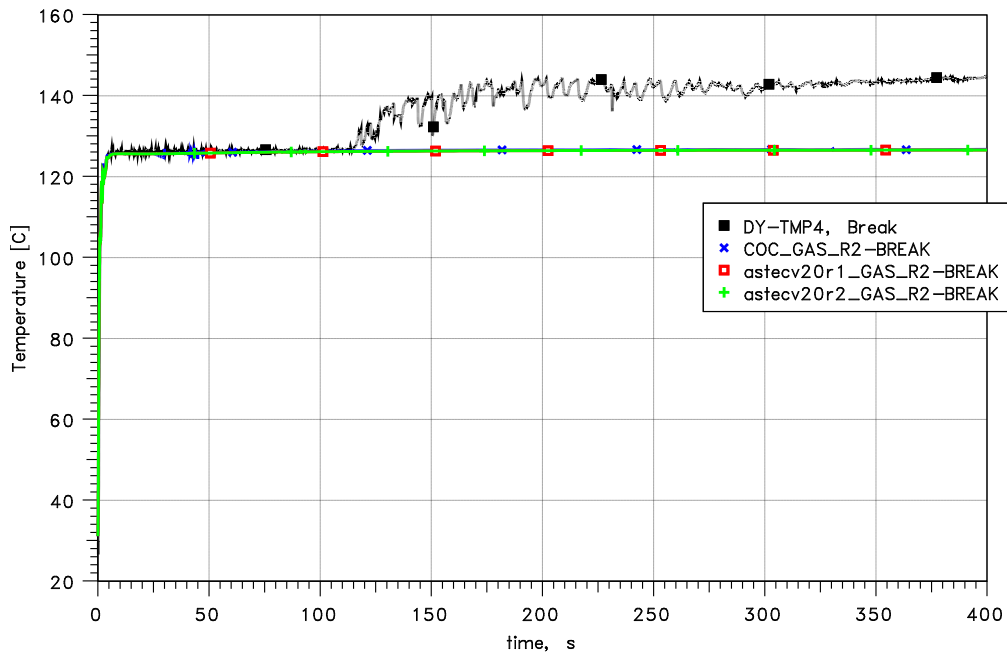


Figure 4.6-5 GKSS, test M1, atmosphere temperature in the break room

GKSS M1 test

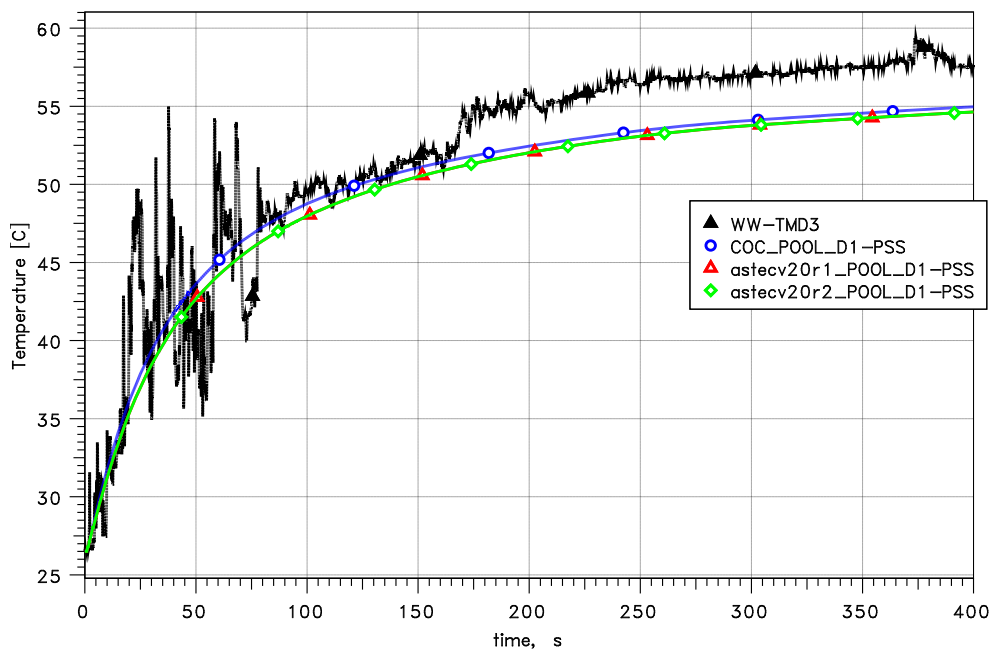
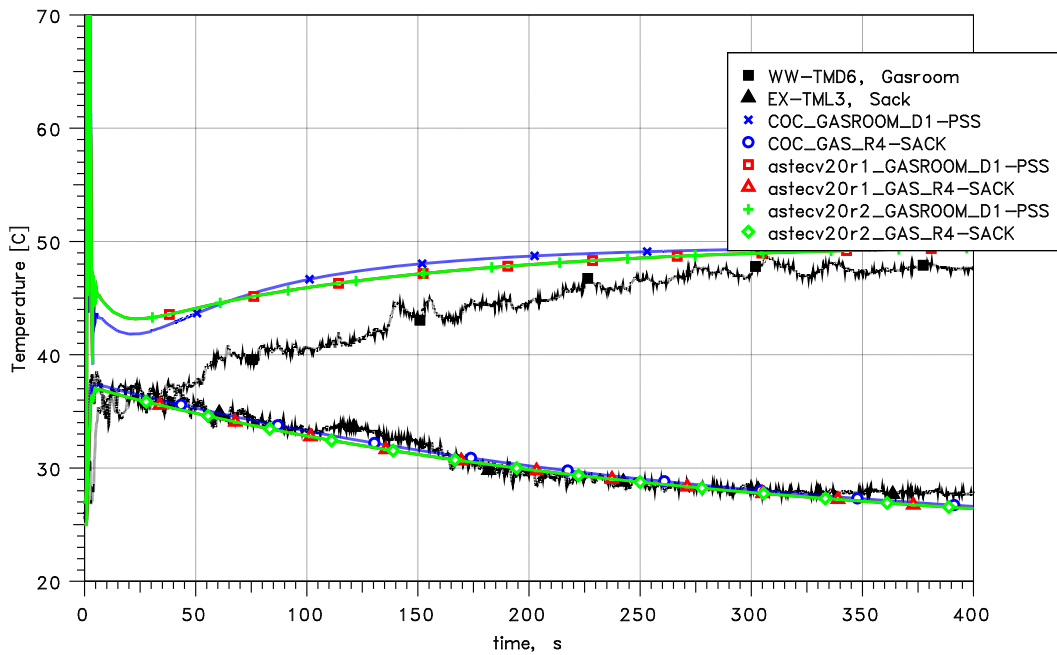


Figure 4.6-6 GKSS, test M1, PSS pool water temperature

The long term temperature development in the atmosphere of the wet-well and in the expansion room is shown in Figure 4.6-7. In all calculations the atmosphere temperature is too high in the wet-well atmosphere. This result is discussed and explained in more detail in /NOW 07/. There is no difference in the temperatures gained by both ASTEC versions and also the differences to COCOSYS are very small.

GKSS M1 test



**Figure 4.6-7 GKSS, test M1, atmosphere temperature in the wet-well zone and expansion room**

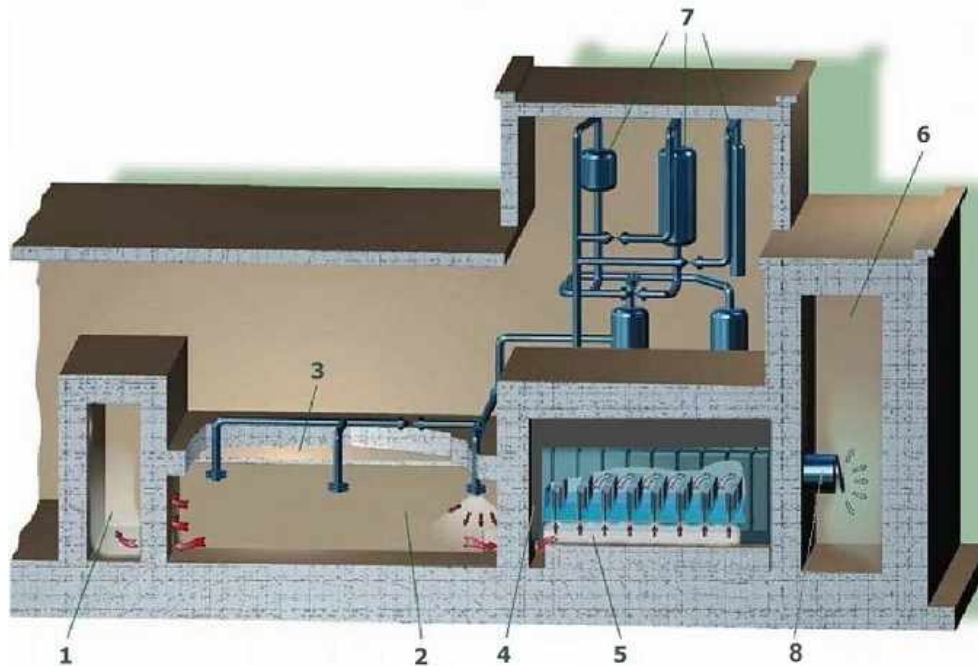
#### 4.6.1.4 Summary

The comparison between both ASTEC versions doesn't show any differences concerning pressure and temperature. The comparison with COCOSYS shows marginal differences concerning the pressure build up in the long term phase. The pressure gained with ASTEC is about 0.05 bar lower than the COCOSYS results. Compared with the experiment the ASTEC results are more close to the measured pressures.

### 4.6.2 EREC BC-V213 SLB-G02

#### 4.6.2.1 EREC test facility

The EREC test facility BC V-213 was designed for thermal hydraulic testing of the Bubble Condenser (BC) of NPP with WWER-440/W-213. Reinforced concrete boxes model the Bubble Condenser Containment of the Paks NPP in a volume scale of 1:100. The facility includes a fragment of the BC with 18 full-scale gap/cap systems. A schematic view of the BC V-213 is given in Figure 4.6-8. The BC V-213 is designed for a maximum pressure of 300 kPa and a minimum pressure of 80 kPa. A high pressure system consisting of up to 5 vessels ( $V_{V1} - V_{V5}$ ) is designed for preparing the mass and energy release into the steam generator box V1 at one of three possible break locations.



1 - dead end volume (termed as V0), 2 - steam generator box with three possible break locations (V1), 3 - steam generator box (V2), 4 - bubble condenser shaft (V3), 5 - bubble condenser (V4) 6 - air trap (V5), 7 - high pressure vessel system, 8 - check valve

**Figure 4.6-8 EREC BC V-213, schematic view of the test facility**

The BC V-213 consists of 5 hermetic compartments: dead end volume (V0), two steam generator boxes (V1 and V2), accident localisation shaft (V3) with a full-scale BC fragment (V4) and air trap (V5). The total volume of the model including the BC water is about 510 m<sup>3</sup>. The BC section, i.e. two prototype segments containing 18 gap/cap systems, is located in the accident localisation shaft at a concrete pedestal. The shaft volume V3 is diminished by volume displacers to meet the volume scale ratio of 1:100. The BC is connected with the air trap V5 via a check valve. The structure of the check valve model is consistent with one full-scale DN500 valve, but its cross section area is 0.0235 m<sup>2</sup> (reduced according to 1:100 facility scaling). The cross section area of the DN250 relief valve from BC gas room into BC shaft is reduced by an upstream orifice DN122 to fulfil the area ratio of 1:100 of the two parallel relief valves per floor in the plant.

The thickness of the hermetic compartments walls is 0.8 m. The internal surfaces of all boxes are lined with 6 mm thick steel plates. Main elements of the BC model are made of stainless steel with a thickness of 3 mm. To make the ratio of the inner surface area of compartment walls to their volumes in the test facility equal to that of Paks NPP, some walls of the hermetic compartments V1, V2, V3 and V5 are insulated with wooden plates of 12 mm thickness.

More information on the test facility (volumes, main geometrical compartment dimensions, junctions between the compartments, measuring devices positions) can be found in /MEL 01, BCE 99, ARN 03/.

### 4.6.2.2 CPA input deck

This test case is only calculated applying the DRASYS zone model for the Bubble Condenser section. The alternative modelling option with the more simple INSERTION option /ARN 07/ is tested in the BWR-72 case (section 4.7.1).

For the post-test analyses a detailed nodalisation is required, which represents in a sufficient manner the facility geometry and considers also the position of measuring gauges. However, considering identified uncertainties in boundary conditions a medium sized nodalisation was compiled, in which the 18 gap-cap systems, the water pool and the gas room of the BC module are simulated with one zone (termed as V4-BC, see Figure 4.6-9) of the DRASYS type (detailed model for PSS simulation, see /KLE 00/). Thus, an average BC behaviour is simulated. The nodes in which a large water mass can be accumulated are simulated by the non-equilibrium zone type (e.g. V0-SUMP or V1-SUMP), whereas the other nodes are of equilibrium type.

To simulate the EREC BC V-213 test facility a CPA input deck with 24 zones, 35 atmospheric and 21 drain junctions, 4 pump systems and 109 heat conducting structures was developed. It bases on the COCOSYS input deck used for the original post-calculations of this experiment. Details can be found in /ARN 03, PER 03/. The nodalisation scheme is presented in Figure 4.6-9.

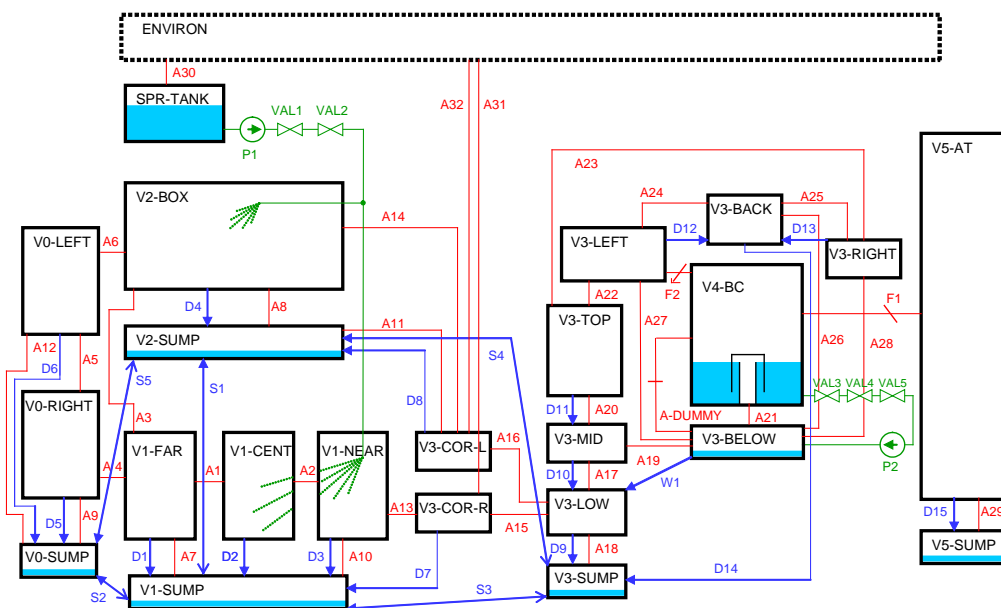


**Figure 4.6-9 BC V-213, nodalisation with 24 zones**

The first two digits of the zone names point to the association to facility compartments. The subdivision of the SG box V1 into three zones reflects the three possible break locations, which is the zone V1-FAR for the test SLB-G02. In the lower parts of the facility compartments, simulated as separate sumps with special tables for the zone water level as function of water volume. Special attention was paid to the modelling of the BC shaft volume V3 which has a complex geometry.

Zones are connected by atmospheric junctions (A1 to A32) to simulate the mass flow of accident generated 2-phase 2-component mixture between the zones. The gas room of the BC is connected with the air trap V5-AT via the dynamic flap F1. The DN250 relief valve equipped with the DN122 orifice is simulated by the dynamic flap model (junction

F2). It will be locked in closed position, if the pressure in BC shaft rises higher than the flap set-point, what is controlled by the signal SIG1. The facility compartment system is assumed to be leak tight. Drain junctions in CPA are defined to simulate flow processes of water, for instance the drainage of injected water or condensate (drain junctions D1 to D15, see Figure 4.6-9) or the flow between different sumps to equalise the water surface levels (S1 to S5). The spray system, which can inject water into both SG boxes V1 and V2, is not active in this experiment and not modelled in the used CPA dataset. The passive spray, i.e. the reverse flow of water from BC pool to the BC shaft due to the negative pressure difference across the gap-cap systems, does not occur during this experiment. Thus, it was not modelled in the dataset.

In each zone the relevant structure surfaces were defined as floor, side wall or ceiling (concrete walls covered by steel layers) and the BC stainless steel walls are subdivided into different heat slabs to consider that wall sides are linked with the pool water, the gas room or the gap-cap system. The standard options are used for heat transfer calculation, i.e. a combination of free and forced convection, condensation and wall-gas-radiation. The initial wall temperature profiles are calculated according to steady state conditions.

The input deck had to be adjusted separately for the post-test calculation of each test, i.e. initial zone condition, break location and so on. For that adjustment Quick Look Reports were produced. Main uncertainties of the test facility come from the wooden insulation (is it really perfect or non-tight or "wet" with much larger heat conductivity) and the fact that the initial relative air humidity was not measured for all facility compartments (air humidity and atmosphere temperature determine the initial air mass in the facility and so influences the long term pressure level).

#### 4.6.2.3 Results

In the figures the comparison between the experiment (black line), the current COCOSYS development version V2.4 (blue line), the previous ASTEC version V2.0r1 (red line) and the current version V2.0r2 (green line) is given for some relevant parameters.

The test SLB G02 simulates a steam line break in the Bubble Condenser Containment of NPP with VVER-440/213. The high pressure vessel system provides the scaled down steam mass and energy release into the SG box V1 (break location is the zone V1-FAR). A process time of 1 800 s (0.5 h) is simulated in the experiment. To reduce uncertainties in the initial conditions the test was started with "cold" conditions of about 20 °C, i.e. without test facility pre-heating. The results of the original COCOSYS post-calculations (validation) are described in detail in /ARN 03/ and summarised in /PER 03/.

In Figure 4.6-10 the calculated pressures for V1, V4 and V5 (see Figure 4.6-8 and Figure 4.6-9) are compared with the experiment. The pressure behaviour is good post-calculated, i.e. during the important time intervals (pressure peak and long term pressure level) the calculation is inside the uncertainty bandwidth, which is given as  $\pm 4$  kPa. In the short-term up to 50 s the pressure increase is somewhat too high in the COCOSYS calculation. This phase is much better calculated by both ASTEC CPA versions. In the period of 150 – 400 s the COCOSYS results for V1-NEAR and for V4-BC are at the upper uncertainty band. The CPA results are closer to the measurement. However, between 300 and 1 400 s ASTEC gives too low temperatures for nodes V1

and V4 compared to the experiment. Overall, ASTEC calculates lower pressures than COCOSYS. The results of both ASTEC versions are identical.

BC V-213, EREC Test SLB-G02

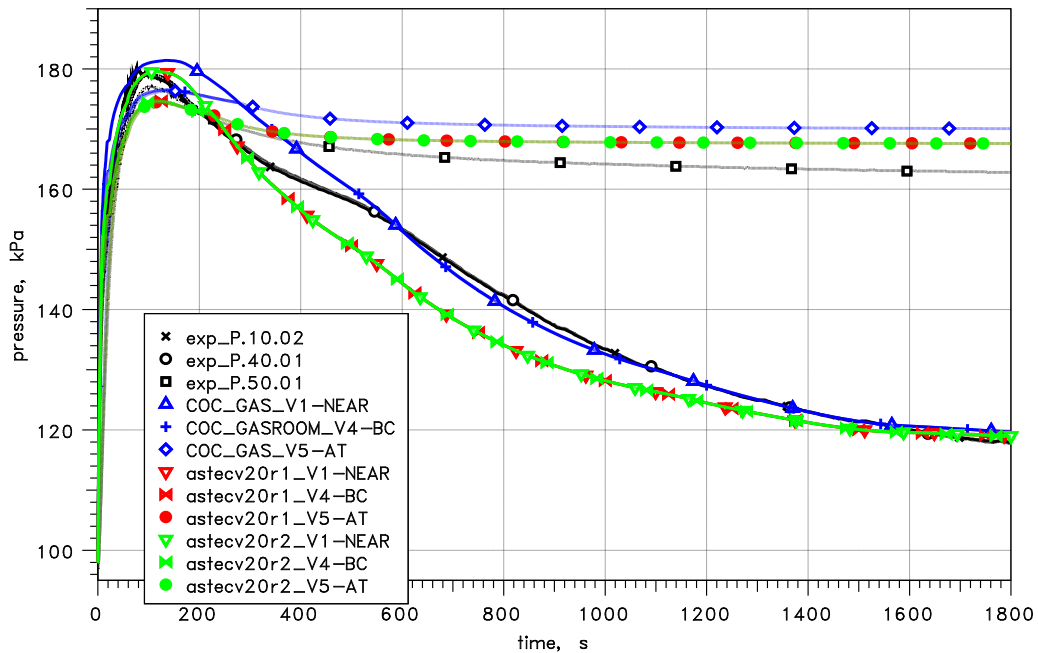


**Figure 4.6-10 BC V-213, test SLB G02, pressure in the break compartment V1, in the BC gas room V4 and the air trap V5**

The calculated temperature for the box V1 (labelled as V1-NEAR, Figure 4.6-11) is up to 50 K higher than measured, because COCOSYS and CPA calculate superheated atmosphere conditions. (The temperature gauges uncertainty amounts to  $\pm 1.5$  K /MEL 03/). For COCOSYS also the saturation temperature termed as T-sat is presented. A comparison of the saturation temperature with the measurement shows a good coincidence. Until about 700 s the COCOSYS saturation temperature is inside the uncertainty bandwidth of the relevant gauges. However, in the long-term also the calculated saturation temperature is up to 10 K higher and outside the uncertainty. Looking carefully at the time interval 250 – 450 s the gauge T.10.03 shows some temperature peaks indicating a possible superheated atmosphere. It is still an unresolved question whether COCOSYS and CPA overestimate the temperature or/and condensation effects at the thermocouple head falsify the measurement. In comparison to COCOSYS the CPA results are closer to the experiment. No difference occurs between both ASTEC versions.

BC V-213, EREC Test SLB-G02

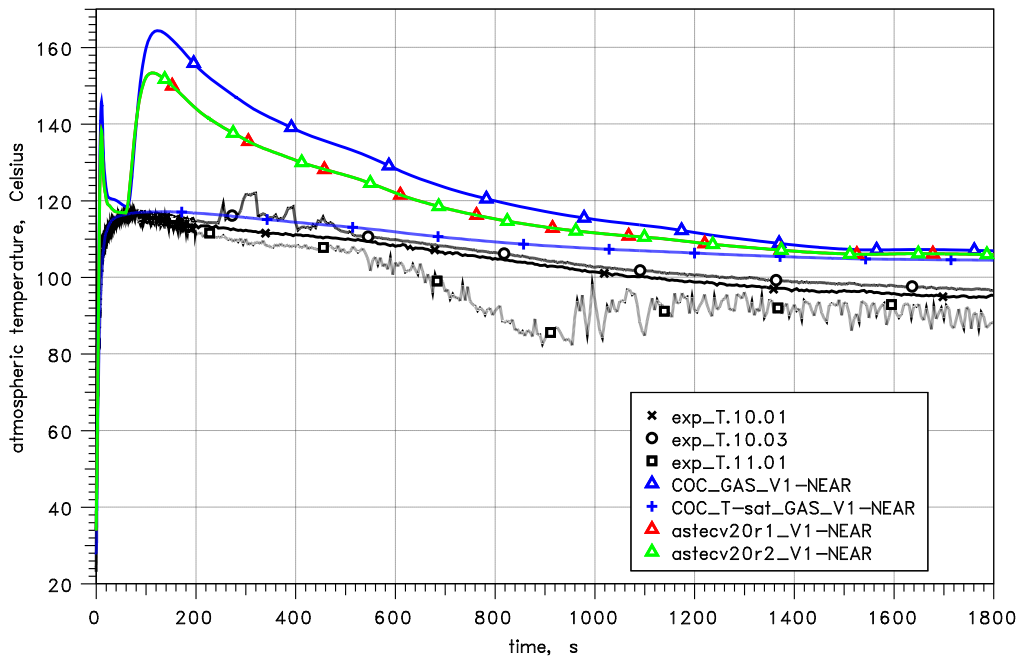


**Figure 4.6-11 BC V-213, test SLB G02, atmosphere temperature in the box V1**

The calculated development of the temperatures in the BC gas room (compartment V4 modelled as zone V4-BC) is not the same as the measured temperature. However the maximum temperature is close to the experimental curve (Figure 4.6-12). After 600 s the temperature drop is larger than measured for COCOSYS and both ASTEC versions. The COCOSYS temperatures are about 5 to 10 K higher than CPA.

BC V-213, EREC Test SLB-G02

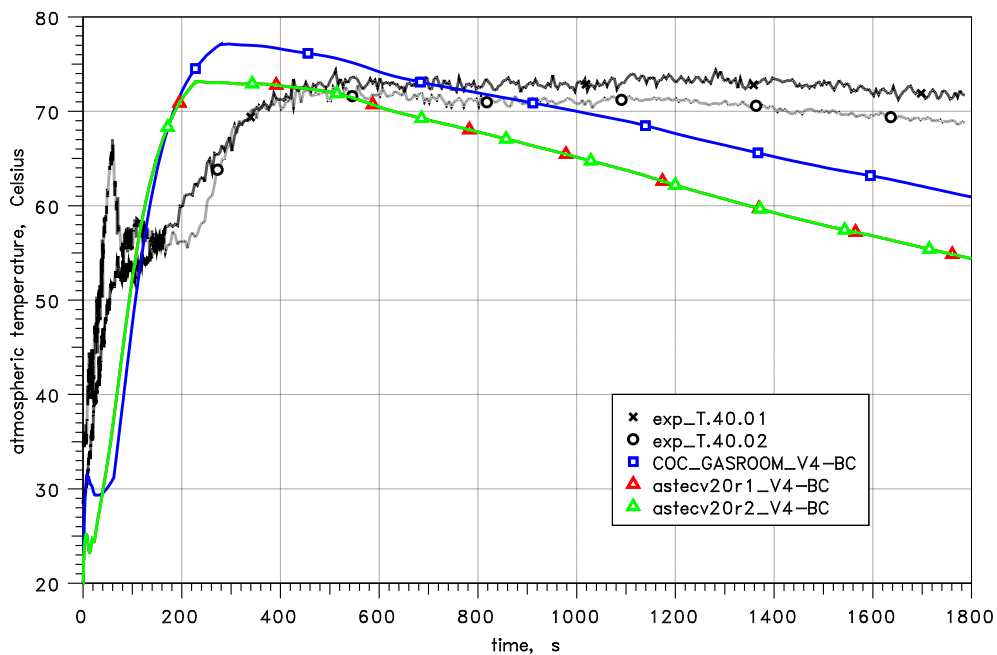


**Figure 4.6-12 BC V-213, test SLB G02, atmosphere temperature in the BC gas room V4**

The comparison of the calculated and the experimental pressure difference across the BC walls for the first 4 s is given in Figure 4.6-13. From the available measurements the gauge PD3040.03, the only one with 50 Hz sampling rate, was selected. For the first peak a good agreement of the calculated pressure difference of 6.9 kPa with the experimental value of 6.4 kPa can be stated. In this SLB experiment not the first pressure difference peak is the absolute maximum. The absolute maximum was reached during the second peak (7.6 kPa). Due to simplifying assumptions in the DRASYS model (switch from pool swell to steady modes /KLE 00/) after the first oscillation the pressure difference is kept constant according to the caps insertion depth. In general the theoretical results are in the gauge uncertainty bandwidth of  $\pm 1.2$  kPa, except during 1.2 to 1.7 s. Only minor differences between COCOSYS and CPA and no differences between both ASTEC versions occur.

BC V-213, EREC Test SLB-G02

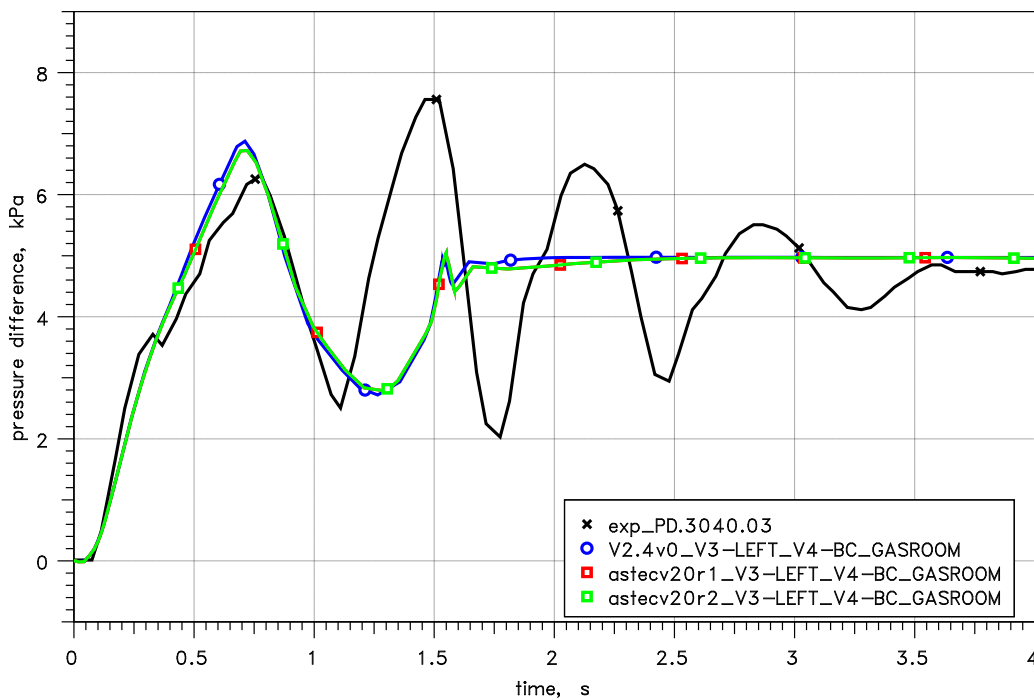


**Figure 4.6-13 BC V-213, test SLB G02, pressure difference across the BC walls**

The calculated and measured heat-up of the water are given exemplarily for the right side of the BC pool in Figure 4.6-14. Due to the simulation of the BC fragment by one node in COCOSYS as well as in CPA an average pool water temperature is calculated. In difference to that the available 53 gauges give local temperatures. The spreading of the measured water temperatures is result of the restricted water mixing due to the relative strong separation of the pool by the gap/caps. One can state a quite good coincidence of calculated and measured temperatures, i.e. the calculated temperature is well inside the different gauges. To facilitate the comparison the arithmetic average of all gauges is included in the figures as well. ASTEC CPA calculates slightly higher pool temperatures than COCOSYS. Both CPA versions are identical.

BC V-213, EREC Test SLB-G02

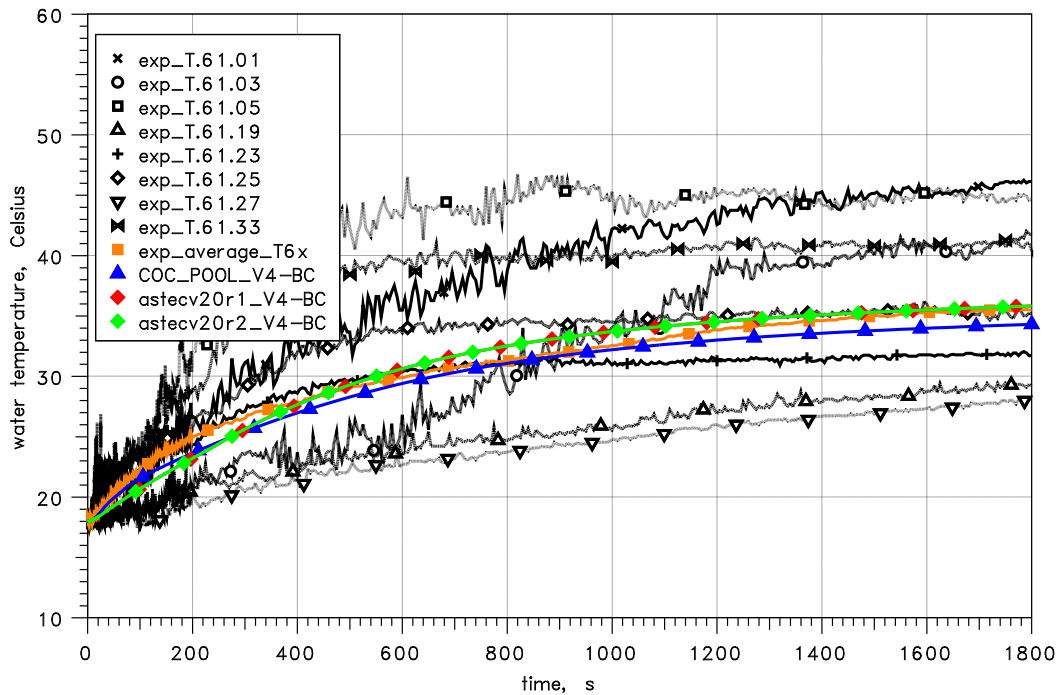


**Figure 4.6-14 BC V-213, test SLB G02, water temperature in the right side of the BC pool**

#### 4.6.2.4 Summary

The above results show, that ASTEC CPA is capable to post-calculate the SLB G02 test. The main parameters as maximum pressure, pressure difference across Bubble Condenser walls and BC pool water heat up were well post-calculated by both versions of CPA. There are no differences between both ASTEC versions, what demonstrates that no unintended side effects occur due to source code changes in CPA or new models implemented.

### 4.7 Typical NPP test cases

#### 4.7.1 BWR-72 (KRB II – C)

The containment of the German 1 344 MW boiling water reactor KRB II – C (NPP Gundremmingen II, unit C) of the 72 series is modelled in this calculation. The input is built up to calculate the hydrogen distribution in case of a fictive severe accident ‘Loss of main heat sink plus loss of pressure limitation’, in the German PSA study for BWR’s shortly abbreviated as ‘HWDB’ case /KER 98, page 305/. Within this scenario a failure of the reactor pressure vessel cover flange is assumed at 12 MPa that is modelled by a constant leakage of 0.2 m<sup>2</sup>. The ASTEC CPA dataset is based on the original COCOSYS input deck.

### 4.7.1.1 ASTEC CPA input deck

The nodalisation of the containment is given in Figure 4.7-1. It consists of 50 zones. Zone names belonging to the dry-well are preceded by an R, R10 for instance, and zone names of the wet-well are preceded by a K, K21 for instance. The pool parts of the pressure suppression system are simulated by two zones K21 and K22. The atmosphere of the dry-well is connected to the atmosphere part of the wet-well (same zones K21 and K22) by connections (vent pipes) from the rooms R10 and R11. The vent pipes are simulated by the INSERTION option for an ATM\_VALVE junction between the dry-well and wet-well. The INSERTION option is a fast running simplified model for pressure suppression systems, which concentrates on the simulation of quasi-steady flows of steam/gas mixtures into a water pool (compare section 4.6.1).

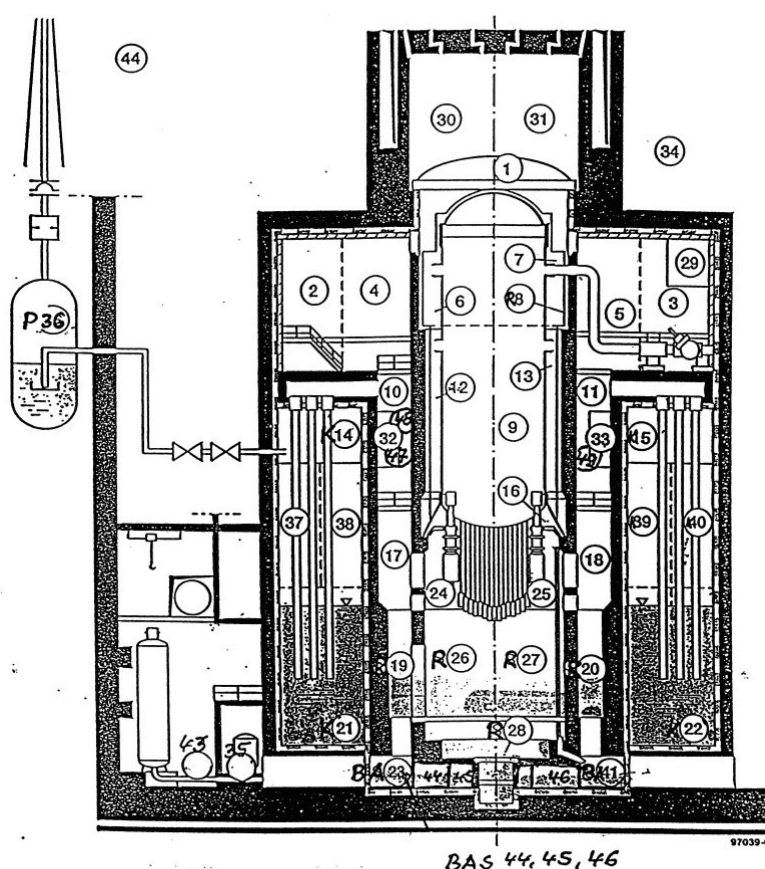


**Figure 4.7-1 Nodalisation of BWR-72**

This calculation uses only the thermal hydraulics module of CPA. No aerosol behaviour or molten corium concrete interaction is considered yet. All data concerning the accident scenario in the reactor cooling system are based on MELCOR 1.8.3 calculations /KER 98, page 305/. An overview of the corresponding accident sequence is given in Table 4.7-1. In the accident sequence a total failure of the steam discharge to the wet-well by the safety valves was assumed. An initial transient caused the SCRAM. The isolation of the main steam line stopped the heat removal of the RPV and the pressure started to rise. A pressure in the RPV larger than 120 bar caused an RPV head leak and the flow was directed into the upper dry-well. Through several vent pipes steam and air is released from the dry-well into the wet-well. The steam is condensed in the

wet-well, but the heat removal from the wet-well failed so that the water temperature is rising until saturation is reached. As ASTEC CPA does not calculate the mixing between the two water zones K21 and K22, its temperature might become different.

In order to simulate this scenario with CPA mass and energy flow rates have to be transferred into the containment which is done via table input. These input tables are based on the results of the previous MELCOR calculation of the above mentioned HWDB scenario /KER 98, page 305/. This input is summarized in Table 4.7-2.

There are some inconsistencies in comparison to the accident sequence in Table 4.7-1. The hydrogen and CO injection of MCC1 starts at 3110 s, i.e. 70 s before the failure of the reactor pressure vessel at 3180 s. The origin of these discrepancies is linked to the coarse plot time step from the old MELCOR calculations (3110 s = last plot time step before RPV failure) and accepted to have comparable results to the original COCOSYS calculation. The zone numbers in this table correspond to the nodalisation of the containment as shown in Figure 4.7-1.

**Table 4.7-1 Event table of the BWR-72 HWDB scenario**

| Event                                                                                                                              | Time (s)           |
|------------------------------------------------------------------------------------------------------------------------------------|--------------------|
| Unintended opening of turbine bypass valve                                                                                         | 0                  |
| SCRAM<br>Coast down of reactor coolant pump<br>Isolation of main steam line<br>Turbine trip<br>Stop of main steam bypass equipment | 0.5                |
| Shutdown of reactor coolant pump                                                                                                   | 172                |
| Shutdown of control rod flush water pump                                                                                           | 180                |
| Shutdown of seal water pump                                                                                                        | 315                |
| Pressure in RPV > 120 bar: RPV cover break                                                                                         | 450                |
| Begin of fission product release into dry-well                                                                                     | 1140               |
| Begin of molten corium relocation into lower plenum of RPV                                                                         | 1620               |
| Core slump to lower plenum and subsequent local RPV failure                                                                        | 3180               |
| Melt discharge to dry-well and MCC1                                                                                                | 3180 - 85000       |
| Containment venting                                                                                                                | ~24000 &<br>~63000 |

**Table 4.7-2 Injection rates for the BWR-72 plant calculation**

| Name   | Remarks               | Time (s) | Release zone: |
|--------|-----------------------|----------|---------------|
| BDAMDE | steam from cover leak | ~450     | R1, R6, R7    |

| Name    | Remarks                                                             | Time (s) | Release zone:                      |
|---------|---------------------------------------------------------------------|----------|------------------------------------|
| BH2DE   | H <sub>2</sub> from cover leak                                      | ~1080    | R1, R6, R7                         |
| BWAEX   | residual water from primary system                                  | ~3200    | R26, R27                           |
| BDAMEX  | steam from primary system                                           | ~3240    | R28                                |
| BDACEX  | steam from MCCI                                                     | ~34400   | R28                                |
| BH2CEX  | H <sub>2</sub> from MCCI                                            | ~3110    | R28                                |
| BCO2CEX | CO <sub>2</sub> from MCCI                                           | ~28800   | R28                                |
| BCOCEX  | CO from MCCI                                                        | ~3110    | R28                                |
| BLFRI   | energy from fission products in air (dry-well)                      | ~1730    | R1, R2, R3, R4, R5, R29            |
| BLPOOL  | energy from fission products in pool (wet-well)                     | ~3200    | K21, K22                           |
| BLAB    | energy of settled fission products on diverse structures (dry-well) | ~3200    | R2, R3, R4, R5, R19, R20, R23, R41 |
| BLSRDB  | system heat from RPV into dry-well                                  | ~0       | R6, R7, R12, R13                   |
| BLSTR   | radiation heat from melt in cavity                                  | ~3200    | R28, BA23                          |

#### 4.7.1.2 Results

The following results show a comparison between the ASTEC versions V2.0r1 (red line) and V2.0r2 (green) as well as with latest release version of COCOSYS (blue).

Figure 4.7-2 shows the temperature during the calculation in the dry-well zone R10 atmosphere and the corresponding wet-well atmosphere in zone K21 and the pool temperature. These zones are connected via an ATM\_VALVE with the INSERTION option. The temperatures in the new ASTEC version are only slightly higher compared to the old version up to 23 000 s, but significantly lower than in COCOSYS. After the first venting phase the temperature difference between both versions is about 10 K. COCOSYS calculates even 20 K higher temperatures in the dry-well as the V2.0r2 ASTEC version. In the wet-well the difference is up to 80 K after 60 000 s. The new ASTEC version calculates the highest pool temperature. At the end of the simulation the old versions temperature is about 10 K less and the COCOSYS result 20 K lower. Figure 4.7-3 shows the same graphic for the dry-well zone R11 and the corresponding wet-well zone K22. The trend for the atmospheric temperatures is the same with a even hotter atmosphere in COCOSYS compared to both ASTEC versions, but the temperature difference between atmosphere and pool is smaller. In contrast to zone K21, COCOSYS calculates a higher pool temperature compared to ASTEC. In future

this nodalisation should be modified, as COCOSYS and ASTEC CPA do not calculate mixing processes between two connected pool regions. As well for the corresponding atmosphere region in K21 and K22 the temperatures are significantly different.

KRB – HWDB case

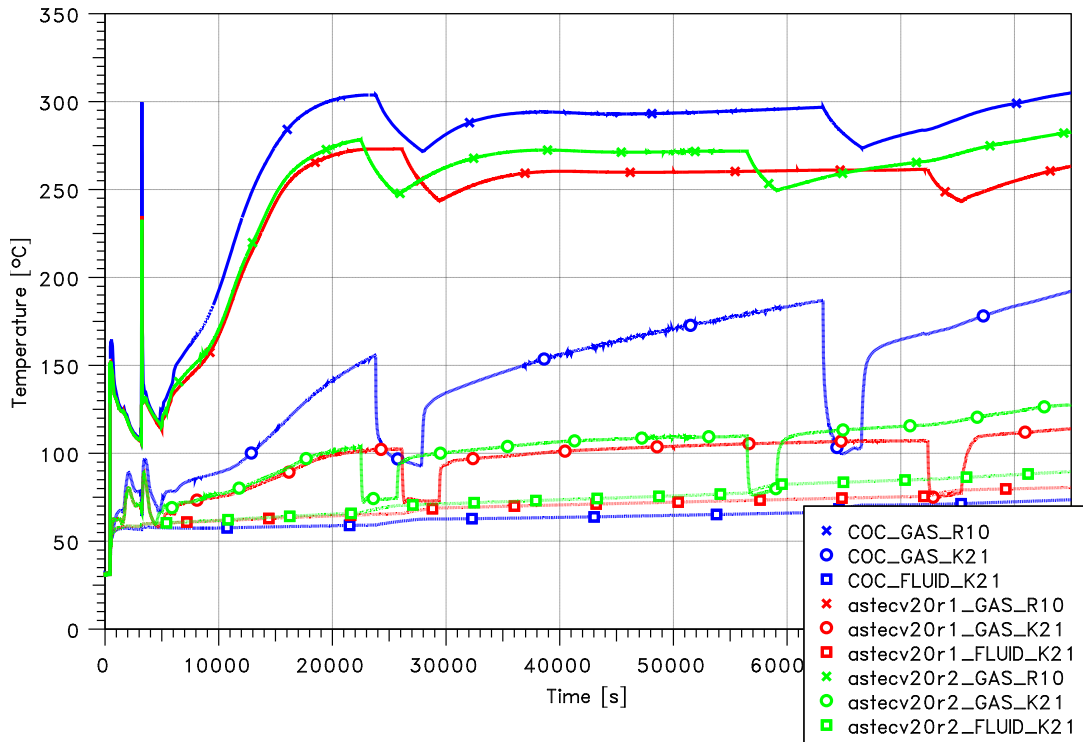


**Figure 4.7-2 BWR-72, temperature in a wet-well zone (K21) and a dry-well zone (R10)**

KRB – HWDB case

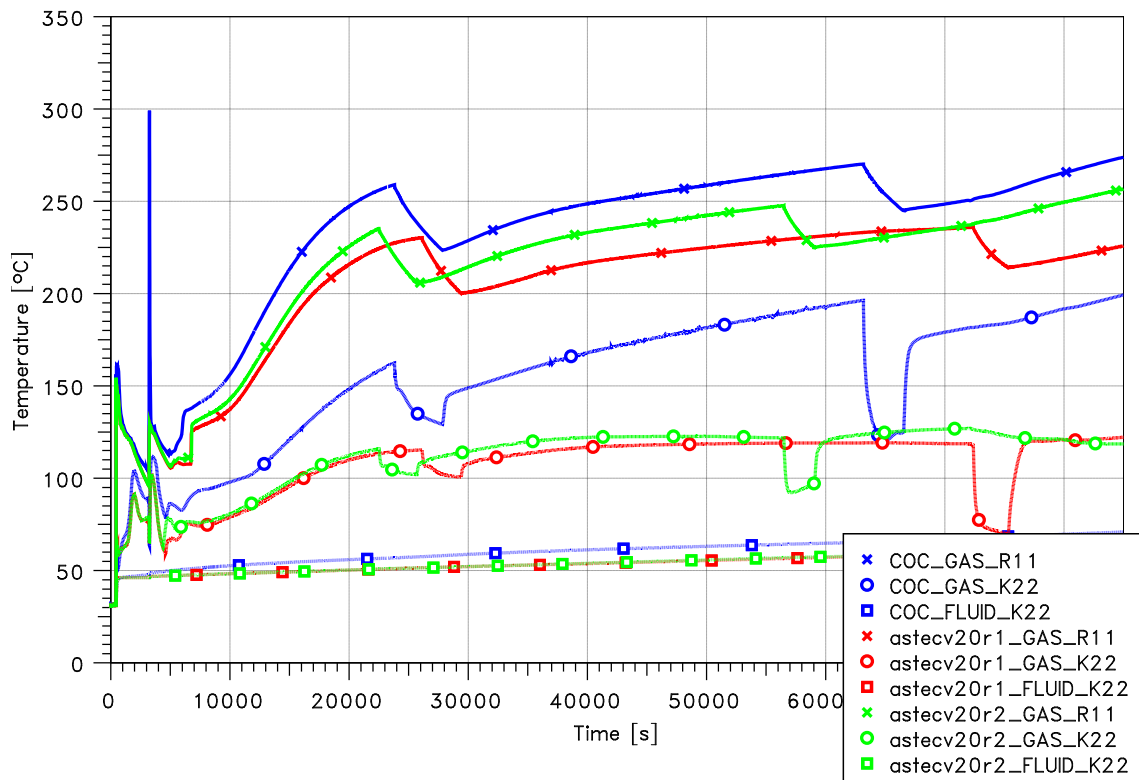


**Figure 4.7-3 BWR-72, temperature in a wet-well zone (K22) and a dry-well zone (R11)**

The pressure behaviour in the dry-well and the wet-well is shown in Figure 4.7-4. In the new ASTEC version at 23 000 s the containment pressure limit is reached first time and the venting is initiated. In the old version the venting starts about 3 000 s later (see Figure 4.7-4). The long term phase is significantly different between all three versions compared.

KRB – HWDB case

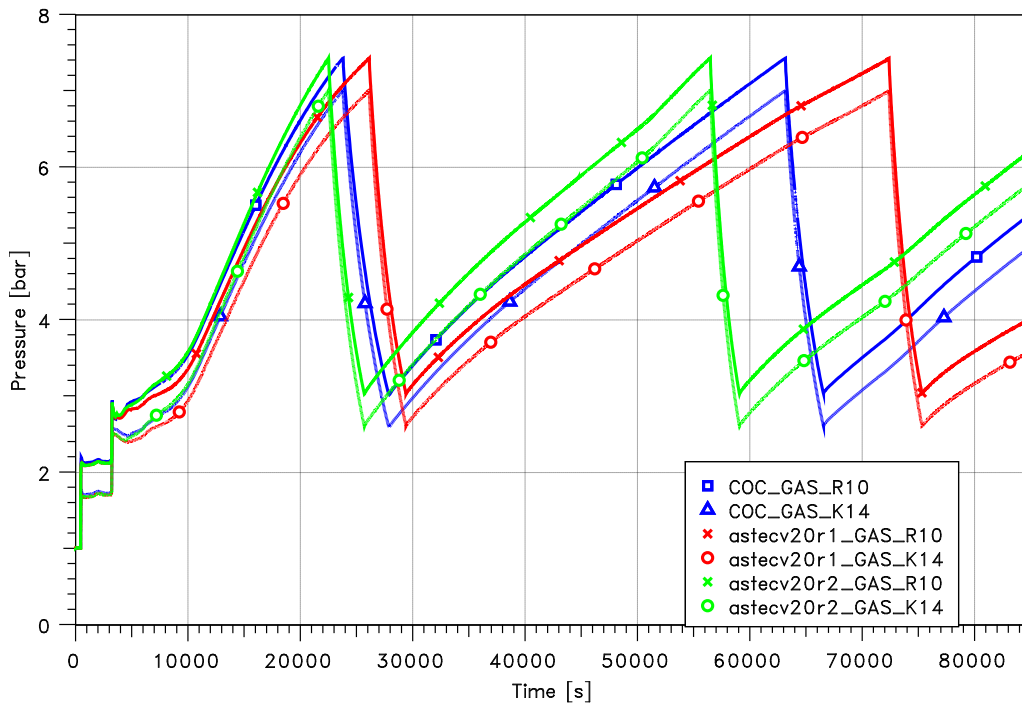


**Figure 4.7-4 BWR-72, pressure in dry-well and wet-well**

The mass flow rate through the vent pipes of the pressure suppression system, i. e. the INSERTION junction, during the first 1 000 s is given in Figure 4.7-5. All calculations show a similar flow rate, except the peak at 450 s, which is significantly higher in COCOSYS.

KRB – HWDB case

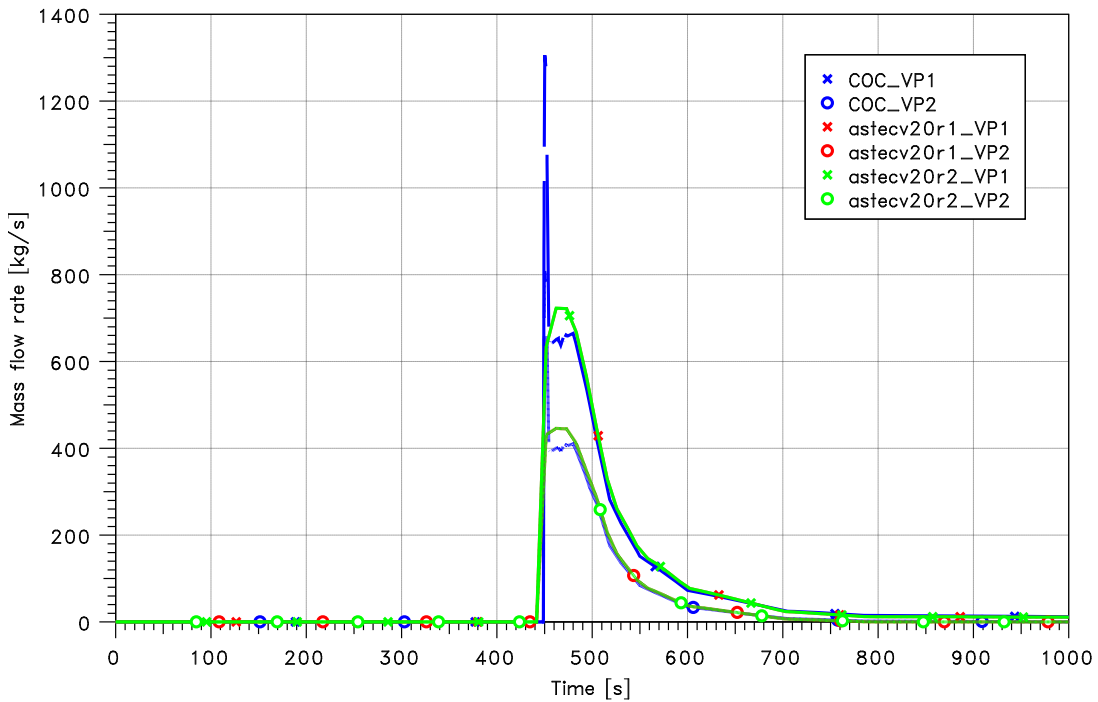


**Figure 4.7-5 BWR-72, mass flow rate through vent pipes up to 1000 s**

The hydrogen concentrations in the dry-well zone R10 and the wet-well zone K21 are shown in Figure 4.7-6. Up to the time the containment venting is initiated, COCOSYS and ASTEC V2.0r1 calculate almost the same results. ASTEC V2.0r2 calculates a lower concentration that is caused by higher steam content (Figure 4.7-7) in the dry-well. Consequently, also the pressure increase is faster in the new version.

After the first venting all three codes show still the same hydrogen concentration in the wet-well, but different concentrations in the dry-well with the highest concentration in V2.0r1 and the lowest in version V2.0r2. The COCOSYS result is in between. As already mentioned the differences between the codes/versions are increasing in the long term.

Figure 4.7-7 shows the corresponding steam concentrations for the same zones. The new ASTEC version calculates a much higher steam concentration for the dry-well in comparison to the old version. This is the explanation for the lower hydrogen concentration in Figure 4.7-6. The COCOSYS result is in between.

KRB – HWDB case

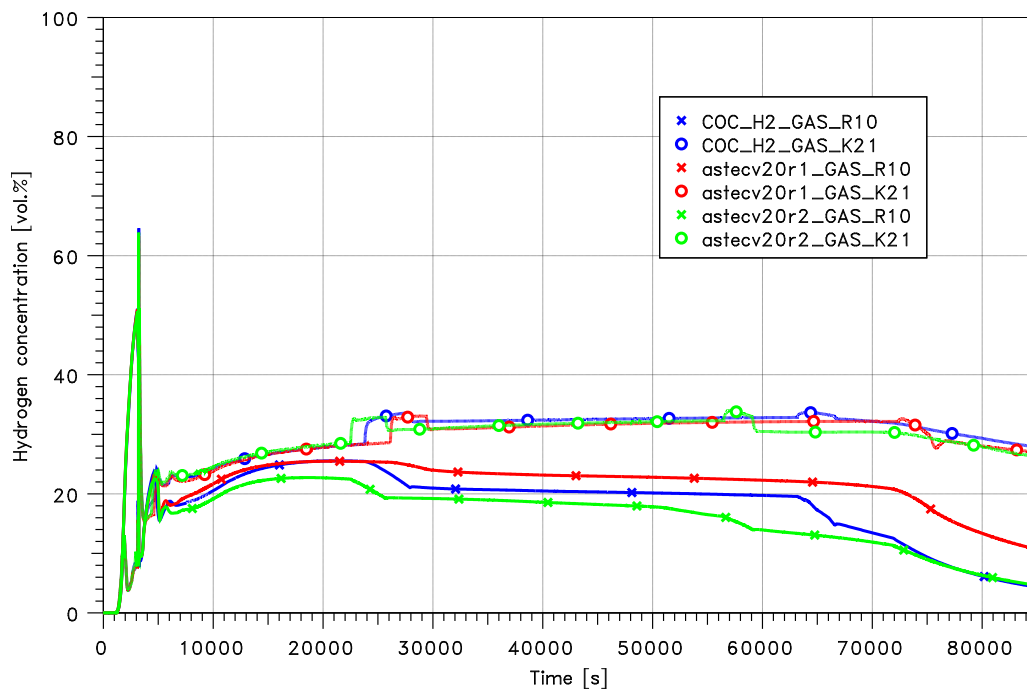
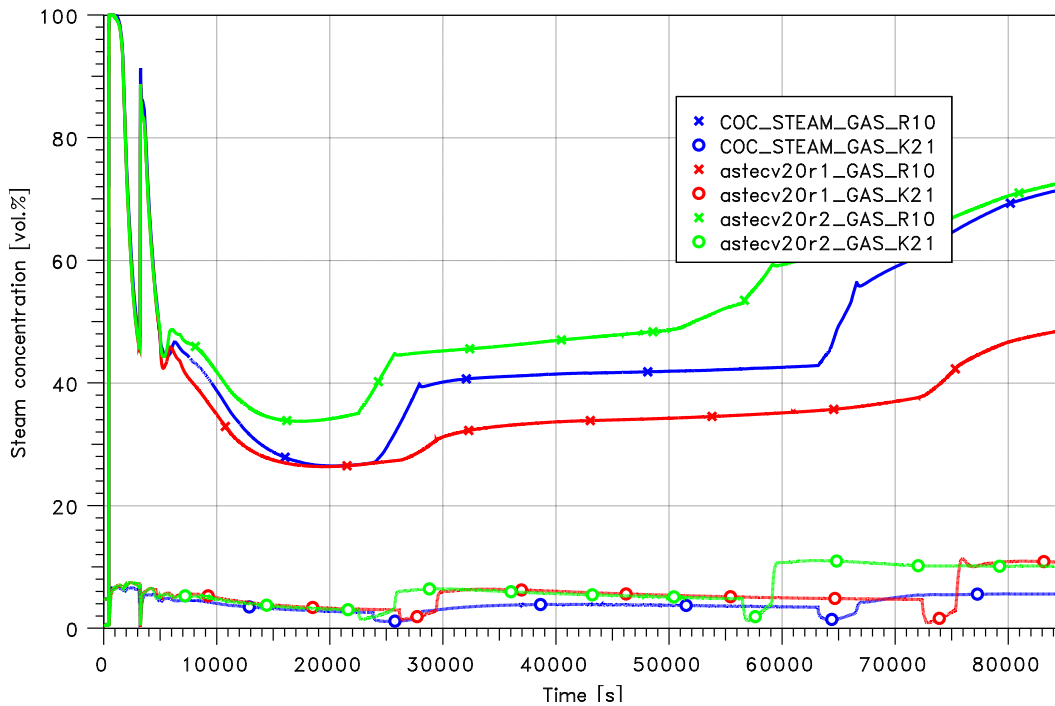


Figure 4.7-6 BWR-72, hydrogen concentration in dry- and wet-well

KRB – HWDB case



**Figure 4.7-7 BWR-72, steam concentration in a wet-well zone (K21) and a dry-well zone (R10)**

### 4.7.1.3 Summary

The calculations performed show that the INSERTION option of an ATM\_VALVE junction for the simulation of pressure suppression systems implemented into the new version V2.0r2 of ASTEC improves the simulation of ASTEC CPA for BWR type containments. However, different dry-well atmosphere and wet-well water temperatures and a different increase of the containment pressures between both ASTEC versions and in comparison to COCOSYS show relevant differences. The differences get more important in the late phase after the first venting was stopped.

A detailed investigation showed that this test case also uses a heat injection into a structure, so some differences between the two ASTEC versions have the same origin as the differences in the THAI Iod-11 test case (bug in the subroutine simulating heat injection into structures). An ASTEC calculation without heat injection into structure gives the same results as the old ASTEC version.

The differences between the used COCOSYS version and ASTEC are caused by the different heat transfer models for the sump surface in NONEQUILIBRIUM zones. This is important for the water pool in the wet-well (K21 and K22). Also different models for the heat transfer for condensation and wall condensation by DRAIN\_WALL junctions are used. In the current development version of COCOSYS this was changed and it is now possible to use the ASTEC models for these heat transfer models, too. A test calculation has been performed with heat transfer models COD+CDW replaced by the ASTEC models CDA+CWA. Also the heat transfer model for the sump surface in NONEQUILIBRIUM zones has been used by the option SUHT=AST. The results of this

calculation show a much better agreement between COCOSYS and ASTEC, but not completely identical behavior (Figure 4.7-8 and Figure 4.7-9).

KRB – HWDB case

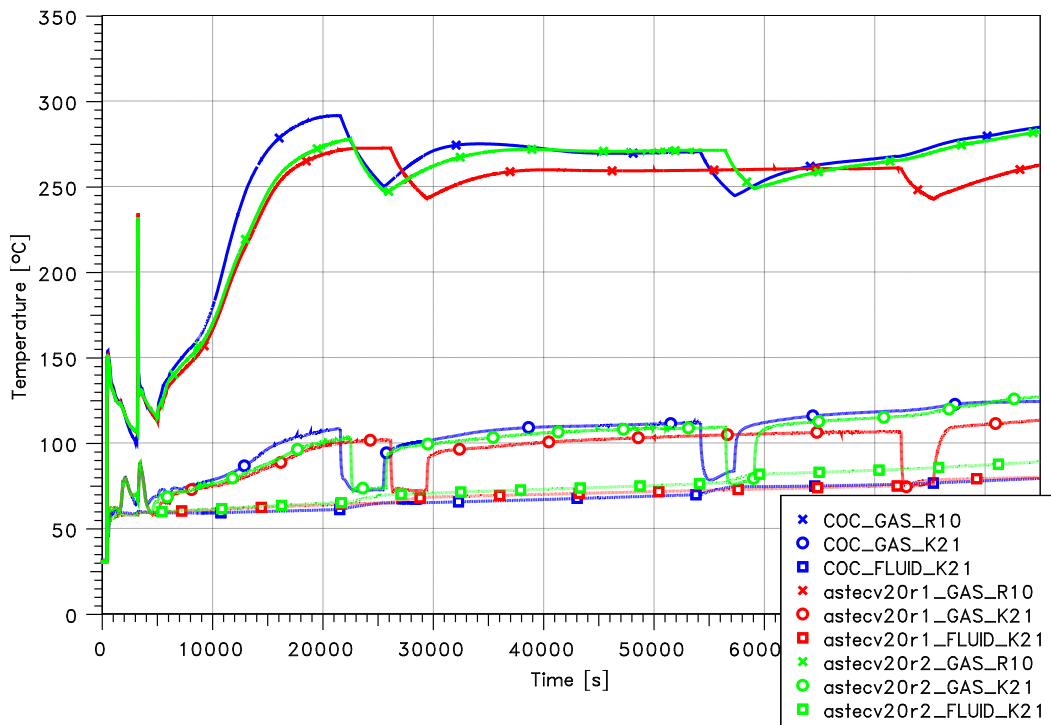


Figure 4.7-8 BWR-72, temperature in a wet-well zone (K21) and a dry-well zone (R10); calculation with COCOSYS developed version

KRB – HWDB case

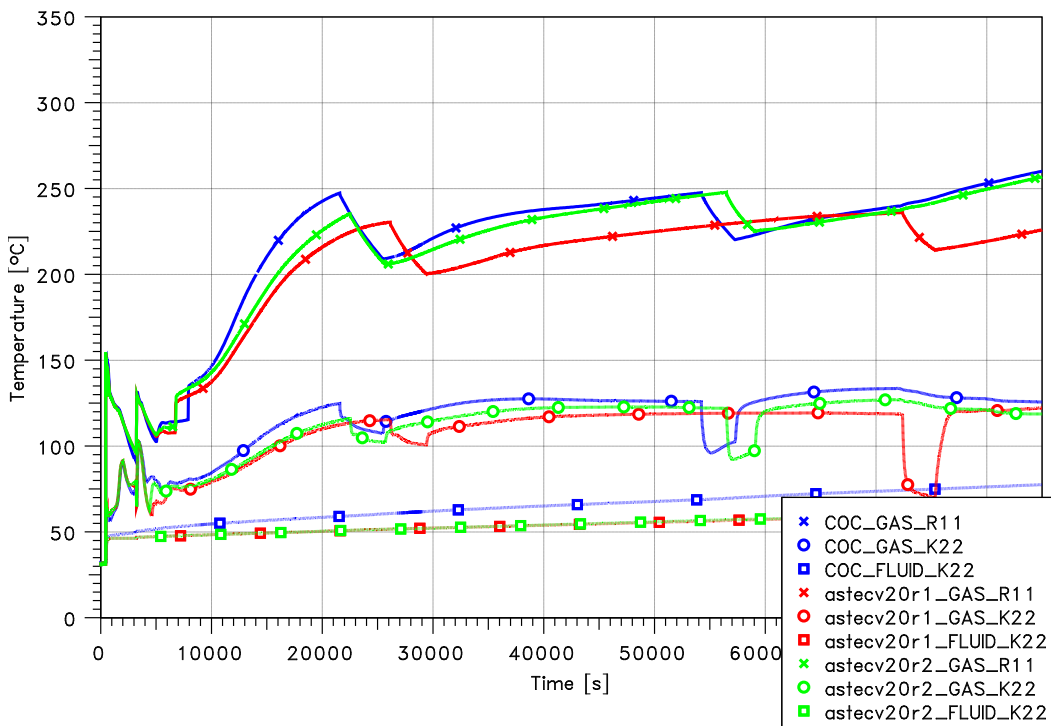


Figure 4.7-9 BWR-72, temperature in a wet-well zone (K22) and a dry-well zone (R11); calculation with COCOSYS developed version

---

#### **4.7.2 KONVOI PWR**

The test case will be added later to the regression test matrix.

#### **4.7.3 WWER-1000**

The test case will be added later to the regression test matrix.

## 5 Summary

A procedure for the regression testing of ASTEC has been successfully installed. It is based on the regression testing procedure already used for COCOSYS /ARN 08/. The calculations performed show larger differences between the ASTEC versions V2.0r1 and V2.0r2 for various calculations, which can be explained by code modifications. For some test cases the comparison with COCOSYS gives additional information.

The THAI Iod-11 test case now shows a realistic distribution of the light gas helium, because the new version solved a bug that caused that heat injection into structures was not considered. This improvement is not mentioned in /CHA 11/. The iodine behaviour in the RTF-Phebus 1 calculation is different in comparison to the initial version. This is understandable, as the IODE module was strongly improved between the versions compared.

Also the hydrogen deflagration cases ENACCEF RUN 153 and BMC Hx23 display strong differences due to the development process done on the new FRONT model.

The COMET L3 test case shows a difference in the heat transfer coefficients between the metal and the oxide layer. The used Greene correlation has not been modified. A further investigation showed also a change in the superficial gas velocity in the oxide layer and of the viscosity in the metal layer. In /CHA 11/ it is described that the Stedman correlation for the calculation of viscosity in the metal layer has changed. This could explain the differences, but it could not be resolved in detail.

In addition, the test case for the German boiling water reactor BWR-72 reveals strong differences in the temperatures of the wet-well water pool and the dry-well atmosphere that lead to a different pressure history between the ASTEC versions compared and especially in comparison to the latest COCOSYS release version. Therefore, also the starting point of the venting as well as the distribution of hydrogen on both sides of the pressure suppression system pool is different. The reason for these differences between the ASTEC versions is the usage of heat injection into structures that didn't work in the old ASTEC version. This is related to the same bug fix as in the THAI Iod-11 test case. The reason for the remaining differences to COCOSYS can be partially explained by the different heat transfer models used in the COCOSYS release version used for comparison here. A comparison with the latest COCOSYS developer version shows significant better agreement.

In total, 6 of 13 test cases show differences/improvements, although the change between the compared versions is only 1 revision. Most of them can be explained by the developments that have been made. The strong model development on the FRONT and IODE modules explain the differences visible in the test cases using these modules.

## 6 References

- /ABD 06/ Abdo, D., R. Tomassian, J. Brinster, D. Roumier, I. Tkatschenko, J. L. Widlocher:  
M5-MASP MISTRA experimental results  
CEA/DM2S report SFME/LTMF/RT/06-006/A, 2006
- /ALL 03a/ Allelein, H.-J., S. Arndt, L. Gallner, M. Heitsch, B. Hüttermann, K. Neu, W. Klein-Heßling, J. Langhans, W. Luther, B. Schmitz, S. Schwarz, G. Weber:  
Weiterentwicklung von COCOSYS, GRS-A-2960, 2003
- /ALL 03b/ Allelein, H.-J., S. Arndt, H. Bartalszky, M. Heitsch, B. Hüttermann, W. Klein-Heßling, S. Schwarz, G. Weber:  
Weiterentwicklung und Fortsetzung der Validierung des Containment-Code-Systems COCOSYS und des deutschfranzösischen Integralcodes ASTEC, GRS-A-2961, 2003
- /ALL 06/ Allelein, H.-J., S. Arndt, W. Klein-Heßling, S. Schwarz, C. Spengler, G. Weber:  
COCOSYS: Status of Development and Validation of the German Containment Code System  
Technical Meeting on Severe Accident and Accident Management for Nuclear Power Plants, Tokyo, March 14-16, 2006
- /ALL 07/ Allelein, H.-J., S. Arndt, W. Klein-Heßling, W. Luther, K. Neu, N. Reinke, S. Schwarz, B. Schwinges, C. Spengler, G. Weber:  
Intensivierte Validierung der Rechenprogramme COCOSYS und ASTEC  
GRS-A-3330/I, 2007
- /ALS 07/ Alsmeyer, H. et al.:  
The COMET-L3 Experiment on Long-Term Melt-Concrete Interaction and Cooling by Surface Flooding  
FZKA 7244  
Forschungszentrum Karlsruhe 2007
- /ARN 99/ Arndt, S., H. Bartalszky, A. Breest, F. Ewig, H.-G. Friederichs, B. Hüttermann, W. Klein-Heßling, J. Langhans, B.M. Schmitz, E. Schrödl, S. Schwarz, B. Schwinges:  
Entwicklung und Verifikation eines Containment-Code-Systems (COCOSYS) und eines deutsch-französischen Integralcodes (ASTEC), GRS-A-2737, 1999
- /ARN 03/ Arndt, S., H. Wolff:  
RALOC MOD4 input deck description for the EREC Bubble Condenser Test Facility BC V-213  
Technical Note TN-ARN-2/2002 (GRS - V - INT 9142 - 2/2002)  
GRS, May 2003
- /ARN 07/ Arndt, S.:  
Implementation of a fast running model for the simulation of vent pipes into ASTEC  
Technical Note TN-ARN-1/2007, GRS, 2007

- /ARN 08/ Arndt, S., H. Nowack:  
Status of regression testing - Comparison of COCOSYS V2.4(dev) with V2.3v9, GRS-A-3437, 2008
- /AUS 81/ Aust, E., A. Bültemann, H.-R. Niemann, P. Sattler, H. Schwan, J. Vollbrandt:  
DAS-Experiment der GKSS – Bericht über den Hauptversuch M1  
Versuchsbericht Nr. 23 11 AR E 04  
GKSS-Forschungszentrum Geesthacht GmbH, 1981
- /BAC 08/ Bachratá, A.:  
ASTEC V1 - Validation of the HDR Experiment HDR E11.1  
SARNET-MOBILITY Program report  
Contract EC-SARNET/FI6O-CT-2004-509065, August 2008
- /BAL 04/ Ball, J., C. Marchand:  
ISP-41 – Follow-up Exercise, Phase 2 Iodine Code Comparison Exercise  
against CAIMAN and RTF Experiments  
NEA / CSNI / R(2004)16 (August 2004)
- /BCE 99/ Quick Look Report. Test No.: 1  
Project PH 2.13/95: Bubble Condenser Experimental Qualification  
Task 2: Thermo-hydraulic and fluid-structure interaction test  
BC-D-ER-SI-0025, 1999
- /BEN 10/ Bentaib, A., Chaumeix, N.:  
Blind calculation of SARNET2 Hydrogen Combustion Benchmark on  
ENACCEF tests  
Bureau de Physique des Accidents Graves  
Rapport DSR/SAGR n°xxx  
June 2010  
*to be published*
- /BLU 08/ Blumenfeld, L., S. Arndt, A. Bentaib, F. Dabbene, Z. Parduba, J. Travis, E. Urbonavicius:  
SARNET SPRAY Benchmarks: MISTRA THERMALHYDRAULIC part,  
Comparison report, RAPPORT DM2S, SFME/LTMF/RT/07-015/A  
CEA Saclay, 5. November 2008
- /BON 05/ Bonnet, Jean-Michel:  
Overview of Progress in the Corium Area  
ERMSAR 2005, Aix-en-Provence,  
SARNET Contract: FI6O-CT-2004-509065
- /CHA 10/ Chaumeix, N., A. Bentaib:  
“SARNET H2 Combustion Benchmark: Specification of ENACCEF test”  
Bureau de Physique des Accidents Graves  
Rapport DSR/SAGR n°102  
January 2010
- /CHA 10b/ Chaumeix, N.:  
“Some answers to some questions”

Personal information provided for ISP49 participants  
April 2010

- /CHA 11/ Chatelard, P. et al.:  
Evolution of the integral code ASTEC V2.0-rev2 with respect to the original V2.0 version  
ASTEC V2.0r2 documentation, ASTEC-V2/DOC/11-07, 2011
- /DEI 03/ Deitenbeck, H.  
ASTEC - Konvertierung von COCOSYS (V1.2) Eingabedaten in ASTEC (V1.0) Eingabedaten und umgekehrt  
Technische Notiz, GRS, 10.3.2003
- /ECK 11/ Eckel, J.:  
Das FRONT Modul in ASTEC und COCOSYS  
GRS Technical Note  
February 2011
- /ERD 11/ Erdmann, W.:  
The ASTEC flame front module: Some parameter studies  
GRS Technical Note  
ERD-TN-05/11  
May 2011
- /FAR 04/ Farmer, M.T. et al.:  
2-D Core Concrete Interaction (CCI) Tests: CCI-2 Test Data Report – Thermohydraulic Results (Rev 0)  
OECD MCCI Project  
US NRC, October 2004
- /FIR 02/ Firnhaber, M., Fischer, K, Schwarz, S., Weber, G.:  
KAEVER – Experiments on the Behavior of Core-melt Aerosols in a LWR Containment  
OECD NEA ISP44 Comparison Report  
NEA/CSNI/R(2003)5  
August 2002
- /GLO 08/ Glowa, G. A.:  
The Radioiodine Test Facility  
R&D Reports, 153-126530-440-003 revision 0, 2008, AECL, Canada
- /GRS 90/ Deutsche Risikostudie KERNKRAFTWERKE, Phase B  
GRS 1990, ISBN 3-88585-809-6
- /HOE 10/ Höhne, M.:  
ASTEC Validation of CPA-FRONT: Experiences gained during participation on SARNET WP 7 Benchmark 2 Exercise  
GRS Technical Note  
April 2010
- /HÜT 02/ Hüttermann, B.:  
Validierung des HDR-Versuchs E11.1 mit COCOSYS  
HUE - TN 2/2002, Technical Note 2002

- /IVO 93/ IVO Power Engineering Ltd. (Finnland)  
Description of the inside spray model  
(short description of the spray model implemented in RALOC Mod 2.2 Version)  
internal note Nov 9<sup>th</sup>, 1993
- /KAN 93/ Kanzleiter, T.:  
V ANAM Multi-compartment Aerosol Depletion Test M3 with Soluble Aerosol Material  
Technical Report BleV-R67.098-304, Battelle-Institut e.V, 1993
- /KER 98/ Kersting, E., Löffler H.:  
Sicherheitsanalytische Untersuchungen zu schweren Störfällen in BWR, Band 1: Zusammenfassung, probabilistisches Konzept, integrale Unfallablaufanalysen  
GRS-A-2519, 1998
- /KLE 00/ Klein-Heßling, W. et al.:  
COCOSYS V1.2 User's Manual  
Gesellschaft für Anlagen- und Reaktorsicherheit (GRS) mbH  
GRS-P-3/2, July 2000
- /KLE 07/ Klein-Heßling, W., et al.:  
COCOSYS V2.3 User's Manual, Revision 0  
Gesellschaft für Anlagen- und Reaktorsicherheit (GRS) mbH  
Draft version from April 21, 2008  
COCOSYS page: <http://quickplace.grs.de/QuickPlace/astrid1/Main.nsf>  
(password protected Internet page, assessable by registered COCOSYS users only)
- /KLE 09a/ Klein-Heßling, W., S. Arndt, W. Erdmann, W. Luther, H. Nowack, N. Reinke, B. Schramm, S. Schwarz, C. Spengler, J. Stewering, G. Weber:  
Gezielte Validierung von COCOSYS und ASTEC sowie generische Anwendungsrechnungen mit diesen Rechenprogrammen  
Abschlussbericht zum BMWI Projekt RS 1170, GRS Köln, GRS-A-3489, Juli 2010
- /LAN 96/ Langhans, J.:  
Qualitätssicherungshandbuch für COCOSYS  
Gesellschaft für Anlagen- und Reaktorsicherheit mbH  
GRS-A-2357, Juli 1996
- /LUT 09/ Luther, W.:  
The Flame Front Model in the Containment Module CPA  
ASTEC-V2/DOC/09-17-CPA
- /MAL 06/ Malet, J., E. Porcheron, J. Vendel (IRSN), L. Blumenfeld, I. Tkatschenko (CEA):  
SARNET spray benchmarks: TOSQAN and MISTRA: Specification report, Rev. 1, Specification of the SARNET spray Benchmark  
DSU/SERAC/LEMAC – 06-11
- /MEL 01/ Melikhov, O. I., V. I. Melikhov, M. V. Davydov, A. V. Sokolin:  
Description of EREC Bubble Condenser Test Facility BC V-213

- Project INT 9142, Task 3.1  
 Research and Engineering Centre of NPP Safety  
 Electrogorsk, Russia, 2001
- /MEL 03/ Melikhov, O. I., G. V. Osokin, V. I. Melikhov, A. V. Sokolin:  
 Two SLB tests at BC V-213 test facility - Quick Look Report  
 Project INT 9142, Task 3.1, Subcontract UA-2165  
 Research and Engineering Centre of NPP Safety  
 Electrogorsk, Russia, 2003
- /NOW 07/ Nowack, H., S. Arndt:  
 Post-calculation of the GKSS M1 test with COCOSYS  
 RS 1170: "Gezielte Validierung von COCOSYS und ASTEC sowie generi-  
 sche Anwendungsrechnungen mit diesen Rechenprogrammen"  
 GRS-A-3390, Oktober 2007
- /PER 03/ Performance of independent post-test calculations  
 EU TSO Support to CEEC Nuclear Regulatory Authorities and their TSOs  
 in the safety related evaluation of the VVER 440/213 Bubble Condenser  
 Experimental Qualification Project  
 Phare Contract N° 02-0025, Technical Report of Task 4, Part 1  
 RISKAUDIT Report N° 576, Rev. 4, December 2003
- /PRO 02/ Prošek, A., D'Auria F., Mavko B.:  
 Review of quantitative accuracy assessments with fast Fourier based  
 method (FFTBM)  
 Nuclear Engineering and Design, 217 (2002), 179 - 206
- /SCH 84/ Schwinges, B.:  
 Theoretische Untersuchungen zum Verhalten eines Druckabbausystems  
 bei Störfällen  
 Gesellschaft für Anlagen- und Reaktorsicherheit (GRS) mbH  
 GRS-A-969, Juni 1984
- /SCZ 99/ Schwarz S.:  
 Verifikation und Validierung von COCOSYS an dem Experiment VANAM  
 M3  
 Gesellschaft für Anlagen- und Reaktorsicherheit (GRS) mbH  
 GRS - A – 2686, Februar 1999
- /SCZ 04/ Schwarz, S.:  
 COCOSYS - Hints and recommendations: Simulation of free jets and buoy-  
 ant plumes COCOSYS Internet page:  
[http://quickplace.grs.de/LotusQuickr/astrid1/PageLibraryC1256F7E004C22F2.nsf/h\\_Toc/EDDC2626F552984DC125736700309091/?OpenDocument](http://quickplace.grs.de/LotusQuickr/astrid1/PageLibraryC1256F7E004C22F2.nsf/h_Toc/EDDC2626F552984DC125736700309091/?OpenDocument)  
 July 15, 2004, Revision 0
- /SPE 07/ Spengler, C.:  
 Simplified Description of the Corium/Concrete Interface in MEDICIS Using  
 Effective Heat Transfer Coefficients  
 ASTEC-V1/MEM/A07-17, GRS Cologne, 2007
- /THO 97a/ Thompson, D. H., Farmer, M. T., Fink, J. K., Armstrong, D. R., Spencer, B.  
 W.

---

Compilation, Analysis, and Interpretation of ACE Phase C and MACE Experimental Data: Volume I – MCCI Thermalhydraulics Results  
Argonne National Laboratory, ACEX TR-C-14, November 1997, Proprietary Report

- /THO 97b/ Thompson, D. H., Fink, J. K.:  
Compilation, Analysis, and Interpretation of ACE Phase C and MACE Experimental Data: Volume II – Aerosol Results  
Argonne National Laboratory, ACEX TR-C-14, March 1997, Proprietary Report
- /URB 07/ Urbonavičius, E., B. Čėsna, E. Babilas:  
Analysis of the thermal-hydraulic, chemical and fission products transfer processes in confinement system of RBMK-1500 reactor during BDBA Phare Project No. 2003/5812.04.02, Task 4  
Version 1, October 26, 2007, Lithuanian Energy Institute Kaunas
- /WEB 06/ Weber, G., H.-J. Allelein, F. Funke, T. Kanzleiter:  
COCOSYS and ASTEC analyses of iodine multicompartments tests in the THAI facility  
ICONE-14, Miami, Florida, USA 2006
- /WEB 09/ Weber, G., Funke F.:  
Description of the Iodine Model AIM-F3 in COCOSYS  
Gesellschaft für Anlagen- und Reaktorsicherheit (GRS) mbH  
GRS - A – 3508, November 2009

---

**List of tables**

|             | Page                                                                                                                                                                                                                                                   |
|-------------|--------------------------------------------------------------------------------------------------------------------------------------------------------------------------------------------------------------------------------------------------------|
| Table 2.1-1 | Calculations chosen for regression testing ..... 3                                                                                                                                                                                                     |
| Table 4.2-1 | Phases of the VANAM-M3 experiment /KAN 93/ ..... 27                                                                                                                                                                                                    |
| Table 4.2-2 | Aerosol deposition surfaces in ASTEC input ..... 35                                                                                                                                                                                                    |
| Table 4.2-3 | Aerosol parameters in K148 and K187 ..... 35                                                                                                                                                                                                           |
| Table 4.4-1 | Input parameters for FRONT module for ENACCEF ..... 63                                                                                                                                                                                                 |
| Table 4.4-2 | Input parameters for FRONT module for Hx23 (for their<br>signification see /DEI 03/ Deitenbeck, H. ASTEC -<br>Konvertierung von COCOSYS (V1.2) Eingabedaten in ASTEC<br>(V1.0) Eingabedaten und umgekehrt Technische Notiz, GRS,<br>10.3.2003 ..... 69 |
| Table 4.5-1 | Composition of Corium in OECD-CCI-2 ..... 74                                                                                                                                                                                                           |
| Table 4.5-2 | Composition of concrete in COMET facility ..... 79                                                                                                                                                                                                     |
| Table 4.5-3 | Composition of the melt in COMET L3 test ..... 79                                                                                                                                                                                                      |
| Table 4.5-4 | Heat transfer coefficients for the different orientations in<br>W/m <sup>2</sup> K in both calculations ..... 81                                                                                                                                       |
| Table 4.7-1 | Event table of the BWR-72 HWDB scenario ..... 100                                                                                                                                                                                                      |
| Table 4.7-2 | Injection rates for the BWR-72 plant calculation ..... 100                                                                                                                                                                                             |

## List of figures

|               | Page                                                                                                                                 |
|---------------|--------------------------------------------------------------------------------------------------------------------------------------|
| Figure 2.2-1  | Directory structure for the regression testing ..... 4                                                                               |
| Figure 2.2-2  | Graphical user interface of the regression testing ..... 5                                                                           |
| Figure 2.2-3  | Definition of ASTEC versions and input files - definition.py ..... 5                                                                 |
| Figure 4.1-1  | HDR containment ..... 8                                                                                                              |
| Figure 4.1-2  | Injection, spray, and venting mass flow rates ..... 9                                                                                |
| Figure 4.1-3  | HDR Nodalisation ..... 10                                                                                                            |
| Figure 4.1-4  | HDR E11.1, Total pressure ..... 11                                                                                                   |
| Figure 4.1-5  | HDR E11.1, Temperatures in lower part of containment ..... 12                                                                        |
| Figure 4.1-6  | HDR E11.1, Temperatures on injection height ..... 12                                                                                 |
| Figure 4.1-7  | HDR E11.1, Temperatures in dome ..... 13                                                                                             |
| Figure 4.1-8  | HDR E11.1, Light gas concentration in lower part of containment ..... 14                                                             |
| Figure 4.1-9  | HDR E11.1, Light gas concentration on injection height ..... 14                                                                      |
| Figure 4.1-10 | HDR E11.1, Light gas concentration in dome ..... 15                                                                                  |
| Figure 4.1-11 | MISTRA test facility, general and schematic views showing external circuits of three annular condensers ..... 16                     |
| Figure 4.1-12 | MISTRA test facility, vertical cut including 3 condensers (yellow) and spray jet (grey) indications and spray nozzle detail ..... 17 |
| Figure 4.1-13 | MISTRA test facility, instrumentation mesh ..... 18                                                                                  |
| Figure 4.1-14 | MISTRA test facility, instrumentation of reference half-plane P0 (used in MASPn experiments) ..... 18                                |
| Figure 4.1-15 | MISTRA, M5 - MASP1 test sequence ..... 19                                                                                            |
| Figure 4.1-16 | MISTRA, MASP1, 58 zone model including with zone names ..... 21                                                                      |
| Figure 4.1-17 | MISTRA, MASP1, 58 zone model, heat conducting structures ..... 21                                                                    |
| Figure 4.1-18 | MISTRA, MASP1, comparison of measured and calculated pressure ..... 23                                                               |
| Figure 4.1-19 | MISTRA, MASP1, measured and calculated atmosphere temperatures in radius R2 ..... 23                                                 |
| Figure 4.1-20 | MISTRA, MASP1, measured and calculated sump water level ..... 24                                                                     |
| Figure 4.1-21 | MISTRA, MASP1, calculated and measured condensation rate at all condensers ..... 25                                                  |
| Figure 4.2-1  | BMC VANAM-M3, test geometry ..... 26                                                                                                 |
| Figure 4.2-2  | BMC VANAM-M3, simple nodalisation ..... 28                                                                                           |
| Figure 4.2-3  | BMC VANAM-M3, total pressure ..... 29                                                                                                |
| Figure 4.2-4  | BMC VANAM-M3, temperature stratification in R6 ..... 30                                                                              |
| Figure 4.2-5  | BMC VANAM-M3, relative humidity in R8 ..... 30                                                                                       |
| Figure 4.2-6  | BMC VANAM-M3, aerosol concentration in R8 ..... 31                                                                                   |
| Figure 4.2-7  | BMC VANAM-M3, aerosol concentration in R9 ..... 31                                                                                   |
| Figure 4.2-8  | BMC VANAM-M3, aerosol concentration in R10 ..... 32                                                                                  |
| Figure 4.2-9  | KAEVER test vessel /FIR 02/ ..... 33                                                                                                 |
| Figure 4.2-10 | Top view of the KAEVER test vessel /FIR 02/ ..... 34                                                                                 |
| Figure 4.2-11 | Pressure in K148 test phase II ..... 36                                                                                              |
| Figure 4.2-12 | Gas temperature in the KAEVER test vessel for K148 ..... 37                                                                          |
| Figure 4.2-13 | Volume condensation rates in K148 test calculations ..... 37                                                                         |
| Figure 4.2-14 | Sum of all wall condensation rates in the KAEVER test vessel in K148 calculations ..... 38                                           |
| Figure 4.2-15 | Dry aerosol concentration in K148 ..... 39                                                                                           |
| Figure 4.2-16 | Wet aerosol concentration in K148 ..... 39                                                                                           |
| Figure 4.2-17 | Geometric number mean diameter of the aerosol ..... 40                                                                               |
| Figure 4.2-18 | Volumetric /mass median diameter of the aerosol ..... 40                                                                             |
| Figure 4.2-19 | Pressure evolution in K187 experiment ..... 41                                                                                       |
| Figure 4.2-20 | Gas temperature in KAEVER test vessel in K187 experiment ..... 42                                                                    |
| Figure 4.2-21 | Volume condensation rate in K187 experiment ..... 42                                                                                 |
| Figure 4.2-22 | Wall condensation rate in K187 experiment ..... 43                                                                                   |
| Figure 4.2-23 | Total dry aerosol concentration in K187 ..... 43                                                                                     |

|               |                                                                                                                                                                      |    |
|---------------|----------------------------------------------------------------------------------------------------------------------------------------------------------------------|----|
| Figure 4.2-24 | Dry aerosol concentration of Ag in K187 .....                                                                                                                        | 44 |
| Figure 4.2-25 | Dry aerosol concentration of CsI in K187 .....                                                                                                                       | 44 |
| Figure 4.2-26 | Dry aerosol concentration of CsOH in K187 .....                                                                                                                      | 45 |
| Figure 4.2-27 | Total wet aerosol concentration in K187 .....                                                                                                                        | 45 |
| Figure 4.2-28 | Mean aerosol particle diameters for K187 .....                                                                                                                       | 46 |
| Figure 4.2-29 | Experimental measured particle (droplet) size distribution<br>1 000s after end of aerosol injection (at 7.5h) /FIR 02/.....                                          | 46 |
| Figure 4.3-1  | Multi-compartment configuration of the THAI-facility for the<br>Iodine tests .....                                                                                   | 48 |
| Figure 4.3-2  | THAI Iod-11, CPA and COCOSYS-AIM nodalisation of the<br>THAI-facility .....                                                                                          | 49 |
| Figure 4.3-3  | THAI Iod-11, pressure in the facility .....                                                                                                                          | 50 |
| Figure 4.3-4  | THAI Iod-11, temperature in a lower and a upper zone.....                                                                                                            | 51 |
| Figure 4.3-5  | THAI Iod-11, helium concentration in a lower and a upper<br>zone 52                                                                                                  |    |
| Figure 4.3-6  | THAI Iod-11, gaseous iodine concentration in different levels<br>of the facility .....                                                                               | 53 |
| Figure 4.3-7  | THAI Iod-11, calculation effort.....                                                                                                                                 | 54 |
| Figure 4.3-8  | Schematic of the PHEBUS/RTF Facility from /GLO 08/ .....                                                                                                             | 55 |
| Figure 4.3-9  | RTF-1, Total liquid iodine concentration .....                                                                                                                       | 56 |
| Figure 4.3-10 | RTF-1, Liquid compound concentration .....                                                                                                                           | 57 |
| Figure 4.3-11 | RTF-1, Wall deposition in liquid phase .....                                                                                                                         | 58 |
| Figure 4.3-12 | RTF-1, Total gaseous iodine concentration .....                                                                                                                      | 58 |
| Figure 4.3-13 | RTF-1, Gaseous compound concentration .....                                                                                                                          | 59 |
| Figure 4.3-14 | RTF-1, Wall deposition from gaseous phase.....                                                                                                                       | 60 |
| Figure 4.4-1  | Overview and sketch of the ENACCEF facility /CHA 10/.....                                                                                                            | 61 |
| Figure 4.4-2  | Measured flame front velocities .....                                                                                                                                | 62 |
| Figure 4.4-3  | ASTEC nodalization for ENACCEF facility .....                                                                                                                        | 63 |
| Figure 4.4-4  | Calculated flame front velocity; compare with Figure 4.4-2 .....                                                                                                     | 64 |
| Figure 4.4-5  | Pressure evolution at the dome entrance (2.877m from<br>ignition).....                                                                                               | 65 |
| Figure 4.4-6  | Gas temperatures in the facility.....                                                                                                                                | 66 |
| Figure 4.4-7  | Hydrogen concentration at different locations in ENACCEF .....                                                                                                       | 66 |
| Figure 4.4-8  | Battelle Model Containment.....                                                                                                                                      | 67 |
| Figure 4.4-9  | Five-room geometry for Hx23 experiment .....                                                                                                                         | 68 |
| Figure 4.4-10 | ASTEC nodalization for Hx23 *) .....                                                                                                                                 | 69 |
| Figure 4.4-11 | Pressure in the BMC Hx23 experiment.....                                                                                                                             | 70 |
| Figure 4.4-12 | Temperature in the BMC Hx23 experiment .....                                                                                                                         | 71 |
| Figure 4.4-13 | Hydrogen concentration in Hx23 experiment.....                                                                                                                       | 72 |
| Figure 4.5-1  | General view of the OECD-CCI-2 Test Section /FAR 04/.....                                                                                                            | 73 |
| Figure 4.5-2  | Side view (left) and top view (right) of the MCCI-part of OECD-<br>CCI-2 Test Facility (in blue: Tungsten electrodes for direct<br>electrical heating /FAR 04/)..... | 74 |
| Figure 4.5-3  | Cavity Erosion Profile at the end of OECD-CCI-2 - maximal<br>vertical and maximal horizontal erosion lengths are<br>approximately the same /FAR 04/.....             | 75 |
| Figure 4.5-4  | Temperature of the melt (single layer) .....                                                                                                                         | 76 |
| Figure 4.5-5  | Maximal horizontal (lateral) ablation (at +10cm elevation, see<br>Figure 4.5-3).....                                                                                 | 77 |
| Figure 4.5-6  | Vertical (axial) ablation.....                                                                                                                                       | 77 |
| Figure 4.5-7  | Overview: COMET test facility /ALS 07/ .....                                                                                                                         | 78 |
| Figure 4.5-8  | Picture of the N-S-plane cut of COMET L3 cavity; white lines<br>indicate the initial cavity /ALS 07/.....                                                            | 80 |
| Figure 4.5-9  | Time dependent erosion of the cavity in COMET L3 /ALS 07/ .....                                                                                                      | 80 |
| Figure 4.5-10 | MEDICIS calculated heat transfer coefficients between metal<br>and oxide layer .....                                                                                 | 81 |
| Figure 4.5-11 | MEDICIS calculated temperature of the metal layer in COMET<br>L3 82                                                                                                  |    |

|               |                                                                                                                                                                      |     |
|---------------|----------------------------------------------------------------------------------------------------------------------------------------------------------------------|-----|
| Figure 4.5-12 | MEDICIS calculated temperature of the oxide layer bulk in COMET L3 (red / green). Black/ grey: IR-measured maximal and minimal oxide layer surface temperature. .... | 83  |
| Figure 4.5-13 | Maximal axial ablation .....                                                                                                                                         | 83  |
| Figure 4.5-14 | Maximal radial ablation .....                                                                                                                                        | 84  |
| Figure 4.5-15 | Total eroded mass of concrete.....                                                                                                                                   | 84  |
| Figure 4.6-1  | Schematic configuration of the GKSS experimental facility .....                                                                                                      | 86  |
| Figure 4.6-2  | Simple 4 zones model of the GKSS M1 experiment with the DRAYS zone D1-PSS .....                                                                                      | 87  |
| Figure 4.6-3  | GKSS, test M1, short term pressure build-up in break room and wet-well zone (DRASYS zone) .....                                                                      | 88  |
| Figure 4.6-4  | GKSS, test M1, pressure build-up in break room and wet-well zone                                                                                                     | 89  |
| Figure 4.6-5  | GKSS, test M1, atmosphere temperature in the break room.....                                                                                                         | 90  |
| Figure 4.6-6  | GKSS, test M1, PSS pool water temperature .....                                                                                                                      | 90  |
| Figure 4.6-7  | GKSS, test M1, atmosphere temperature in the wet-well zone and expansion room.....                                                                                   | 91  |
| Figure 4.6-8  | EREC BC V-213, schematic view of the test facility .....                                                                                                             | 92  |
| Figure 4.6-9  | BC V-213, nodalisation with 24 zones .....                                                                                                                           | 93  |
| Figure 4.6-10 | BC V-213, test SLB G02, pressure in the break compartment V1, in the BC gas room V4 and the air trap V5.....                                                         | 95  |
| Figure 4.6-11 | BC V-213, test SLB G02, atmosphere temperature in the box V1                                                                                                         | 96  |
| Figure 4.6-12 | BC V-213, test SLB G02, atmosphere temperature in the BC gas room V4.....                                                                                            | 96  |
| Figure 4.6-13 | BC V-213, test SLB G02, pressure difference across the BC walls                                                                                                      | 97  |
| Figure 4.6-14 | BC V-213, test SLB G02, water temperature in the right side of the BC pool.....                                                                                      | 98  |
| Figure 4.7-1  | Nodalisation of BWR-72.....                                                                                                                                          | 99  |
| Figure 4.7-2  | BWR-72, temperature in a wet-well zone (K21) and a dry-well zone (R10).....                                                                                          | 102 |
| Figure 4.7-3  | BWR-72, temperature in a wet-well zone (K22) and a dry-well zone (R11).....                                                                                          | 103 |
| Figure 4.7-4  | BWR-72, pressure in dry-well and wet-well .....                                                                                                                      | 104 |
| Figure 4.7-5  | BWR-72, mass flow rate through vent pipes up to 1000 s.....                                                                                                          | 104 |
| Figure 4.7-6  | BWR-72, hydrogen concentration in dry- and wet-well.....                                                                                                             | 105 |
| Figure 4.7-7  | BWR-72, steam concentration in a wet-well zone (K21) and a dry-well zone (R10) .....                                                                                 | 106 |
| Figure 4.7-8  | BWR-72, temperature in a wet-well zone (K21) and a dry-well zone (R10); calculation with COCOSYS developed version .....                                             | 107 |
| Figure 4.7-9  | BWR-72, temperature in a wet-well zone (K22) and a dry-well zone (R11); calculation with COCOSYS developed version .....                                             | 107 |



**Gesellschaft für Anlagen-  
und Reaktorsicherheit  
(GRS) mbH**

Schwertnergasse 1  
**50667 Köln**  
Telefon +49 221 2068-0  
Telefax +49 221 2068-888

Forschungszentrum  
**85748 Garching b. München**  
Telefon +49 89 32004-0  
Telefax +49 89 32004-300

Kurfürstendamm 200  
**10719 Berlin**  
Telefon +49 30 88589-0  
Telefax +49 30 88589-111

Theodor-Heuss-Straße 4  
**38122 Braunschweig**  
Telefon +49 531 8012-0  
Telefax +49 531 8012-200

**[www.grs.de](http://www.grs.de)**